

Copyright is owned by the Author of the thesis. Permission is given for a copy to be downloaded by an individual for the purpose of research and private study only. The thesis may not be reproduced elsewhere without the permission of the Author.

**Convergence properties of Fock-space
based approaches in strongly correlated
Fermi gases**

A dissertation presented in partial fulfilment of the
requirements for the degree of

Doctor of Philosophy

in
Physics

at
Massey University, Albany
New Zealand

Peter Jeszenszki

2019

Abstract

The main objective of this thesis is the efficient numerical description of strongly correlated quantum gases. Due to the complex many-body structure of the wave function, usually, numerical methods are required for its computation. The exact diagonalization approach is considered, where the energies and the wave functions are obtained by diagonalizing the Hamiltonian in a many-body basis. The dimension of the space increases combinatorially with the number of particles and the number of single-particle basis functions, which limits the characterization of few-body systems to intermediate interactions. One of the main components of the convergence rate originates from the particle-particle interaction itself. The bare contact interaction introduces a singularity in the wave function at the particle-particle coalescence point. This is responsible for the slow convergence in the finite basis expansion in one dimension and it even causes pathological behavior in higher dimensions.

Firstly, the Gaussian interaction potential is examined as an alternative pseudopotential. After the description of the accurate calculation of the s -wave scattering length of this potential, the convergence properties are investigated. As this function is smooth, by construction the wave function is free from any singularity implying an exponentially fast convergence rate. If the resolution of the basis set is not fine enough, the finite-range pseudopotential is indistinguishable from the pathological contact potential. Through the example of few particles in a two-dimensional harmonic trap, we show that in order to reach the necessary resolution, the number of harmonic-oscillator single-particle basis functions must increase quadratically with the inverse characteristic length of the pseudopotential. This scaling property combined with the combinatorial growth of the many-body space makes the physically realistic short-range potentials computationally inaccessible.

We have also applied the so-called transcorrelated approach, where the singular part of the wave function is isolated in a Jastrow-type factor. This factor can be transformed into the Hamiltonian reducing the irregularity of the eigenfunction

and improving the convergence rate. We will show through the example of the homogeneous gas in one dimension that this transformation efficiently improves the convergence from M^{-1} to M^{-3} , where M is the number of the single-particle plane-wave basis functions.

Acknowledgements

First of all, I would like to thank my supervisor, Joachim Brand, for introducing me to the topic of ultracold atoms and strongly correlated quantum materials. I am really thankful for the thorough discussions and for his questions, which always pointed to the right direction. These years were really eye-opening to me, I see now physics and science from a completely different point of view.

I also would like to thank Ali Alavi for his constant enthusiasm about our topics and for the enlightening discussions. Although these focused especially on the Full Configuration Quantum Monte Carlo algorithm, it frequently spread out to more general topics like many-particle correlations and principles of numerical algorithms. I also really appreciate the active five months, which I spent in his group in Stuttgart as a visitor.

I am also really grateful to those researchers, which I collaborated with the most during my Ph.D. I would like to thank Hongjun Luo, who taught me the transcorrelated method and more generally the principles of mathematical physics, which formed the way to see the numerical methods in a more rigorous and precise manner. I would like to acknowledge the help of Tal Levy, who taught me the basic elements of the NECI code, which I have intensively used the past few years. I would like to thank Alexander Yu. Cherny, who taught me some important principles of scattering theory, which helped me to see this field in a clearer way.

Additionally, I would like to thank the former and the current group members of the Brand group. I am grateful to Ulrich Ebling and Mingrui Yang, the discussions with them helped a lot to understand the strongly correlated quantum matter and the numerical approaches we apply for them. I am thankful to Sophie S. Shamaliov, who explained the complicated Bethe ansatz technique to me in a very simple way. I would like to acknowledge the discussions with Antonio M. Mateo, who taught me a lot about traditional fermionic theories. I would like to thank Jayson G. Cosme, with whom we discussed a lot about the connection between different theoretical and experimental techniques. I am also grateful to Oleksandr Fialko, Lauri Toikka, Shreyoshi Gosh, and Jan Mayor, the discussions with them were extremely useful to understand the general properties of ultracold atoms.

I am also grateful to the people at the Center of Theoretical Chemistry and Physics (CTCP) and the Max Planck Institute in Stuttgart for providing a friendly atmosphere and keeping company even outside the academic environment. Additionally, I would like to acknowledge the funding from the Dodd-Walls Center during these three and half years.

Finally, I would like to thank my partner, Nikolett Nemet, for proofreading this thesis and for the constant patience and company for these three and half years. I also would like to thank my family members and my friends in Hungary for keeping close connections despite the large geographical distance.

Contents

1	Introduction	1
1.1	Publication list	5
2	Theoretical Background	6
2.1	Description of the interaction between ultracold atoms	6
2.1.1	Approximation of the interaction potential with scattering theory	6
2.1.2	Contact interaction	12
2.1.3	Connection between wave function derivatives and the decay rate of expansion coefficients	16
2.2	Introduction to the exact diagonalization approach	19
2.2.1	Exact diagonalization approach	19
2.2.2	Propagation in imaginary time	21
3	The s-wave scattering length of a Gaussian potential	26
3.1	Introduction	26
3.2	Numerical determination of the S -wave scattering length	28
3.2.1	Solution of the two-body problem and connection with the s -wave scattering length	28
3.2.1.1	Two-body scattering problem	28
3.2.1.2	The s -wave scattering and boundary conditions	30
3.2.1.3	Scattering length	30
3.2.2	One and three dimensions	31
3.2.3	Two dimensions	32
3.2.4	The Gaussian potential and the convergence of numerical results	33
3.3	Approximate expressions for Gaussian potential	37
3.3.1	Three-dimensional case	37
3.3.2	One-dimensional case	40
3.3.3	Two-dimensional case	42
3.4	Conclusion	44
4	Are smooth pseudopotentials a good choice for representing short-range interactions?	46
4.1	Introduction	46

4.2	Hamiltonian	50
4.3	Basis set expansion	50
4.4	Resolving the Gaussian pseudopotential	52
4.4.1	Unscaled harmonic oscillator basis	52
4.4.2	Length scale resolution	53
4.4.3	Scaled harmonic oscillator basis	56
4.4.4	Estimating the interaction-dependent prefactor	57
4.5	Conclusion and outlook	61
5	Accelerating the convergence of exact diagonalization with the transcorrelated method: Quantum gas in one dimension with contact interactions	63
5.1	Introduction	63
5.2	Theory	67
5.2.1	One-dimensional quantum gas with contact interaction: cusp of the wave function	67
5.2.2	Correlation factor for 1D system with contact interaction	69
5.2.3	Transcorrelated Hamiltonian in real space	71
5.2.4	Smoothness of the transcorrelated wave function	72
5.2.5	Convergence rate for ground-state energy	77
5.2.5.1	Standard method	78
5.2.5.2	Transcorrelated method	79
5.2.6	Transcorrelated Hamiltonian in second quantization and three-body term	80
5.3	Numerical examinations	82
5.3.1	Methods and implementation	82
5.3.2	Two particles	83
5.3.2.1	Correlation factor with fixed parameter k_c	85
5.3.2.2	Correlation factor with sliding parameter k_c	86
5.3.2.3	Comparison with the renormalization approach	87
5.3.2.4	Single-particle momentum density	88
5.3.3	Three fermions	91
5.3.3.1	Correlation factor with fixed parameter k_c : Bias from the approximation of the three-body term	92
5.3.3.2	Correlation factor with sliding parameter k_c : Treatment of the three-body term	93
5.3.3.3	Single-particle momentum density	94
5.3.4	Six fermions	95
5.4	Conclusion and outlook	98
6	Summary	100
7	Outlook	103
A	Boundary conditions for the scattering problem	105

B Accuracy of the s-wave scattering length in three dimensions at the singularity	108
C Alternative derivation of the approximate expressions for the s-wave scattering length	110
C.1 Three-dimensional case	110
C.2 One-dimensional case	112
C.3 Two-dimensional case	112
D Derivation of approximate formula (3.32) for the one-dimensional s-wave scattering length	114
E Fock-Darwin orbitals	119
F Evaluation of the matrix elements	121
F.1 Evaluation of one-particle integrals	121
F.2 Evaluation of two-particle integrals	122
G Evaluation of the infinite sum in Eq.(5.47)	126
Bibliography	129

Chapter 1

Introduction

The study of strongly correlated matter has attracted increasing research interest in the past decades [1]. These systems cannot be explained with a simple single-particle theory due to a significant role of the particle-particle interaction term. Therefore, a many-body theory should be considered to obtain a correct description even at a qualitative level. It is essential to understand the underlying physics of these systems in order to explain such interesting phenomena as high-temperature superconductivity [2–5] or the fractional quantum Hall effect [6–8]. Moreover, the same theory is required for the description of exotic astronomical objects like neutron stars [9–12].

Due to the complexity of many-body systems, the theoretical description becomes extremely difficult. It is widely believed that the fundamental phenomenon of high-temperature superconductivity can be modeled with the Hubbard model in two dimensions [13], where only the on-site and nearest neighbor interactions are considered. Even in this simple model there are no exact analytical solutions available, hence efficient numerical approaches are required [14]. Unfortunately, all of these techniques scale exponentially with the size of the system, restricting the applicability to the few-particle and intermediate interaction regimes.

An alternative solution can be an experimental realization of these strongly correlated systems in a well-controlled laboratory environment on an analog quantum simulator [15]. Ultracold atoms have been widely used for these purposes thanks to the experimental developments of the past two decades [16]. The optical and

magnetic traps can be finely tuned to mimic the desired external potential [16, 17]. Moreover, it is also possible to confine the system to lower dimensions [18] and to even examine dimensional crossovers [19]. Additionally, due to Feshbach resonances [20] the particle-particle interaction strength can be well-controlled with an external magnetic field. In this way, they have managed to create and dissociate ultracold molecules [21], realize strongly interactive two-dimensional systems [22, 23] or perform direct examinations of the occupation numbers in the two-dimensional Hubbard model [24].

Another important experimental development is the microtrap [25], where the ultracold few-particle regime becomes accessible. This enables the investigation of the transition from few- to many-body regimes [26, 27] or examination of pairing [28] and the effect of the quantum statistics in few-particle systems [29]. These experiments provide significant developments for the description of strongly correlated materials as they have the potential to realize the fractional quantum Hall effect, where it is believed that the fundamental phenomenon can be observed in the strongly interacting few-particle regime [30, 31].

The theoretical description of strongly correlated systems is usually done by using efficient numerical methods. One of the most elegant approaches is based on the Bethe ansatz [32], which provides exact results by numerically solving a nonlinear set of equations [33–35]. This approach is restricted to the homogeneous gas in one dimension. Although the strongly attractive limit of inhomogeneous systems can be accurately approximated with this approach [36–39] for the general cases and especially for higher dimensions a different approach is required.

As bosons are symmetric under particle exchange, the ground state of the wave function is nodeless. The wave function can be easily calculated with polynomially scaling Quantum Monte Carlo (QMC) [40] approaches. As fermions are antisymmetric under particle exchange the wave function has several nodes, where the wave function can change sign. In this case the wave function and the energy cannot be calculated with a polynomially scaling algorithm, which is frequently referred to as the sign-problem [41]. A popular solution to this problem is to expand the wave function in terms of antisymmetric many-body basis functions

(determinants) where the antisymmetry of the particles is satisfied. However, the sign problem can be still present due to the unknown sign of the expansion coefficients [41, 42]. Apart from some special cases [43, 44] they can be determined only with those techniques, which scales exponentially with the size of the system [41].

The most straightforward way to determine the energy and the wave function is the exact diagonalization approach [45, 46], where the Hamiltonian is diagonalized in a many-body basis. This basis set is usually constructed by selecting a single-particle basis set, where all the configurations with a given particle number are produced. The number of the many-body basis functions increases combinatorially with the number of particles and the number of the single-particle functions. Generally, for larger interactions more basis functions are needed, limiting the exact diagonalization approach to few-body systems and weakly correlated regimes [47].

In order to improve this method the coefficients are determined with efficient numerical techniques such as Auxiliary Field Quantum Monte Carlo [48, 49], Full Configuration Interaction Quantum Monte Carlo [50, 51], Matrix Product State approaches [52], Artificial Neural Network [53]. Although these methods provide significant improvements compared to the exact diagonalization approach they are still limited by the exponential scaling of the Hilbert space. Our principal goal in this thesis is to develop and investigate possible methodologies, which can decrease the necessary number of single-particle basis functions extending the applicability of these approaches to larger particle numbers and stronger interactions.

This thesis is organized as follows. In the first part of Chapter 2, we discuss the theoretical background of the particle-particle interaction models. We consider interaction and temperature regimes, where the s -wave scattering length alone is enough to describe the interaction between ultracold atoms and we can substitute the complex interaction potential with a simpler pseudopotential. Then we discuss one of the most popular pseudopotentials, the contact potential, in detail. This potential leads to a singularity in the wave function or in its first derivative causing a slow convergence rate in one dimension and straightforward application of it

leads to pathological results in higher dimensions. In the last part of this chapter, we briefly overview the exact diagonalization approach. Finally, we discuss the imaginary time propagation technique, which is used in the further chapters of the thesis.

In Chapter 3, the finite-range Gaussian pseudopotential is considered. We provide accurate expressions for the s -wave scattering length in one, two and three spatial dimensions. We first describe a numerical procedure to compute the value of the s -wave scattering length from the parameters of the Gaussian but find that its accuracy is limited in the vicinity of singularities that result from the formation of new bound states. We then derive simple analytical expressions that capture the correct asymptotic behavior of the s -wave scattering length near the bound states. Expressions that are increasingly accurate in wide parameter regimes are found by a hierarchy of approximations that capture an increasing number of bound states. The small number of coefficients that enter these expressions are determined from accurate numerical calculations. The new approximate formulae combine the advantages of the numerical and approximate expressions, yielding an accurate and simple description from the weakly to the strongly interacting limit.

In Chapter 4, we investigate the convergence properties of the above mentioned Gaussian potential. As this function is smooth the finite basis set expansions are guaranteed to converge exponentially fast. Nevertheless, if the finite basis expansion cannot resolve the finite-range of the Gauss potential, it is indistinguishable from the contact interaction leading to the same pathological behavior. We discuss scaling relations for the required size of the basis set and demonstrate the basis set convergence on the example of a two-dimensional system of few fermions in a harmonic trapping potential. In particular, we show that the number of harmonic-oscillator basis functions needed to reach the regime of exponential convergence for a Gaussian pseudopotential scales with the fourth power of the pseudopotential length scale, which can be improved to quadratic scaling when the basis functions are re-scaled appropriately. Numerical examples for three fermions with up to a few hundred single-particle basis functions are presented and implications for the feasibility of accurate numerical multi-particle simulations of interacting ultra-cold

atom systems are discussed.

In Chapter 5 we apply a different philosophy to improve the convergence properties. The transcorrelated approach is applied, where the singularity of the wave function is treated exactly and folded into the many-body Hamiltonian with a similarity transformation. The resulting transcorrelated Hamiltonian is not Hermitian but can be treated numerically with a standard projection approach. The smoothness of the wave function increases by at least one order and thus the convergence rate for the ground-state energy improves. By numerical investigation of a one-dimensional gas of spin- $\frac{1}{2}$ fermions, we find the error in the transcorrelated energy to scale as M^{-3} with a single-particle basis of M plane waves compared to M^{-1} for the expansion of the original Hamiltonian and M^{-2} using conventional lattice renormalization.

Finally, in Chapter 6, the results of the two methodologies are concluded and compared.

1.1 Publication list

In Chapters 3-5 we discuss independent research projects, which were published in scientific journals. The contents of these chapters completely agree with the articles below, only editorial works were performed to match the style of the thesis.

- **Chapter 3:** Peter Jeszenszki, Alexander Yu. Cherny, and Joachim Brand, *s* -wave scattering length of a Gaussian potential, [Physical Review A **97**, 042708 \(2018\)](#)
- **Chapter 4:** Peter Jeszenszki, Ali Alavi and Joachim Brand, *Are smooth pseudopotentials a good choice for representing short-range interactions?*, [Physical Review A **99**, 033608 \(2019\)](#)
- **Chapter 5:** Peter Jeszenszki, Hongjun Luo, Ali Alavi and Joachim Brand *Accelerating the convergence of exact diagonalization with the transcorrelated method: Quantum gas in one dimension with contact interactions*, [Physical Review A **98**, 053627 \(2018\)](#)

Chapter 2

Theoretical Background

2.1 Description of the interaction between ultracold atoms

In this section, the physical interaction between the ultracold atoms is discussed through the perspective of the scattering theory. It will be shown that at sufficiently low temperature the physics can be described by only one parameter, the so-called *s*-wave scattering length. This parameter is used to define pseudopotentials, which can describe the interaction between the particles more efficiently. The contact pseudopotential and its effect on the wave function are discussed in detail at the end of this section.

2.1.1 Approximation of the interaction potential with scattering theory

We are considering a dilute atomic gas at low temperatures (typically on a μK scale), which is trapped in a magnetic or optical trap. Thus, the full Hamiltonian contains, besides the kinetic term, the external potential due to the magnetic and optical fields and the particle-particle interaction term. The most general description of the latter requires the Hamiltonian to explicitly contain all the possible interactions between the electrons and the nuclei constituting the atoms. In practice such a detailed description is not necessary, as at low temperature

ionization or internal atomic excitation processes are negligible [54, 55]. Hence, these atoms can be well approximated by composite particles, where the total spin of the composite particle determines the permutation symmetry (Fermi or Bose) to be applied in a quantum mechanical description.

The interaction potential between the atoms is described by a complicated many-body potential, which is difficult to treat with theoretical methods. Therefore, let us investigate the main contributions of this interaction in the usual experimental conditions. The traps are finely tuned to specific hyperfine states [17, 56], therefore, in order to avoid the loss of particles it is required to eliminate every process, which leads to different hyperfine states [17, 54]. These are typically the particle-particle collisions, where more than two particles are involved. The frequency of these events are mainly determined by the probability to find three or more particles within the volume R^3 , where R is the range of the interaction [17]. This probability can be controlled by the particle-number density, which should be sufficiently low to avoid these collision processes [17].

As the two-body collisions dominate the particle-particle interactions, we can simplify the complicated many-body interaction potential to pair interactions. Therefore, the Hamiltonian can be written in the following form,

$$H = \sum_i^N \left(-\frac{\hbar^2}{2m} \nabla_i^2 + V_{\text{trap}}(\mathbf{r}_i) \right) + \sum_{i < j}^N V(|\mathbf{r}_i - \mathbf{r}_j|), \quad (2.1)$$

where term $-\frac{\hbar^2}{2m} \nabla_i^2$ is the kinetic energy operator of atom i , V_{trap} is the trapping potential and $V(|\mathbf{r}_i - \mathbf{r}_j|)$ is the interaction potential between the atoms.

The determination of the pair potential is numerically demanding due to the complicated interaction between the atoms [54, 57]. Moreover, the experimentally measurable quantities are sensitive to the potential curve, which makes it difficult to compare the results of the theoretical calculations and the experimental measurements [54, 57]. Therefore, scattering theory is applied to introduce a simpler pseudopotential instead of the physical interaction potential.

In order to determine the main properties of the potential during the scattering,

let us investigate a two-particle system without trapping potential in three dimensions. The Hamiltonian can be separated into centre-of-mass and relative motion. The first describes the motion of the free particle, whereas the latter considers the non-trivial interaction potential,

$$H_{\text{rel}} = -\frac{\hbar^2}{2\mu}\nabla^2 + V(r) , \quad (2.2)$$

where $\mu = m/2$ is the reduced mass, and r is the distance between the particles.

In a scattering process we consider an incoming plane wave from one of the spatial direction with momentum k and an outgoing scattered wave, ψ_{scatt} ,

$$\psi = e^{ikz} + \psi_{\text{scatt}} ,$$

where the spatial direction z is chosen for the direction of the incoming wave. The scattered wave at large interparticle separation can be expressed with a spherical wave,

$$\psi = e^{ikz} + f(\vartheta)\frac{e^{ikr}}{r} , \quad (2.3)$$

where $f(\vartheta)$ is the scattering amplitude, and ϑ is the scattering angle, which is the angle between the relative momenta before and after the scattering. Due to the spherical symmetry of the Hamiltonian, the scattering amplitude depends only on the scattering angle, which also imposes an axial symmetry on the wave function. The scattering amplitude includes all the effects of the interaction potential during the scattering process. Therefore, in the following we concentrate on the determination of $f(\vartheta)$ in the low temperature limit, when $k \rightarrow 0$.

The wave function can be expanded in partial waves [17],

$$\psi = \frac{1}{r} \sum_{\ell=0}^{\infty} A_{\ell} P_{\ell}[\cos(\vartheta)] u_{3\text{D},\ell}(r) , \quad (2.4)$$

where A_{ℓ} is the expansion coefficient, $u_{3\text{D},\ell}(r)/r$ describes the radial part of the wave function, and $P_{\ell}(x)$ is the Legendre polynomial [58]. The radial part of the

wave function is determined by a differential equation [59],

$$\left[-\frac{\hbar^2}{2\mu} \frac{d^2}{dr^2} + \frac{\ell(\ell+1)\hbar^2}{2\mu r^2} + V(r) \right] u_{3D,\ell}(r) = E u_{3D,\ell}(r), \quad (2.5)$$

where $E = \hbar^2 k^2 / 2\mu$ is the kinetic energy of the incoming wave.

Assuming that the potential $V(r)$ has a finite range R , the function $u_{3D,\ell}(r)$ can be given as a sine function [17, 54, 60],

$$u_{3D,\ell}(r) \underset{r \gg R}{\sim} \frac{1}{k} \sin \left[kr - \frac{\pi}{2} \ell + \delta_\ell(k) \right], \quad (2.6)$$

where \sim stands for the asymptotical equality. The effect of the scattering potential is encoded in $\delta_\ell(k)$, which is called the phase shift. The relation between the scattering amplitude and the phase shift can be determined by comparing Eqs.(2.3), (2.4), and (2.6) [17, 61],

$$f(\vartheta) = \sum_{\ell=0}^{\infty} (2\ell+1) f_\ell P_\ell[\cos(\vartheta)], \quad (2.7)$$

$$f_\ell = \frac{1}{k \cot(\delta_\ell) + ik} \quad (2.8)$$

where f_ℓ is the partial scattering amplitude.

The weight of the different partial scattering amplitudes can be determined by considering Eq.(2.5). Note that the only difference between the ℓ -states appears in the so-called repulsive centrifugal potential $\ell(\ell+1)\hbar^2/2\mu r^2$, which increases with ℓ . This potential keeps the particles with higher angular momenta further apart, which in turn decreases the contribution of the scattering processes with larger angular momentum. It can be explicitly expressed in the phase shift [60, 61],

$$\delta_\ell \underset{k \rightarrow 0}{\sim} \begin{cases} k^{2\ell+1} & \text{if } \ell < (n-3)/2, \\ k^{n-2} & \text{if } \ell \geq (n-3)/2, \end{cases} \quad (2.9)$$

where $V(r) \stackrel{r \rightarrow \infty}{\sim} r^{-n}$. The ultracold atoms interact with van der Waals interaction, where $n = 6$, which provides the following expressions for the phase shift:

$$\delta_0 \stackrel{k \rightarrow 0}{\sim} k, \quad (2.10)$$

$$\delta_1 \stackrel{k \rightarrow 0}{\sim} k^3, \quad (2.11)$$

$$\delta_2 \stackrel{k \rightarrow 0}{\sim} k^4 \stackrel{k \rightarrow 0}{\sim} \delta_3 \stackrel{k \rightarrow 0}{\sim} \delta_4 \stackrel{k \rightarrow 0}{\sim} \dots \quad (2.12)$$

The values of δ_ℓ decreases with the angular momentum for small k from $\ell = 0$ to $\ell = 2$, then the values of δ_ℓ at $\ell \geq 2$ will be asymptotically equivalent.

The argument above means that it is enough to consider the smallest possible ℓ state, which is determined by the permutational symmetry of the wave function. In case of bosons, the wave functions is symmetric under particle exchange, which can be represented in the wave function of the relative motion (2.4) by a 180° rotation in the scattering angle. Therefore, using the symmetry of Legendre polynomials [58],

$$P_\ell [\cos(\vartheta)] = (-1)^\ell P_\ell [\underbrace{\cos(\pi - \vartheta)}_{-\cos(\vartheta)}],$$

it can be seen that only the even values of ℓ are allowed as for these states there is no sign-flip under particle exchange. Hence, the lowest possible angular momentum state corresponds to $\ell = 0$ (*s*-wave). In the case of two identical fermions, the wave function is antisymmetric under particle exchange. Thus, it allows only odd values of ℓ with the lowest angular momentum $\ell = 1$ (*p*-wave).

In this thesis, we consider the spin-1/2 Fermi gas, where besides the previously discussed interaction between identical fermions, another interaction is present between fermions with different spin. In this case the spatial part of the wave function is symmetric under particle exchange, therefore similarly to the bosonic case they interact via the *s*-wave process. As the contribution of the *s*-wave scattering is much larger than the contribution from the *p*-wave scattering, the interaction between the identical fermions is negligible.

An explicit expression for f_0 can be obtained by considering the limit of $k \rightarrow 0$ in Eq.(2.5), where the effect of $V(r)$ is negligible,

$$-\frac{\hbar^2}{2\mu} \frac{d^2}{dr^2} u_{3D,0}(r; k=0) = 0 . \quad (2.13)$$

This equation can be solved,

$$u_{3D,0}(r; k=0) = C(r - a_s^{3D}) , \quad (2.14)$$

where C and a_s^{3D} are just two arbitrary constants.

Calculating the logarithmic derivative of Eq.(2.14), we can eliminate the coefficient C ,

$$\frac{u'_{3D,0}(r; k=0)}{u_{3D,0}(r; k=0)} = \frac{1}{r - a_s^{3D}} . \quad (2.15)$$

The same logarithmic derivative can be calculated for Eq.(2.6), where the limit of $k \rightarrow 0$ should give back Eq.(2.15),

$$\lim_{k \rightarrow 0} \left[\frac{u'_{3D,0}(r)}{u_{3D,0}(r)} \right] = \lim_{k \rightarrow 0} [k \cot(kr + \delta_0)] = \frac{1}{r - a_s^{3D}} . \quad (2.16)$$

Applying the addition theorem for the cotangent function, and considering only the leading order term of $\tan(kr) = kr + \mathcal{O}(k^3)$, the equation (2.16) can be further simplified,

$$\lim_{k \rightarrow 0} \left[\frac{u'_{3D,0}(r)}{u_{3D,0}(r)} \right] = \lim_{k \rightarrow 0} \left[\frac{1}{r + \frac{1}{k \cot(\delta_0)}} \right] = \frac{1}{r - a_s^{3D}} .$$

Hence, the relationship between δ_0 and a_s^{3D} can be easily determined,

$$\lim_{k \rightarrow 0} k \cot(\delta_0) = -\frac{1}{a_s^{3D}} , \quad (2.17)$$

where a_s^{3D} is called the three dimensional scattering length. Substituting it into Eq.(2.8), the scattering amplitude in the zero energy limit can be determined,

$$f_0 = -a_s^{3D} .$$

Of course, in reality the momentum of the particles is larger than zero. For bosons it is predominantly caused by the finite temperature. For fermions there is a larger effect due to the Pauli exclusion principle. Therefore, in some special cases as the narrow Feshbach resonance [56, 62], the momentum dependent terms should also be considered in the phase shift (2.17) and it can be taken into account with a finite range expansion [63, 64].

In spite of these, most of the collisions with the same value of a_s^{3D} cannot be distinguished from each other at low energies [17, 56, 62]. Therefore, we choose the pseudopotential in a way to have a simple form for the theoretical calculations and to reproduce the desired value of a_s^{3D} . As a_s^{3D} can be measured with experimental techniques it provides an easy way to compare the theoretical calculations with the experimental measurements [17, 54].

Generalizations of pseudopotentials in lower dimensions are introduced in a similar manner. The one-dimensional scattering length, a^{1D} [65], and the two-dimensional s -wave scattering length, a_s^{2D} [66, 67], are applied to parametrize the pseudopotential [65].

2.1.2 Contact interaction

One of simplest possible pseudopotentials is the contact pseudopotential, where the particles only interact if they are on top of each other. For the sake of simplicity let us start with particles in one dimension, where the contact interaction can be expressed with a Dirac- δ function [33, 65]

$$V_{1D}(x) = -\frac{2\hbar^2}{ma^{1D}}\delta(x) . \quad (2.18)$$

The Dirac- δ function is singular at the particle-particle coalescence point, $x = 0$ leading to an irregular behavior in the wave function [65]. This can be easily

shown for two particles in a homogeneous system. The Schrödinger equation has the following form in the relative-motion coordinate (x):

$$-\frac{\hbar^2}{2\mu} \frac{d^2}{dx^2} \psi_{1D}(x) - \frac{\hbar^2}{\mu a_{1D}} \delta(x) \psi_{1D}(x) = E \psi_{1D}(x) ,$$

where $\mu(= m/2)$ is the reduced mass. Let us take the integral of this equation over a small interval $[-\epsilon, \epsilon]$ around the singularity,

$$-\frac{\hbar^2}{2\mu} \int_{-\epsilon}^{\epsilon} \frac{d^2}{dx^2} \psi_{1D}(x) dx - \frac{\hbar^2}{\mu a_{1D}} \int_{-\epsilon}^{\epsilon} \delta(x) \psi_{1D}(x) dx = E \int_{-\epsilon}^{\epsilon} \psi_{1D}(x) dx . \quad (2.19)$$

Assuming that the wave function is continuous and finite everywhere, as $\epsilon \rightarrow 0$ the right-hand side of Eq.(2.19) vanishes leading to a step in the first derivative,

$$-\frac{2}{a_{1D}} \psi_{1D}(0) = \lim_{\epsilon \rightarrow 0} \left[\left. \frac{d}{dx} \psi_{1D}(x) \right|_{x=\epsilon} - \left. \frac{d}{dx} \psi_{1D}(x) \right|_{x=-\epsilon} \right] . \quad (2.20)$$

It means the wave function has a cusp at the particle-particle coalescence point, which can be described by an absolute value function,

$$\psi_{1D}(x) = \left(1 - \frac{|x|}{a_{1D}} \right) \psi_{1D}(0) + \mathcal{O}(x^2) . \quad (2.21)$$

The expressions (2.20) and (2.21) can be considered as boundary conditions for the wave function. If the boundary conditions are satisfied, the eigenfunction can be determined by considering only the interaction free Hamiltonian. This idea was first introduced in the context of nuclear physics to describe the deuteron (diplon) by Hans Bethe and Rudolf Peierls [68], and it is thus referred to as Bethe-Peierls boundary conditions.

The boundary conditions have been successfully applied in one dimension as they lead to exactly solvable models for the homogeneous gas [33–35] and for the trapped systems in the strongly interacting limit [36, 38, 69]. However, in more general cases, due to the effect of the trap the direct implementation of the boundary conditions is difficult. In these cases except of the two-body system [70] the exact solutions are unknown. Therefore, instead of introducing the boundary

conditions in the wave function, the Dirac- δ pseudopotential (2.18) is considered in the Hamiltonian. Approximating the wave function with a finite basis expansion, perturbative and exact diagonalization approaches can be applied for the determination of the wave function and the energy [47, 71, 72].

In higher dimensions, the representation of the contact potential is not as straightforward as in one dimension. However, before we discuss the possible pseudopotentials in more details let us start with the Bethe-Peierls boundary conditions in two and three dimensions [73],

$$\psi_{2D}(r) = \ln\left(\frac{r}{a_s^{2D}}\right) + \mathcal{O}(r) \quad , \quad (2.22)$$

$$\psi_{3D}(r) = \frac{a_s^{3D}}{r} - 1 + \mathcal{O}(r) \quad . \quad (2.23)$$

Comparing these expressions with the one-dimensional case in Eq.(2.21), where only the first derivative of the wave function was discontinuous, in higher dimensions the wave functions is already singular. This extreme behavior at the boundaries restricts the application of the boundary conditions to two- and three-body systems [74, 75].

For larger particle numbers, a zero-range pseudopotential has to be defined. In higher dimensions the bare Dirac- δ potential cannot be applied straightforwardly. As the wave function is divergent at the coalescence point it would lead to infinite potential energy, which causes the lack of scattering processes for repulsive interaction and the nonphysical divergence of the energy for attractive interactions [76, 77]. Therefore, the Dirac- δ potential has to be regularized with a differential operator $\frac{\partial}{\partial r}$, which handles the singularity in the wave function and reproduces the correct s -wave scattering length [78–80],

$$V_{2D}(\mathbf{r}) = -\frac{2\pi\hbar^2}{m \ln(a_s^{2D})} \delta(\mathbf{r}) \left[1 - \ln(a_s^{2D}) r \frac{\partial}{\partial r} \right] \quad , \quad (2.24)$$

$$V_{3D}(\mathbf{r}) = \frac{4\pi a_s^{3D} \hbar^2}{m} \delta(\mathbf{r}) \frac{\partial}{\partial r} r \quad . \quad (2.25)$$

These potentials have been successfully applied in the description of few-body systems [70] or in the perturbation theory of ultracold atomic gas [78]. However,

evaluating the effect of the potentials (2.24) and (2.25) over the smooth functions, we obtain back the matrix elements of the pathological Dirac- δ potential [47, 81]. In order to see this, let us calculate the matrix element for the pseudopotential (2.25) between the non-singular spherically symmetric smooth functions $f(r)$ and $g(r)$,

$$\langle f | V_{3D} | g \rangle = \frac{4\pi a_s^{3D} \hbar^2}{m} \int_0^\infty dr r f^*(r) \frac{\delta(r)}{r} \frac{\partial}{\partial r} [r g(r)]$$

where the Dirac- δ function is transformed into polar coordinates and we integrate out for the spherical angles. After simplifying with variable r and evaluating the differentiation, we obtain two terms,

$$\langle f | V_{3D} | g \rangle = \frac{4\pi a_s^{3D} \hbar^2}{m} \left(\int_0^\infty dr f^*(r) \delta(r) g(r) + \underbrace{\int_0^\infty dr f^*(r) \delta(r) r \frac{\partial g(r)}{\partial r}}_{f^*(r) r \frac{\partial g(r)}{\partial r} \Big|_{r=0} = 0} \right).$$

The second term on the right-hand side is zero due to the factor r and the first term on the right-hand side corresponds to a matrix element of a Dirac- δ function. This means that we cannot apply the pseudopotentials (2.24) and (2.25) in any numerical approach, which is based on the finite basis expansion with smooth basis functions.

Alternatively, two approaches have been commonly used for the numerical calculations of these high dimensional systems. One of them is the so-called renormalization approach. This approach is based on the fact that the finite basis expansion cannot resolve the singularity of the Dirac- δ potential, hence the potential in this representation has a finite range leading to physically meaningful scattering length [73]. The potential strength is renormalized according to the number of the applied single-particle functions to obtain the correct scattering properties. Exact mathematical descriptions can be derived for a homogeneous system using a plane-wave basis set to determine the interaction strength corresponding to a given scattering length [73]. Such explicit expressions are unknown

for inhomogeneous systems. However, the renormalization is performed in a way to reproduce the exactly solvable two-body results that seemingly give a reliable approximation for the energy and the wave function even at larger particle numbers [77, 82]. The renormalization approach can also be applied to accelerate the convergence of the finite basis expansions [83, 84], which we will examine in detail in Chapter 5.

An alternative approach is to use a finite-range pseudopotential [81, 85, 86], instead of the zero-range contact potential. In this case, the scattering length is well defined, but due to the finite length scale the scattering processes can be biased [81]. In order to eliminate this bias, besides extrapolating to the infinite basis limit, an additional extrapolation to the zero-range is required [81, 87]. In Chapter 3 and Chapter 4 we present a detailed discussion about the scattering and convergence properties of a specific finite-range potential, the Gauss pseudopotential.

2.1.3 Connection between wave function derivatives and the decay rate of expansion coefficients

In numerical approaches it is a standard approximation to expand the wave function over a finite number of basis functions [47, 81]. In terms of analyzing the convergence behavior of this expansion the derivatives of the wave function have an important role. This can be easily demonstrated on the example of the plane wave basis functions.

Let us consider a periodic function $f(x)$ with period L ,

$$f(x + L) = f(x) .$$

We also assume that the $(p-1)$ th derivative of the function $f(x)$ is discontinuous at x_0 , and its p th derivative at this point is related to the Dirac- δ function ¹

$$\frac{d^p f(x)}{dx^p} \sim \delta(x - x_0) A(x) , \quad (2.26)$$

¹The discontinuous function cannot be differentiated in a rigorous way. However, the differentiation can be generalized with the so-called weak derivative [88], which can be calculated for these functions. This leads to the expected Dirac-delta function for the weak derivative of the Heaviside step function.

where $A(x)$ is a continuous regular function, which describes the p -th derivative everywhere else.

Let us expand the function $f(x)$ in a plane wave basis set,

$$f(x) = \sum_j c_j \frac{1}{\sqrt{L}} e^{ik_j x}, \quad (2.27)$$

where c_j is the expansion coefficient and $1/\sqrt{L}$ is the norm of the plane wave function. We require the basis functions to be periodic with L as well, therefore, the value of k_j is set to

$$k_j = \frac{2\pi n_j}{L},$$

where n_j is an integer.

In a numerical approach, we can consider only a finite number of basis functions in the expansion (2.27). Therefore, it is advantageous if the coefficients c_j decay rapidly.

Let us determine this decay rate by calculating c_j with the overlap of function $f(x)$ and the corresponding plane wave basis function,

$$c_j = \frac{1}{\sqrt{L}} \int_0^L dx f(x) e^{ik_j x}. \quad (2.28)$$

Using partial integration, c_j can be expressed with the integral of the derivative of $f(x)$,

$$c_j = \frac{1}{ik_j \sqrt{L}} \underbrace{[f(x) e^{ik_j x}]_0^L}_0 - \frac{1}{ik_j \sqrt{L}} \int_0^L dx \frac{df(x)}{dx} e^{ik_j x},$$

where the first term on the right hand side is zero as $f(0) = f(L)$ and $e^{i2\pi n_j} = e^0 = 1$. The partial integration can be repeated p times,

$$c_j = \frac{1}{\sqrt{L}} \int_0^L dx f(x) e^{ik_j x} = \frac{1}{\sqrt{L}} \left(\frac{-i}{k_j} \right)^p \int_0^L dx \frac{d^p f(x)}{dx^p} e^{ik_j x} \sim \frac{1}{\sqrt{L}} \left(\frac{-i}{k_j} \right)^p e^{ik_j x_0},$$

where the relation (2.26) is used and we assumed that the Dirac- δ function predominantly determines the integral expression above. As $e^{ik_j x_0}$ is bounded,

$$|e^{ik_j x_0}| = 1 ,$$

in the limit of large value of k_j , the value of c_j decays polynomially,

$$c_j \stackrel{k \rightarrow \infty}{\sim} \frac{1}{k_j^p} . \quad (2.29)$$

It gives us the general rule that the functions, which are differentiable in higher orders, converge more rapidly in their plane wave expansions. If the function is differentiable infinitely many times, then it converges faster than any polynomial convergence and it can also be shown that this convergence is exponentially fast [89].

Applying relation (2.29) for the contact interaction in one dimension, we find that it converges with $1/k_j^2$ as the second derivative of the absolute value function in Eq.(2.21) leads to a Dirac- δ function.

The relation (2.29) also describes a more general connection between the short-range interaction and the high momentum-tail. Due to the contact interaction, in the asymptotic limit of large momentum the wave function decays with $1/k^2$, which leads to a $1/k^4$ decay in the density [65]. Interestingly the same $1/k^2$ decay for the wave function and $1/k^4$ decay for the density can be obtained in higher dimensions as well [73]. This can be visualized easily if we recognize that the second derivative of the wave functions (2.22) and (2.23) are related to the Dirac-delta function [73],

$$\begin{aligned} \nabla^2 [\ln(r)] &= 2\pi\delta(\mathbf{r}) , & \text{in two dimensions ,} \\ \nabla^2 \left(\frac{1}{r} \right) &= -4\pi\delta(\mathbf{r}) , & \text{in three dimensions .} \end{aligned}$$

In the upcoming chapters, we focus more on the applicability of these relations for the ultracold atoms with short-range interactions. In Chapter 4 instead of the plane wave basis set we examine the convergence in the harmonic oscillator basis set. In this basis set the convergence rate is still connected with the differentiability

of the wave function. The energy converges polynomially with $1/n_j^{(p+1)/2}$ [90]. Though it is slower than the convergence in the plane wave basis set, it is still expected to be exponentially fast if the wave function is smooth. In Chapter 4 we apply the Gauss pseudopotential, which is not singular, hence the exact wave function is smooth and it converges exponentially fast at the asymptotic limit.

We follow a different philosophy in Chapter 5, where we introduce a similarity transformation, which improves the convergence by increasing the smoothness leading to a faster converging basis expansion. We found that the differentiability can be improved at least two orders for the homogeneous Bose gas leading to $1/k_j^4$ decay for the coefficients of the plane waves. For the homogeneous Fermi gas the differentiability improves with one order, which results in a $1/k_j^3$ decay in momentum space.

2.2 Introduction to the exact diagonalization approach

In this section, the exact diagonalization approach is introduced. The basis set representation and the problem of the exponential scaling are discussed. After that a specific diagonalization technique, the imaginary time evolution, is thoroughly discussed.

2.2.1 Exact diagonalization approach

In order to determine the ground-state wave function, $|\Psi_0\rangle$, and energy, E_0 , let us start with the time-independent Schrödinger equation,

$$H|\Psi_0\rangle = E_0|\Psi_0\rangle. \quad (2.30)$$

In exact diagonalization approach the Schrödinger equation is solved by introducing a finite many-body basis set. The basis vectors are the Fock-state vectors,

which can be constructed by a product of creation operators,

$$|\Phi_{\underline{n}}\rangle = \prod_i \prod_{\sigma} \left(a_{i\sigma}^{\dagger} \right)^{n_{i\sigma}} |\text{vac}\rangle ,$$

where $|\Phi_{\underline{n}}\rangle$ is the Fock-state vector, $\underline{n} = (n_{1\sigma_1}, n_{2\sigma_2}, \dots, n_{i\sigma}, \dots)$, where $n_{i\sigma}$ is the occupation number of the i th single-particle state with spin σ , $a_{i\sigma}^{\dagger}$ creates a particle to the same single-particle, $|\text{vac}\rangle$ is a vacuum state, which is a Fock-state without any particles.

The wave function is expanded in the Fock-state basis,

$$|\Psi_0\rangle = \sum_{\underline{n}} c_{\underline{n}0} |\Phi_{\underline{n}}\rangle , \quad (2.31)$$

where $c_{\underline{n}0}$ is the expansion coefficient. Substituting Eq.(2.31) into Eq.(2.30) and projecting with $\langle \Phi_{\underline{m}} |$ we obtain the following linear equation:

$$\sum_{\underline{n}} H_{\underline{m}\underline{n}} c_{\underline{n}0} = E_0 c_{\underline{m}0} , \quad (2.32)$$

where $H_{\underline{m}\underline{n}} = \langle \Phi_{\underline{m}} | H | \Phi_{\underline{n}} \rangle$ and the orthonormality of the basis vectors is used. Hence, the diagonalization of the matrix \mathbf{H} provides the ground-state energy and wave function as the lowest eigenvalue and the corresponding eigenvector.

In order to define the many-body basis set we select a set of single-particle states, which can be determined from the non-interacting or mean-field solutions. Subsequently, we consider all the possible occupation numbers corresponding to these states for a given number of particles.

The number of the many-body basis states can be determined by considering the number of the single-particle states, M_{σ} , and the number of the particles, N_{σ} , for all the spin components. Usually, the number of single-particle states does not change with the σ , thus in the following we drop the index σ in M_{σ} . In the case of bosons the number of basis functions can be determined by a combinatorial expression,

$$M_{\text{mb}}^b = \prod_{\sigma} \binom{M + N_{\sigma} - 1}{N_{\sigma}} , \quad (2.33)$$

where M_{mb}^b is the number of many-body basis functions. For fermions we obtain a different expression as the identical fermions cannot occupy the same single-particle state due to the Pauli exclusion principle,

$$M_{\text{mb}}^f = \prod_{\sigma} \binom{M}{N_{\sigma}}, \quad (2.34)$$

where M_{mb}^f is the number of many-body basis functions for fermions.

These combinatorial scalings lead to enormous number of basis functions even for few particles and small number of single-particle states. For 10 bosons and 20 single-particle basis functions it means $M_{\text{mb}}^b = 2 \cdot 10^8$ many-body basis functions, which translates into about 360 TByte memory usage just to store the Hamiltonian matrix. It is even larger for 5 spin-up and 5 spin-down fermions and 20 single-particle basis functions, where the number of the many-body basis functions increases to $M_{\text{mb}}^f = 2.4 \cdot 10^9$ with a required memory of 53000 TByte. These huge matrices cannot be stored in the currently available computer architectures. Moreover, the standard diagonalization algorithms cannot be applied as the number of operations scales with the third power of the dimension of the space [91]. In the following subsection we introduce a more efficient numerical algorithm, where both the memory requirements and the number of operations improve significantly.

2.2.2 Propagation in imaginary time

In order to find an efficient way to determine the ground-state solution let us consider the Schrödinger equation in imaginary time (setting $\hbar = 1$),

$$-\frac{\partial}{\partial \tau} |\Psi\rangle = H |\Psi\rangle. \quad (2.35)$$

The differential equation can be solved formally

$$|\Psi(\tau)\rangle = e^{-H\tau} |\Psi(0)\rangle, \quad (2.36)$$

where we assumed that H does not depend on τ . The exponential operator on the right hand side in Eq.(2.36) propagates $|\Psi(0)\rangle$ to the ground state at large τ

values. In order to see this let us evaluate the effect of $e^{-H\tau}$ by expanding the Hamiltonian in the basis of the eigenstates,

$$H = \sum_I E_I |\Psi_I\rangle \langle \Psi_I|. \quad (2.37)$$

Substituting Eq.(2.37) into Eq.(2.36), we can obtain the contributions from the different eigenstates to the state $|\Psi(\tau)\rangle$,

$$|\Psi(\tau)\rangle = e^{-\tau \sum_I E_I |\Psi_I\rangle \langle \Psi_I|} |\Psi(0)\rangle = \sum_i e^{-\tau E_I} \langle \Psi_I | \Psi(0) \rangle |\Psi_I\rangle. \quad (2.38)$$

During the imaginary time propagation, the state with $E_I > 0$ decays exponentially to zero, the state with $E_I < 0$ increases exponentially, whereas the state with $E_I = 0$ stays constant. Hence, in the infinite imaginary time limit, $|\Psi(\tau)\rangle$ decays to the ground state,

$$\lim_{\tau \rightarrow \infty} |\Psi(\tau)\rangle = |\Psi_0\rangle.$$

In the limit of $\tau \rightarrow \infty$, the norm of $|\Psi(\tau)\rangle$ is exponentially large or small depending on the sign of E_0 . In order to prevent this, a shift, S , is introduced in the exponential,

$$|\Psi(\tau)\rangle = e^{-(H-S)\tau} |\Psi(0)\rangle. \quad (2.39)$$

The value of the shift is determined by keeping the norm to be constant. This leads to an exponential decay of the excited states, while the value of the shift naturally gives us the ground-state energy.

This imaginary time propagation requires an initial guess $|\Psi(0)\rangle$, which has to have a non-zero overlap with the ground state, $\langle \Psi_0 | \Psi(0) \rangle \neq 0$, otherwise $|\Psi(\tau)\rangle$ converges to one of the excited states. Although this condition theoretically cannot be satisfied without the prior knowledge of $|\Psi_0\rangle$, in the most of the cases, the non-interactive or the mean-field solutions has a non-zero overlap with the ground state. Therefore, in the practice the condition $\langle \Psi_0 | \Psi(0) \rangle \neq 0$ is usually satisfied.

Although the direct application of the exponential form of the Hamiltonian is not possible due to the non-linear parametrization, the operator can be simplified by using the following identity of the exponential function [92],

$$e^x = \lim_{k \rightarrow \infty} \left(1 + \frac{x}{k}\right)^k . \quad (2.40)$$

Hence, the exponential in (2.39) can be considered as a successive effect of the Hamiltonian,

$$|\Psi(\tau)\rangle = \lim_{k \rightarrow \infty} [1 - (H - S) \Delta\tau]^k |\Psi(0)\rangle , \quad (2.41)$$

where $\Delta\tau = \tau/k$, which can be easily transformed to an iterative equation,

$$|\Psi^{(k+1)}\rangle = [1 - (H - S) \Delta\tau] |\Psi^{(k)}\rangle . \quad (2.42)$$

Substituting the finite basis expansion Eq.(2.31) into Eq.(2.42) and projecting onto $\langle \Phi_{\underline{m}} |$, we obtain the iterative expression for the coefficients,

$$c_{\underline{m}}^{(k+1)} = c_{\underline{m}}^{(k)} - \sum_{\underline{n}} (H_{\underline{mn}} - S\delta_{\underline{mn}}) \Delta\tau c_{\underline{n}}^{(k)} . \quad (2.43)$$

The shift is iteratively updated to preserve the norm of the wave function in every A -th step [50],

$$S^{(k)} = S^{(k-A)} - \frac{\zeta}{A\Delta\tau} \ln \left(\frac{N_w^{(k)}}{N_w^{(k-A)}} \right) ,$$

where ζ is a damping parameter and $N_w^{(k)}$ is L_1 norm of the wave function,

$$N_w^{(k)} = \sum_{\underline{m}} |c_{\underline{m}}^{(k)}| .$$

In the calculations parameters ζ is typically chosen between 0.05-0.1, while the parameter A is chosen between 5-10.

There is an alternative way to obtain the energy and the wave function by simply setting $S = 0$ and normalizing $c_{\underline{m}}^{(k)}$ in Eq.(2.43) at every iteration step.

This algorithm does not require the optimization of the shift and the energy is obtained by simply the L_2 norm of the wave function after the multiplication with the Hamiltonian. However, in this case, this methodology requires to calculate the square of the coefficients and the normalization of the coefficient with every (or every A -th) iteration step. This increases the number of floating point operations compared to the previously discussed approach.

There are several diagonalization procedures, which determine the eigenvectors and eigenvalues by the successive multiplication of the Hamiltonian, such as power iterative methods [93], Lanczos algorithm [94] or Arnoldi algorithm [95]. These methods are usually applied if only a few low-lying eigenvalues and the corresponding eigenvectors are of interest. The Hamiltonian is usually sparse, which improves the scaling of the number of operations from the third power to the first power with the dimension of the Hilbert space [96].

Another advantage of the imaginary time propagation is the lower memory requirement. It is not necessary to store the Hamiltonian matrix, only the effect of the matrix on the coefficients is needed.

This can be easily shown by considering the second quantized representation of the Hamiltonian [97],

$$H = \sum_{ij} \sum_{\sigma} h_{ij} a_{i\sigma}^{\dagger} a_{j\sigma} + \sum_{ijkl} \sum_{\sigma\sigma'} V_{ijkl} a_{i\sigma}^{\dagger} a_{j\sigma'}^{\dagger} a_{l\sigma'} a_{k\sigma} \quad (2.44)$$

$$h_{ij} = \int d\mathbf{r} \varphi_i(\mathbf{r}) \left(-\frac{\hbar^2}{2m} \nabla^2 + V_{\text{trap}}(\mathbf{r}) \right) \varphi_j(\mathbf{r}), \quad (2.45)$$

$$V_{ijkl} = \int d\mathbf{r} \int d\mathbf{r}' \varphi_i(\mathbf{r}) \varphi_j(\mathbf{r}') V(|\mathbf{r} - \mathbf{r}'|) \varphi_k(\mathbf{r}') \varphi_l(\mathbf{r}). \quad (2.46)$$

where $\varphi_i(\mathbf{r})$ is the i th single-particle function, h_{ij} is the one-particle integral, V_{ijkl} is the two-particle integral.

The effect of the Hamiltonian (2.44) can be considered as moving one or two particles to different single-particle states. Thus all the matrix elements are zero between those basis functions, which cannot be transformed to each other by changing the single-particle states of maximum two particles. The remaining matrix elements can be easily expressed with the one- and two-particle integrals in Eqs.(2.45) and (2.46) [98–100].

Therefore, it is enough to store the one- and two-particle integrals and the coefficients from two consecutive iteration steps in Eq.(2.43). As the number of one- and two-particle integrals have a polynomial scaling with the single-particle orbitals, their memory requirement is usually negligible compared to the combinatorially scaling memory requirement of the coefficients. This means a linear scaling with the dimensions of the space, which is a significant improvement compare to the quadratic scaling of the Hamiltonian matrix. Considering the previous example with 10 bosons and 20 single-particle orbitals, it decreases the memory usage from 360 TByte to 38 Mbyte. For 5 spin-up and 5 spin-down fermions, the improvement is from 53000 TByte to 460 MByte. Both examples become easily calculable on a desktop computer.

In Chapter 4 and 5 we used imaginary time propagation to determine the ground-state energy and eigenvector. The algorithm has been implemented in the N-electron Configuration Interaction (NECI) code by the Ali Alavi's group [50]. This group has developed the NECI code to calculate the Full Configuration Interaction Quantum Monte Carlo (FCIQMC) algorithm, which is based on the stochastic sampling of Eq.(2.43). It also provides the possibility to apply the more efficient, but further approximated FCIQMC algorithm to ultracold atoms in the future.

Chapter 3

The s -wave scattering length of a Gaussian potential

3.1 Introduction

The interest in the accurate determination of s -wave scattering length has increased in the past decades due to its importance in the description of systems of ultracold atoms [17, 101]. As the range of the inter-particle interactions are usually much smaller than the average inter-particle distances, the effects of interactions can be expressed in terms of the scattering amplitude between pairs of particles. For dilute gases at ultracold temperatures the kinetic energies are low and, therefore, the main contribution to the amplitude comes from the s -wave scattering at zero momentum. Particle interactions are thus determined completely by a single parameter, the s -wave scattering length [17, 102]. In theoretical calculations, it is therefore not necessary to consider the detailed interaction potential between the particles. Instead, a pseudopotential may be chosen in a way to reproduce the desired value of the s -wave scattering length, which can simplify the required computations considerably [17].

One of the simplest and most popular pseudopotentials is the Dirac-delta potential. Its straightforward application is, however, restricted to one dimension, since in two or three dimensions it is meaningless without renormalisation [76, 77, 103]. An alternative option is to use finite-range pseudopotentials, e.g. the finite square

well [81, 87], Troullier-Martins [85, 104], Pöschl-Teller [86, 105] or Gaussian potential [81, 87, 103, 106–111]. The scattering length is finite for these pseudopotentials, but an extrapolation to zero range might be necessary to avoid an unphysical shape dependence [81, 87, 105]. The relationship between the parameter(s) of the potential and the scattering length is not always trivial. Apart from some special cases [105, 112] numerical techniques are required to determine this relation [60, 66, 113].

For Gaussian potentials no closed-form analytic expressions are available and for this reason numerical approaches have been applied [64, 106, 110, 114]. In two dimensions an approximate expression was derived by Doganov *et al.* [103]. These authors considered two particles in a harmonic trap, where the Gaussian interparticle interaction is treated in a perturbative framework. The obtained second order correction combined with the analytical result of the contact pseudopotential [70, 115] provides the approximate expression. Due to the perturbative approach, this approximation works quite well in the weakly interacting limit, but it deteriorates with increasing interaction strength.

In this chapter, we derive approximate analytical expressions for the *s*-wave scattering length of a Gaussian pseudopotential in one, two and three dimensions¹. These expressions qualitatively describe the singularities of the *s*-wave scattering length at the formation of the first bound state, which is problematic for purely numerical approaches. Analytical formulae for weak interactions are derived in one and two dimensions, where the *s*-wave scattering length has a singularity at zero interaction strength. In order to improve the accuracy, the approximate expressions are generalized by including the effects of additional bound states. The unknown parameters in this ansatz are determined by non-linear fitting to accurate numerical results. The obtained formulae are robust and simple and accurately provide the values for the *s*-wave scattering length in wide regime of attractive interaction.

We describe and carefully benchmark a numerical method to accurately determine the scattering length of a short-range scattering potential in one, two, and

¹The candidate derived the analytic expression in this chapter and in Appendix D. A. Yu. Cherny worked out the derivations in Appendix C.

three spatial dimensions. The approach is based on previous work of Verhaar [66] and may be useful in its own right as it is able to provide very accurate results except for the immediate vicinity of the singularities. The numerical approach is applicable for general short-range potentials and is not restricted to potentials of Gaussian shape.

This chapter is organized as follows: In Sec. 3.2, after stating the problem and discussing the required asymptotic conditions for scattering wave functions, we present an accurate numerical approach for determining the s -wave scattering length along with benchmark calculations for a Gaussian potential. In Sec. 3.3 approximate analytic expressions for the s -wave scattering length of a Gaussian potential are derived before more accurate, generalized expressions with numerically determined parameters are introduced. Three appendices provide additional details on derivations and numerical issues with determining the position of singularities in the scattering length, respectively.

3.2 Numerical determination of the S -wave scattering length

3.2.1 Solution of the two-body problem and connection with the s -wave scattering length

3.2.1.1 Two-body scattering problem

Let us consider a two-particle scattering process with the following n -dimensional Hamiltonian:

$$H_{2p} = -\frac{\hbar^2}{2m_1}\nabla_1^2 - \frac{\hbar^2}{2m_2}\nabla_2^2 + V(|\mathbf{r}_1 - \mathbf{r}_2|), \quad (3.1)$$

where $V(|\mathbf{r}_1 - \mathbf{r}_2|)$ is a spherically symmetric particle-particle interaction potential, m_i , \mathbf{r}_i and ∇_i^2 are the mass, coordinate and Laplace-operator of the i -th particle, respectively. Although our main target is the Gaussian potential, we here consider

more general classes of potentials for which the numerical procedures can be applied. Specifically, we assume that the interaction is sufficiently short-ranged to justify the existence of the scattering length. This is fulfilled in n dimensions if $V(r)$ obeys the condition [116, 117]

$$\int_A^\infty |V(r)| r^{n-1} dr < \infty$$

for a finite A , where it is sufficient to assume that the potential decreases faster than $1/r^{n+\varepsilon}$ with $\varepsilon > 0$ at sufficiently large distance. In addition, we suppose that the potential is non-singular at the origin (see, e.g., Refs. [117, 118])

$$\int_0^B r |V(r)| dr < \infty, \quad \text{for 2 and 3 D,} \quad (3.2)$$

$$\int_0^B |V(r)| dr < \infty, \quad \text{for 1 D,} \quad (3.3)$$

for a finite B .

The eigenproblem for the Hamiltonian (3.1) can be simplified by introducing the center of mass coordinate $\mathbf{R} = (\mathbf{r}_1 + \mathbf{r}_2)/2$ and relative coordinate $\mathbf{r} = \mathbf{r}_1 - \mathbf{r}_2$. Then the wave function can be separated as [60, 102]

$$\Psi_{nD}^{2p}(\mathbf{r}_1, \mathbf{r}_2) = \exp(i\mathbf{Q} \cdot \mathbf{R}/\hbar) \psi_{nD}(\mathbf{r}),$$

where \mathbf{Q} is the total momentum of the two particles. The relative wave function $\psi_{nD}(\mathbf{r})$ is an eigenfunction of the Hamiltonian of the relative motion,

$$H \Psi_{nD}(\mathbf{r}) = E \Psi_{nD}(\mathbf{r}) \quad (3.4)$$

with

$$H = -\frac{\hbar^2}{2\mu} \nabla^2 + V(r), \quad (3.5)$$

where E is the scattering energy and $\mu = m_1 m_2 / (m_1 + m_2)$ is the reduced mass.

3.2.1.2 The *s*-wave scattering and boundary conditions

Due to the spherical symmetry of the potential, Eq. (3.4) can be further simplified by solving the angular coordinate dependent part separately through eigenstates of the angular momentum operator. By definition, *s*-wave scattering correspond to zero angular momentum with a spherically symmetric wave function. The radial coordinate dependence in Eq.(3.4) can be obtained from the following differential equation for the general *n*-dimensional case [66]²

$$-\frac{\hbar^2}{2\mu} \left(\frac{d^2}{dr^2} + \frac{n-1}{r} \frac{d}{dr} \right) \Phi_{nD}(r) + (V(r) - E) \Phi_{nD}(r) = 0, \quad (3.6)$$

where $\Phi_{nD}(r)$ is the radial part of the relative wave function $\psi_{nD}^{rel}(\mathbf{r})$. For ultracold atoms only low-energy scattering processes are relevant and we may set $E = 0$. As we see in the following subsection, it also provides us with a simple way to define the *s*-wave scattering length. Appropriate boundary conditions for the differential equation (3.6) can be obtained from smoothness and symmetry considerations in the limit $r \rightarrow 0$ (see the detailed description in Appendix A), as

$$\Phi_{nD}(0) = 1, \quad \text{and} \quad \Phi'_{nD}(0) = 0. \quad (3.7)$$

3.2.1.3 Scattering length

As we discussed before in the previous chapter for a short-range potential, the asymptotic of the wave function $\Phi_{nD}(r)$ at distances much larger than the characteristic length scale of the potential ℓ_v is given by a solution of Eq. (3.6) with $V(r) = 0$ and $E = 0$, which is a linear combination of a constant and r in 1D (Eq.(2.21)), $\ln(r)$ in 2D (Eq.(2.22)), and $1/r$ in 3D (Eq.(2.23)). The *s*-wave scattering length can be defined by the ratio of the corresponding constants in this

²The radial Schrödinger equation (3.6), and the asymptotic *s*-wave scattering length expressions (3.8)-(3.13), have been written in different forms in Ref. [60]. Using the relation $u(r) = r^{(n-1)/2} \Phi_{nD}(r)$, these expressions can be easily derived from each other.

linear combination [66]:

$$\Phi_{1D}(r) \stackrel{r \gg \ell_v}{\approx} \mathcal{N}_{1D} (r - a_s^{1D}) , \quad (3.8)$$

$$\Phi_{2D}(r) \stackrel{r \gg \ell_v}{\approx} \mathcal{N}_{2D} \left[\ln \left(\frac{2r}{a_s^{2D}} \right) - \gamma \right] , \quad (3.9)$$

$$\Phi_{3D}(r) \stackrel{r \gg \ell_v}{\approx} \mathcal{N}_{3D} \left(1 - \frac{a_s^{3D}}{r} \right) . \quad (3.10)$$

Here a_s^{nD} is the n -dimensional s -wave scattering length, $\gamma = 0.5772\dots$ is the Euler-Mascheroni constant, and \mathcal{N}_{nD} is a scalar factor. The scattering length can be expressed as a limit of the function $\Phi_{nD}(r)$ and its first derivative by eliminating the unknown parameter \mathcal{N}_{nD} [66]³ as

$$a_s^{1D} = \lim_{r \rightarrow \infty} \left(r - \frac{\Phi_{1D}(r)}{\Phi'_{1D}(r)} \right) , \quad (3.11)$$

$$a_s^{2D} = \lim_{r \rightarrow \infty} 2r \exp \left(-\frac{\Phi_{2D}(r)}{r\Phi'_{2D}(r)} - \gamma \right) , \quad (3.12)$$

$$a_s^{3D} = \lim_{r \rightarrow \infty} \left(r - \frac{r\Phi_{3D}(r)}{r\Phi'_{3D}(r) + \Phi_{3D}(r)} \right) . \quad (3.13)$$

As it can be seen from the expressions above, a_s^{2D} is always positive by definition, while a_s^{1D} and a_s^{3D} can be of either sign. In the limiting case where the scattering potential is absent the solution of Eq. (3.6) becomes a zero-energy plane wave, i.e. the constant 1. Therefore, we have $a_s^{1D} \rightarrow \infty$ and $a_s^{2D} \rightarrow \infty$, while $a_s^{3D} \rightarrow 0$. This means that the scattering length develops a singularity when $V(r) \rightarrow 0$ in one and two dimensions.

3.2.2 One and three dimensions

In three dimensions the radial Schrödinger equation can be simplified by introducing the function [66]

$$u_{3D}(r) = r \Phi_{3D}(r) . \quad (3.14)$$

³The definition of a_s^{2D} differs from the original definition of Verhaar *et al.* [119] with an $e^\gamma/2$ factor. The current definition is more common in the recent ultracold atomic literature [22, 67, 120].

Substituting Eq.(3.14) into the radial Schrödinger equation (3.6) and the expression for the s -wave scattering length (3.13), we obtain identical equations for three and one dimensions

$$\left(-\frac{\hbar^2}{2\mu} \frac{d^2}{dr^2} + V(r) - E \right) u_{1D/3D}(r) = 0 , \quad (3.15)$$

$$a_s^{1D/3D} = \lim_{r \rightarrow \infty} \left(r - \frac{u_{1D/3D}(r)}{u'_{1D/3D}(r)} \right) , \quad (3.16)$$

where we have introduced $u_{1D}(r) \equiv \Phi_{1D}(r)$ for compact notation. The boundary conditions are obtained by substituting Eq.(3.14) into Eq.(3.7) and now differ between one and three dimensions:

$$u_{1D}(0) = 1 , \quad u'_{1D}(0) = 0 , \quad (3.17)$$

$$u_{3D}(0) = 0 , \quad u'_{3D}(0) = 1 . \quad (3.18)$$

In a numerical procedure we may assume that the functions $u_{1D/3D}(r)$ and $u'_{1D/3D}(r)$ can only be given with limited numerical accuracy (p) as

$$\begin{aligned} u_{1D/3D}(r) &= \lim_{p \rightarrow \infty} \tilde{u}_{1D/3D}(r; p) , \\ u'_{1D/3D}(r) &= \lim_{p \rightarrow \infty} \tilde{u}'_{1D/3D}(r; p) , \end{aligned}$$

where p relates to the accuracy of the decimal representation and the numerical method itself. For the numerical determination of the scattering length one should then consider the combined limit

$$\begin{aligned} a_s^{1D/3D} &= \lim_{r, p \rightarrow \infty} \tilde{a}_s^{1D/3D}(r; p) , \\ \tilde{a}_s^{1D/3D}(r; p) &= r - \frac{\tilde{u}_{1D/3D}(r; p)}{\tilde{u}'_{1D/3D}(r; p)} . \end{aligned}$$

3.2.3 Two dimensions

In two dimensions the original radial function $\Phi_{2D}(r)$ is used directly. Here a numerical instability is present as a result of the $1/r$ singularity in the first derivative term of the radial Schrödinger equation (3.6) for two dimensions. The

instability can be avoided by giving the boundary conditions at distance $r = \epsilon$, where ϵ is chosen large enough to avoid the numerical difficulties but small enough to approximately satisfy the conditions of Eq. (3.7)

$$\Phi_{2D}(\epsilon) \approx 1, \quad \Phi'_{2D}(\epsilon) \approx 0. \quad (3.19)$$

Consequently, ϵ becomes another parameter of the numerical evaluation besides the numerical accuracy (p). The scattering length is then obtained from the composite limit

$$a_s^{2D} = \lim_{\substack{r, p \rightarrow \infty \\ \epsilon \rightarrow 0}} \underbrace{2r \exp\left(-\frac{\tilde{\Phi}_{2D}(r; \epsilon, p)}{r \tilde{\Phi}'_{2D}(r; \epsilon, p)} - \gamma\right)}_{\tilde{a}_s^{2D}(r; \epsilon, p)}, \quad (3.20)$$

where $\tilde{\Phi}_{2D}(r; \epsilon, p)$ represents the approximate numerical solution of Eqs.(3.6) and (3.19) with

$$\Phi_{2D}(r) = \lim_{\substack{p \rightarrow \infty \\ \epsilon \rightarrow 0}} \tilde{\Phi}_{2D}(r; \epsilon, p). \quad (3.21)$$

3.2.4 The Gaussian potential and the convergence of numerical results

We now apply this approach to the Gaussian potential

$$V(r) = -\frac{V_0}{2L^2} e^{-\frac{r^2}{L^2}}, \quad (3.22)$$

which depends on parameters for the potential strength V_0 and the length scale L . Since we are free to use L as a scale parameter, we find that the ratio a_s/L depends only on the single dimensionless parameter $V_0\mu/\hbar^2$. The results of the numerical calculations and their physical interpretation will be discussed in Sec. 3.3 along with analytic approximations. Here we discuss the details and convergence properties of the numerical approach.

The numerical calculations are performed with the fourth order Runge-Kutta method of Mathematica [121], where the differential equation is represented on

the usual discretized timesteps. The parameter p is considered here as a composite variable. We set the parameters 'AccuracyGoal' and the 'PrecisionGoal', which quantify the accuracy and precision of the numerical method, respectively, to the same number p , which provides at least 10^{-p} numerical accuracy. The 'WorkingPrecision', which controls the number of the digits in the calculations, is set to $p + 5$ to reduce the error from the finite numerical representation. Ideally, we should consider the infinite limit of p and r , and the zero limit of ϵ . On the computer this limit is considered numerically with a finite accuracy. The accuracy of the calculation are checked with rectangular potential, where analytic solutions are available. We found excellent agreement between the analytical and number calculations for this example.

The convergence properties of the numerical procedure for the Gaussian potential can be seen from Figs. 3.1 and 3.2 for the s -wave scattering length of the Gaussian potential in two and three dimensions, respectively. First, the accurate reference values were calculated by setting $p = 11$, $r = 10L$ and $\epsilon = 10^{-6}L$, which are given in Tables 3.1 and 3.2. Then the relative error of the scattering length compared to the reference value is plotted as a function of the accuracy parameters.

In all cases the relative error decays exponentially until the reference value of the accuracy parameter is reached. At that point, due to the equality of $\tilde{a}_s^{nD} = a_s^{nD}$, the curves abruptly drop to zero. Beyond that point the relative error saturates to a constant value that corresponds to the numerical error of the reference value of the scattering length. In two dimensions (Fig. 3.1) the largest errors occur at $V_0 = 0.002\hbar^2/\mu$ and $V_0 = 11\hbar^2/\mu$, close to divergences of the scattering length (see Fig. 3.5). This demonstrates that a larger numerical effort is required to obtain the same numerical accuracy around the divergences of the scattering length.

In three dimensions the s -wave scattering length diverges near to $V_0 = 2.683\hbar^2/\mu$, where the largest errors in are seen in panel (a) of Fig. 3.2. This singularity corresponds to the appearance of the weakly bound state, where the bound state

$V_0 (\hbar^2/\mu)$	-10	0.002	5	11
$a_s^{2D} (L)$	1.052775727581175	$2.087502897416 \cdot 10^{434}$	1.189350613760202	$1.1340580605359 \cdot 10^{-19}$

TABLE 3.1: Reference values for a_s^{2D} computed with parameters $p = 11$, $r = 10L$, and $\epsilon = 10^{-6}L$ at different V_0 values.

$V_0 (\hbar^2/\mu)$	-10	2.683	5	14
$a_s^{3D} (L)$	1.06471218669307	2992.059356340681	2.25126701647514	0.04887055637493

TABLE 3.2: Reference values for a_s^{3D} computed with parameters $p = 11$ and $r = 10L$ at different V_0 values.

energy, E_b , can be expressed approximately with the s -wave scattering length,

$$E_b = \frac{1}{ma_s^{3D}}.$$

Theoretically, the obtained energy could be compared with the bound-state energy calculated with the exact diagonalization approach, where the function $u_{\text{mathrm}3D}(r)$ is expanded in a finite basis-set. For the accurate description of the weakly bound state, those basis functions have to be considered, which are able to describe both the bounded and unbounded states. The plane-wave basis functions in a rectangular box with periodic boundary condition seem a natural choice. Though in order to eliminate all numerical artifacts two extrapolations are required, one for the infinite basis-set limit and one for the infinite box size limit. These calculations lie outside the scope of this project. Due to the double extrapolations they would most probably suffer from larger numerical inaccuracies than the differential equation solver.

In Fig. 3.2 the case of $V_0 = 14\hbar^2/\mu$ has the second largest numerical error. In that case the scattering length is close to the zero-crossing ($a_s^{3D} \approx 0.05L$). It is difficult to compute it accurately from Eq.(3.16) where a difference of small numbers needs to be taken. This effect is even more notable as a function of the cut-off distance in panel (b) in Fig. 3.2, where the error in the case of $V_0 = 14\hbar^2/\mu$ is at least one order larger at larger distances compared to other values of the potential strength. Numerical rounding errors also explain the jumps in the cases of $V_0 = -10\hbar^2/\mu$ and $V_0 = 5\hbar^2/\mu$, which are the limit of the chosen accuracy.

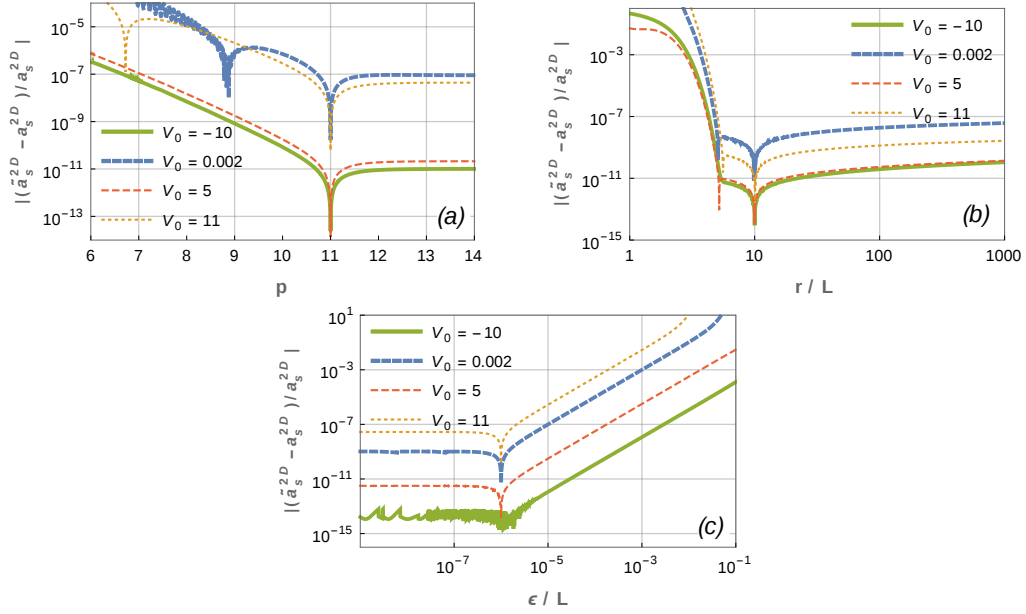


FIGURE 3.1: Relative error in the two-dimensional s -wave scattering length as a function of the numerical precision p in panel (a), on the cut-off distance r in panel (b) and the boundary parameter ϵ in panel (c) for different values of the potential strength V_0 in \hbar^2/μ unit. The reference values a_s^{2D} are computed with parameters $p = 11$, $r = 10L$ and $\epsilon = 10^{-6}L$. The numerical values of a_s^{2D} can be found in Table 3.1.

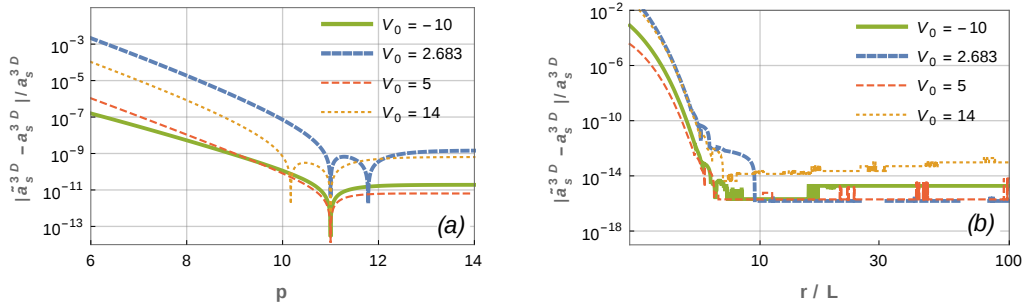


FIGURE 3.2: Relative error in the three-dimensional s -wave scattering length as a function of the numerical precision p in panel (a) and on the cut-off distance r in panel (b) for different values of the potential strength V_0 in \hbar^2/μ unit. The reference value a_s^{3D} computed with parameters $p = 11$ and $r = 10L$. The numerical values of a_s^{3D} can be found in Table 3.2.

3.3 Approximate expressions for Gaussian potential

3.3.1 Three-dimensional case

As it can be seen in the previous section, the numerical approach is accurate in most cases but fails near the divergences of the scattering length. Here we derive analytic approximations that can handle these numerically unstable regions. An alternative derivation based on the Lippmann-Schwinger equation is given in Appendix (C).

In order to derive suitable approximations we can make use of the fact that the Gaussian potential decays rapidly to zero with increasing distance. Therefore, contributions of the long range part of the wave function become negligible, when they are multiplied by this potential. Considering the simplest case of three dimensions, $u_{3D}(r)$ can be approximated in the whole domain $[0, \infty)$ with the first non-zero term of the Taylor expansion around $r = 0$, when it is multiplied by the Gaussian potential (3.22) as

$$e^{-\frac{r^2}{L^2}} u_{3D}(r) \approx e^{-\frac{r^2}{L^2}} r . \quad (3.23)$$

Substituting Eq.(3.23) into Eq.(3.15) at $E_{rel} = 0$, we can obtain the differential equation

$$-\frac{\hbar^2}{2\mu} \frac{d^2}{dr^2} \bar{u}_{3D}(r) - \frac{V_0}{2L^2} e^{-\frac{r^2}{L^2}} r = 0 . \quad (3.24)$$

The function $\bar{u}_{3D}(r)$ can be obtained by integrating Eq.(3.24) twice

$$\bar{u}_{3D}(r) = c_1^{3D} + c_2^{3D} r + \frac{\sqrt{\pi} V_0 \mu}{4\hbar^2} \operatorname{erf}\left(\frac{r}{L}\right) , \quad (3.25)$$

where $\operatorname{erf}(x) = (2/\sqrt{\pi}) \int_0^x \exp(-t^2) dt$ is the error function. The coefficients in Eq.(3.25) can be determined by considering the boundary conditions (3.18) as

$$c_1^{3D} = 0 , \quad c_2^{3D} = \frac{2 - \frac{V_0 \mu}{\hbar^2}}{2L} .$$

Examining these wave functions in the limit when r goes to infinity and using the fact that $\lim_{r \rightarrow \infty} \operatorname{erf}\left(\frac{r}{L}\right) = 1$, if L is finite, we obtained the following asymptotic expression:

$$\bar{u}_{3D}(r) \approx \frac{2 - \frac{V_0 \mu}{\hbar^2}}{2} \left(\frac{r}{L} - \frac{\sqrt{\pi}}{2} \frac{V_0}{V_0 - \frac{2\hbar^2}{\mu}} \right), \quad r \rightarrow \infty. \quad (3.26)$$

Substituting Eq.(3.26) into Eq.(3.16), the approximate relations between the s -wave scattering length and the parameters of the potential can be found as

$$\frac{\bar{a}_s^{3D}}{L} = \frac{\sqrt{\pi}}{2} \frac{V_0}{V_0 - \frac{2\hbar^2}{\mu}}. \quad (3.27)$$

This approximate formula has a pole near the value of V_0 where the Gaussian potential well acquires the first bound state. It qualitatively describes the scattering length near the singularity, but the position of the pole is inaccurate.

As can be seen in Fig. (3.3), further singularities appear when the potential well becomes deeper and these correspond to additional bound states. Although the approximation (3.27) includes only the first singularity, it can be sufficient for the use as a pseudopotential for ultracold atoms if only the qualitative behaviour of the scattering length in the presence of up to one bound state is of interest. In order to reproduce the behaviour of the scattering length across a larger range of potential lengths, we generalize Eq.(3.27) by explicitly introducing a variable number of singularities in the following way:

$$\frac{a_s^{3D}}{L} \approx \sum_{i=1}^n \alpha_i \frac{V_0}{(V_0 - W_i)}. \quad (3.28)$$

Here, W_i and α_i are numerically determined parameters.

The parameters W_i are set to the values of V_0 where the numerically determined scattering length diverges (and changes sign). At these values of V_0 weakly bound states appear (see, e.g., Ref. [122], problem 90). For achieving a high accuracy for approximations of the s -wave scattering length it is important to use accurate values for these parameters (see the detailed description in Appendix B).

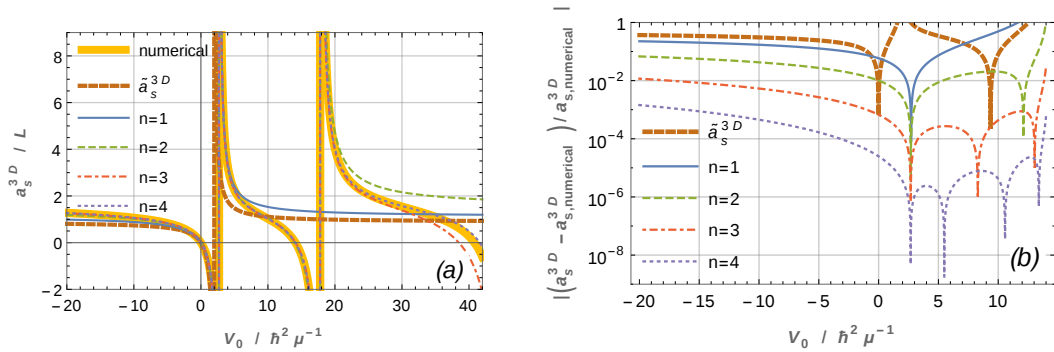


FIGURE 3.3: Panel (a): Three-dimensional s -wave scattering length from the numerical and the approximate expression. Panel (b): The difference between the approximative and numerical scattering length values. The parameters of the numerical simulations are set to $p = 11$ and $r = 10L$. The values of the parameters for the approximative expressions can be found in Table 3.3 and few examples for the numerical values of the s -wave scattering length can be found in Table 3.4.

n	$W_n (\hbar^2/\mu)$	α_1	α_2	α_3	α_4
1	2.68400465092	1.11942413969			
2	17.7956995472	1.12031910105	0.378402820446		
3	45.5734799205	1.12034867267	0.322141242778	0.332600792963	
4	85.9634003809	1.12034897387	0.326461774698	0.135560767226	0.375312300726
\bar{a}_s^{3D}	2	$\sqrt{\pi}/2 \approx 0.8862269$			

TABLE 3.3: Numerical values of parameters for the three-dimensional approximate expression (3.28). The parameters of the analytically approximated scattering length, \bar{a}_s^{3D} , is determined from Eq.(3.27) using the ansatz $\bar{a}_s^{3D}/L = \alpha_1 V_0 / (V_0 - W_1)$.

The parameters α_i are obtained by non-linear fitting of the approximate expression Eq.(3.28) to the numerically obtained scattering length. The fitting procedure is performed on the intervals $V_0 \mu / \hbar^2 \in [0, 2.68] \cup [2.69, 14]$ in order to avoid the singularities. The values of the fitted parameters are shown in Table 3.3. As it can be seen in Fig. 3.3, including even one additional singularity in the model greatly improves upon Eq.(3.27) and qualitatively describes the fitted region. Each additional fitting parameter further improves the relative accuracy by more than one order of magnitude. In addition, the approximate formulas also dramatically improve the approximation of a_s^{3D} outside the fitted regime with each fitting parameter.

$V_0/\hbar^2\mu^{-1}$	numerical	\tilde{a}_s^{3D}	n			
			1	2	3	4
0.1	-0.0459382	-0.0466435	-0.0433213	-0.0454943	-0.0459089	-0.0459372
1.0	-0.6921927	-0.886227	-0.664739	-0.687801	-0.6919302	-0.6921844
2.68	-749.84048	3.49278	-749.143	-749.809	-749.83974	-749.84047
5	2.2512670	1.47704	2.41672	2.27079	2.2518534	2.2512698
10	1.0250876	1.10778	1.53011	1.04593	1.0246425	1.0250833

TABLE 3.4: Examples for the numerical values of the three-dimensional s -wave scattering length in the units of L from Fig. 3.3.

3.3.2 One-dimensional case

We follow an analogous procedure for the three-dimensional case by approximately solving the Schrödinger equation for large r . Although the form of the one-dimensional Schrödinger equation is equivalent to the three-dimensional one [Eq.(3.15)], the boundary conditions of Eqs.(3.17) and (3.18) differ. This has the consequence that the zeroth order term in the Taylor expansion of $u_{1D}(r)$ does not vanish and thus we may approximate the differential equation as

$$-\frac{\hbar^2}{2\mu} \frac{d^2}{dr^2} \bar{u}_{1D}(r) - \frac{V_0}{2L^2} e^{-\frac{r^2}{L^2}} = 0 . \quad (3.29)$$

Equation (3.29) can be solved and provides the following approximate expression for the wave function and the s -wave scattering length:

$$\bar{u}_{1D}(r) = 1 - \frac{V_0\mu}{2\hbar^2} \left[e^{-\frac{r^2}{L^2}} + \sqrt{\pi} \operatorname{erf}\left(\frac{r}{L}\right) \frac{r}{L} - 1 \right] , \quad (3.30)$$

$$\frac{\bar{a}_s^{1D}}{L} = \frac{1}{\sqrt{\pi}} + \frac{2}{\sqrt{\pi}} \frac{\hbar^2}{V_0\mu} . \quad (3.31)$$

Comparing the obtained expression (3.31) with the three-dimensional result (3.27), it can be seen that the first singularity in one dimension is located in the origin, while in three dimensions it is displaced to a finite value of attractive potential strength. As every singularity indicates the creation of a new bound state, the former statement is related to a well-known property: in one dimension there is always a bound-state at any non-zero attractive potential, meanwhile in three dimensions the bound state appears at some finite potential strength.

The approximate expression (3.31) can be further improved if we expand function $u_{1D}(r)$ in a Taylor-series around the origin. As we are interested in the behavior of the singularity in the origin, we can consider the limit of V_0 approaching zero, where the coefficients of the Taylor expansion can be determined (see the detailed description in Appendix D). Examining the asymptotic properties of the wave function we obtain the following approximate formula for the scattering length:

$$\frac{\bar{a}_s^{1D}}{L} = \sqrt{\frac{2}{\pi}} + \frac{2}{\sqrt{\pi}} \frac{\hbar^2}{V_0 \mu}, \quad (3.32)$$

which differs from Eq.(3.31) only in the constant offset. This new expression fits better with the numerically obtained results, but it is still inaccurate at larger absolute values of the potential strength. In analogy to the three dimensional case [Eq.(3.28)], the accuracy of Eq.(3.32) can be further improved by including additional singularities

$$\frac{a_s^{1D}}{L} \approx \sqrt{\frac{2}{\pi}} + \frac{2}{\sqrt{\pi}} \frac{\hbar^2}{V_0 \mu} + \sum_{i=1}^n \alpha_i \frac{V_0}{(V_0 - W_i)}, \quad (3.33)$$

where the parameters W_i are obtained directly from the numerical solution of the differential equation and the parameters α_i are non-linearly fitted to the numerical values in the interval $[1, 8]\hbar^2/\mu$.

A comparison of the approximate and the numerical results is shown in Fig. 3.4. Similarly to the three dimensional case the relative error from the numerical solution gradually decreases with the number of the parameter pairs.

n	$W_n (\hbar^2/\mu)$	α_1	α_2	α_3	α_4
1	8.6490975	0.52689372			
2	30.106280	0.51419392	0.35899733		
3	64.193333	0.51460375	0.20675606	0.36766012	
4	110.88204	0.51459468	0.24033314	0.040512694	0.44420188

TABLE 3.5: Numerically determined parameters for the one-dimensional approximate expression in Eq.(3.39).

$V_0/\hbar^2\mu^{-1}$	numerical					
	0	1	2	3	4	
0.01	113.635079	113.63580	113.6351822	113.635085	113.635080	113.635079
1	1.84604750	1.9262637	1.856341600	1.84647555	1.84605596	1.84604759
3	0.85979335	1.1740109	0.889979118	0.86048843	0.85979610	0.85979330
5	0.24620007	1.0235603	0.290720055	0.24629609	0.24619224	0.24620007
8.64	-487.928498	0.9284840	-507.016304	-487.36624	-487.94067	-487.9285495

TABLE 3.6: Examples for the numerical values of the one-dimensional s -wave scattering length in the units of L from Fig. 3.4.

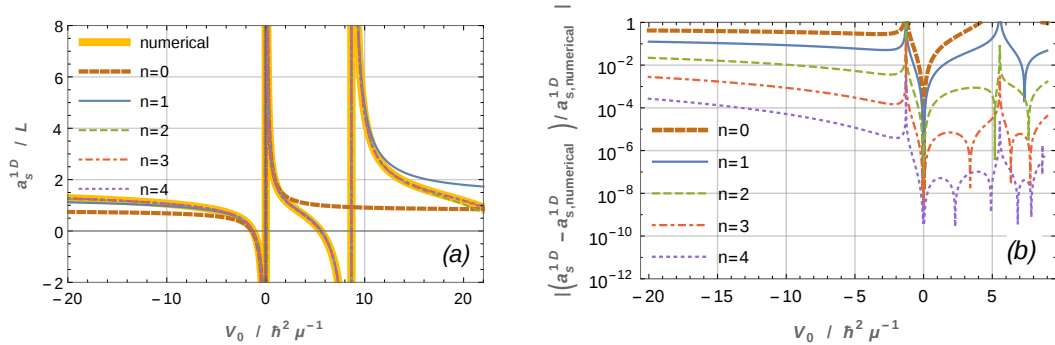


FIGURE 3.4: Panel (a): One-dimensional s -wave scattering length from the numerical and the approximate expression. Panel (b): The difference between the approximate and numerical values of the scattering length. The parameters of the numerical simulations are set to $p = 11$, $r = 10L$. The parameter values for the approximate expressions are tabulated in Table 3.5. The $n = 0$ approximation corresponds to Eq. (3.32). Examples for the numerical values of the s -wave scattering length can be found in Table 3.6.

3.3.3 Two-dimensional case

In two dimensions the function $\Phi_{2D}(r)$ is considered, where the corresponding Schrödinger equation (3.6) at $E_{rel} = 0$ and boundary conditions (3.7) provide the following approximate differential equation:

$$-\frac{\hbar^2}{2\mu} \left(\frac{d^2}{dr^2} + \frac{1}{r} \frac{d}{dr} \right) \bar{\Phi}_{2D}(r) + V(r) = 0. \quad (3.34)$$

Solving Eq.(3.34) the radial function can be obtained as:

$$\bar{\Phi}_{2D}(r) = 1 + \frac{V_0}{4} [\text{Ei}(-r^2) - \gamma - 2\ln(r)], \quad (3.35)$$

where $\text{Ei}(x) = -\int_{-x}^{\infty} \frac{e^{-t}}{t} dt$ is the exponential integral function. At large particle separation the exponential integral function goes to zero, $\lim_{r \rightarrow \infty} \text{Ei}(-r^2) = 0$,

therefore Eq.(3.35) can be approximated with the following expression:

$$\bar{\Phi}_{2D}(r) \approx 1 - \frac{V_0\mu}{4\hbar^2} \left[\gamma + 2 \ln \left(\frac{r}{L} \right) \right], \quad r \rightarrow \infty. \quad (3.36)$$

Using this asymptotic formula, the approximate expression of the s -wave scattering length can be determined from Eq.(3.12) as

$$\frac{\bar{a}_s^{2D}}{L} = 2e^{-\frac{3\gamma}{2} + \frac{2\hbar^2}{V_0\mu}}. \quad (3.37)$$

A singularity appears again in the origin, like in the one-dimensional case, as a consequence of the fact that any arbitrarily weak Gaussian potential well in two dimensions has at least one bound state. In analogy to the procedure of Appendix D in one dimension we can thus determine an improved prefactor to arrive at the approximation

$$\frac{\bar{\bar{a}}_s^{2D}}{L} = \sqrt{8}e^{-\frac{3\gamma}{2} + \frac{2\hbar^2}{V_0\mu}}. \quad (3.38)$$

This approximate formula (3.38) is equivalent to the previously mentioned formula of Doganov *et al.* [103], where Eq.(3.38) was derived in a different manner using perturbation theory. This expression is not very accurate at larger values of potential strength and can be improved by including additional singularities in the same manner as done previously to obtain

$$\frac{a_s^{2D}}{L} \approx \sqrt{8}e^{-\frac{3\gamma}{2} + \frac{2\hbar^2}{V_0\mu} + \sum_{i=1}^n \alpha_i \frac{V_0}{(V_0 - W_i)}}. \quad (3.39)$$

We determined the parameters W_i with the numerical differential equation solver and fitted the parameters α_i on the interval $V_0 \in [1, 10]\hbar^2/\mu$.

The numerical and approximate values for the two-dimensional s -wave scattering length are shown in Fig. 3.5. In contrast to the one- and three-dimensional results, the two-dimensional scattering length is always positive and single poles occur not in the scattering length itself but in its logarithm. Similarly to the previous cases, increasing the number of fitted parameter pairs successively improves the approximate values for the scattering length in and outside the fitted region.

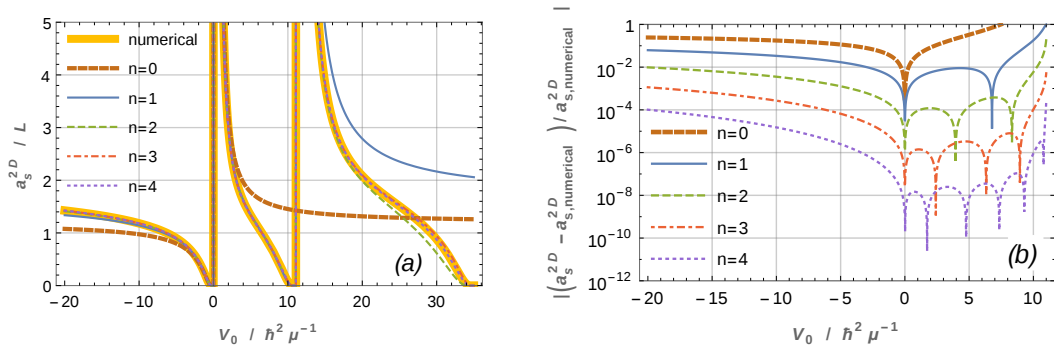


FIGURE 3.5: Panel (a): Two-dimensional s -wave scattering length from the numerical and the approximate expression. Panel (b): The difference between the approximative and numerical scattering length values. The parameters of the numerical simulations are set to the followings: $p = 11$, $r = 10L$, and $\epsilon = 10^{-6}L$. The values of the parameters for the approximative expressions can be found in Table 3.7. The $n = 0$ approximation corresponds to Eq. (3.38). Few examples for the numerical values of the the s -wave scattering length can be found in Table 3.8.

n	$W_n(\hbar^2/\mu)$	α_1	α_2	α_3	α_4
1	11.076903	0.33553384			
2	35.081301	0.30476380	0.20423041		
3	71.774188	0.30609585	0.10986740	0.19295017	
4	121.10485	0.30605919	0.13171195	0.017845686	0.22077743

TABLE 3.7: Numerically determined parameters for the two-dimensional approximate expression in Eq.(3.39).

$V_0/\hbar^2\mu^{-1}$	numerical	n				
		0	1	2	3	4
0.3	925.454378	935.016279	926.323551	925.485608	925.455029	925.454387
1	8.47880838	8.79248407	8.50453845	8.47958092	8.47882030	8.47880849
4	1.60859601	1.96186838	1.62295275	1.60858611	1.60859142	1.60859598
8	0.651404324	1.52790463	0.63858761	0.65127400	0.65140946	0.65140429
10.5	0.005060049	1.43961176	0.00320657	0.00514485	0.00505813	0.00506007

TABLE 3.8: Few examples for the numerical values of the two-dimensional s -wave scattering length in the units of L from Fig. 3.5.

3.4 Conclusion

We have introduced new approximate expressions for the s -wave scattering length for a Gaussian potential in one, two and three dimensions. These may be useful on their own or can improve the accuracy of a numerical determination of the scattering length by providing the correct asymptotic behaviour near singularities. The lowest level expressions can be obtained as simple parameter-free approximations derived from the two-particle Schrödinger equation. They can

qualitatively describe the singularity at the first bound state formation, where numerical methods usually fail or provide inaccurate answers. In one and two dimensions these expressions can be further improved analytically by examining the weakly interacting limit, where the leading terms can be given exactly. More accurate expressions generalize the simple formulas in a straight-forward way by including additional singularities, where the unknown parameters are determined from accurate numerical computations. The obtained formulae improve the accuracy for the whole region of the potential strength. In three dimensions where the singularity due to the appearance of the first bound state appears at a finite value of the potential strength, the accuracy of this value crucially limits the obtainable accuracy for the *s*-wave scattering length.

The Gaussian potential well has its main application for use as a pseudopotential in the description of ultra-cold atoms in the parameter regime between zero interaction and the first non-trivial bound state. In this region the relative error of the parameterized approximate formulas reach below 10^{-4} and thus provide accurate, reliable, and simple formulae to connect the parameters of the Gaussian potential to the *s*-wave scattering length.

Chapter 4

Are smooth pseudopotentials a good choice for representing short-range interactions?

4.1 Introduction

There is increasing interest in the theoretical description of multi-particle systems of interacting ultracold atoms thanks to the recent progress in experimental realizations [23, 24, 28, 123, 124]. In particular we may expect exciting developments in microtraps [25, 29, 125] with tens of particles where accessing strongly-correlated regimes of quantum-Hall-like physics seems feasible [30, 31, 126, 127].

The theoretical description of atom-atom interactions is significantly simplified at ultracold temperatures where details of the interaction potentials can be neglected in favor of a single constant, the s -wave scattering length a_s , to define a physical model with contact interactions [17]. Despite these simplifications, the complexity of many-particle quantum mechanics still makes it a very difficult problem to solve, where exact solutions are only available in special cases in one spatial dimension [33–35, 38, 69] or for up to three particles in a harmonic trap [70, 74, 75].

A straightforward and general approach to representing the many-body problem for computational treatment is to introduce a discrete and necessarily finite basis

of smooth single-particle wave functions from which a finite but still potentially very large Fock-space is constructed to represent the many-body Hamiltonian as a matrix. Finding eigenstates and eigenvalues of the full matrix is known as exact diagonalization or full configuration-interaction [71, 72, 128–131], but many different approximation schemes have also been followed [132]. In particular, standard approaches of *ab initio* quantum chemistry or nuclear physics like the coupled-cluster [47] or multi-configurational self-consistent field theory [133] all can be formulated in this language as they rely on an underlying single-particle basis. Also Monte-Carlo (or other) approaches that rely on a lattice discretization of continuous space fall into the same category [134], as the underlying single-particle space can be represented as a discrete set of plane waves.

One of the complications in the numerical treatment of contact interactions with basis set expansions stems from the non-analytic behavior of the wave function at the point of particle coalescence. At this point, the appropriate Bethe-Peierls boundary conditions demand a cusp in one spatial dimension, i.e. a point of non-differentiability [33], in two dimensions a logarithmic divergence, and in three dimension a $1/r$ divergence of the wave function [65, 68, 73]. While in one dimension a Dirac- δ function pseudopotential provides a well-defined model for contact interactions, the convergence of basis set expansions is algebraic and painfully slow [47, 135]. Basis set expansions in two and three dimensions diverge for bare contact interaction [76, 77, 103] and basis-set-dependent renormalization procedures have to be used in order to obtain convergent and correct results [77, 82–84]. In the best case, renormalized contact interactions will lead to algebraic convergence in the size of the finite single-particle basis set [73, 134, 135].

Here, we consider a different approach where the contact interaction is replaced by a smooth finite-range pseudopotential. This has the advantage that basis set expansions will converge exponentially for appropriately chosen single-particle basis functions [89]. Specifically we will consider what the requirements are for the basis set to reach the regime of exponential convergence and whether this approach is feasible for multi-particle simulations. Examples of finite-range pseudopotentials used in the literature are the Troullier-Martins [85, 104], Pöschl-Teller [86, 105],

and Gaussian potentials [87, 103, 106–111, 136–138], in addition to the square well popular in diffusion Monte Carlo simulations[87].

When using finite range pseudopotentials to represent short-range interactions, an interpolation in the width of the pseudopotential should be done to the zero-range limit [81]. In order to approach this limit, the length scale of the pseudopotential should be significantly smaller than other physically relevant length scales of the problem, in particular the mean particle separation and length scales imposed by external potentials. In order to reach a regime where the basis set expansion converges exponentially, however, the basis set needs to resolve the smallest length scale of the pseudopotential. At the same time, the large length scales of the problem, i.e. the (Thomas-Fermi) size of the cold atom cloud, or size of the container, also have to be represented by the basis set. This hierarchy of length scales, typically spanning at least one but possibly several orders of magnitude presents a challenge for accurate numerical simulations. While the size of the single-particle basis (quantified by the number of single-particle functions M) is determined by this hierarchy of length scales, the size of the full many-body problem also depends strongly on the number of particles N . Specifically for spinless bosons, the size of the relevant part of Fock space is $\binom{N+M-1}{M}$, whereas for spin- $\frac{1}{2}$ fermions the total dimension is $\binom{M}{N_\uparrow}\binom{M}{N_\downarrow}$, where N_\uparrow and N_\downarrow are the number of up- and down-spin particles, respectively.

In this work, we specifically consider ultra-cold fermionic atoms in a harmonic oscillator trapping potential where the potential in one of the three trapping directions is so tight that the problem can be considered two-dimensional. We furthermore choose a Gaussian pseudopotential to model attractive s -wave interactions between spin-up and spin-down particles [139]. For the underlying single-particle basis we consider two cases:

- (a) a basis that is defined by the single-particle eigenstates of the isotropic two-dimensional harmonic trapping potential
- (b) the same set of basis functions with scaled spatial coordinates by a scaling factor γ

Using the known properties of the harmonic oscillator eigenfunctions we show that the basis set size M required to resolve the chosen length scale of the pseudopotential l_{res} scales as $(l/l_{\text{res}})^4$ where $l = \sqrt{\hbar/m\omega}$ is the harmonic oscillator length scale of the trapping potential for case (a). The typical value of (l/l_{res}) has been examined in three-dimensions for the unitary regime with a diffusion Monte-Carlo approach [87]. The zero-range limit can be achieved by choosing (l/l_{res}) about $10^{-3} - 10^{-4}$, which is also consistent with the rate of the length-scale of the physical atomic interaction potential and the typical length-scale of the trap [17].

Allowing the basis functions to be scaled by γ as in case (b) leads to an improved scaling of $(l/l_{\text{res}})^2$ while still faithfully resolving the small length scale l_{res} and a fixed large length scale that is determined by the particle-number and interaction strength. We provide estimates for these length scales and the required scaling parameters. Numerical examples show the convergence of the ground state energy for three fermions obtained by exact diagonalization with single-particle basis sets of up to 231 Fock-Darwin orbitals. In order to compute the matrix elements four dimensional integrals have to be calculated. The number of integrals to be computed scales with the fourth power of the number of the basis functions. In order to reduce the numerical effort of the integral calculations, a careful algorithm based on recursion formulas was developed, which is described in Appendix F.

This chapter is organized as follows: After defining the Hamiltonian in Sec. 4.2 and introducing the methodology in Sec. 4.3, we discuss the main results of the chapter in Sec. 4.4. Examples for the numerical convergence with a harmonic oscillator basis are presented in Sec. 4.4.1 before deriving analytical formulas for the required minimum basis set size in Sec. 4.4.2 for the unscaled and in Sec. 4.4.3 for a scaled harmonic oscillator basis. The required scaling factor is estimated in Sec. 4.4.4 where also numerical results for the scaled basis are presented. Implications of our findings for the feasibility of accurate computations of larger multi-particle problems are discussed in Sec. 4.5. Two appendices define the Fock-Darwin orbital basis used (App. E) and detail the explicit formulas and the algorithm used to compute the matrix elements (App. F).

4.2 Hamiltonian

We consider ultracold fermions in a two-dimensional harmonic trap,

$$H = H_{\text{osc}} + \sum_i^{N_\uparrow} \sum_j^{N_\downarrow} V(\mathbf{r}_{i\uparrow}, \mathbf{r}_{j\downarrow}), \quad (4.1)$$

$$H_{\text{osc}} = \sum_\sigma \sum_i^{N_\sigma} \left(-\frac{\hbar^2}{2m} \nabla_{i\sigma}^2 + \frac{m\omega^2}{2} r_{i\sigma}^2 \right), \quad (4.2)$$

where m is the mass of the fermions, ω is the harmonic oscillator strength, $r_{i\sigma}$ is the position of the i -th particle with the spin σ and $V(\mathbf{r}_{i\uparrow}, \mathbf{r}_{j\downarrow})$ is the interaction potential between the fermions. Dividing the operator H_{osc} with $\hbar\omega$, Eq.(4.2) takes the form

$$\frac{H_{\text{osc}}}{\hbar\omega} = \sum_\sigma \sum_i^{N_\sigma} \left(-\frac{l^2}{2} \nabla_{i\sigma}^2 + \frac{1}{2l^2} r_{i\sigma}^2 \right),$$

where $l = \sqrt{\frac{\hbar}{m\omega}}$ is the harmonic oscillator length scale of the trapping potential. The interaction between the particles is described with a Gaussian pseudopotential

$$V(\mathbf{r}_{i\uparrow}, \mathbf{r}_{j\downarrow}) = -\frac{V_0}{R^2} e^{-\frac{(\mathbf{r}_{i\uparrow} - \mathbf{r}_{j\downarrow})^2}{R^2}}. \quad (4.3)$$

The parameters V_0 (given in units of $\hbar\omega$) and R (given in the units of l) control the strength and width of the interaction potential, respectively. These parameters can be converted to the s -wave scattering length with approximate formulas or by direct numerical computation as is discussed in detail in Ref. [139].

4.3 Basis set expansion

For our numerical approach, we compute the ground state energy of a multiple fermion system following the exact diagonalization approach. Starting from a finite single-particle basis of size M (i.e. with M spin-orbitals), the multi-particle

wave function is expanded as a linear combination

$$|\Psi\rangle = \sum_{\underline{n}} C_{\underline{n}} |\Phi_{\underline{n}}\rangle, \quad (4.4)$$

of states in the Fock basis

$$|\Phi_{\underline{n}}\rangle = \prod_{i=1}^M (\hat{c}_i^\dagger)^{n_i} |\text{vac}\rangle, \quad (4.5)$$

where $\underline{n} = (n_1, \dots, n_i, \dots, n_M)$ and n_i is the occupation number of the n -th single-particle basis function (spin-orbital). The fermionic Fock states $|\Phi_{\underline{n}}\rangle$ (often referred to as Slater determinants) are constructed from the complete set of index vectors \underline{n} for fixed particle number N , with

$$N = \sum_{i=1}^M n_i. \quad (4.6)$$

The exact diagonalization approach (also referred to as full configuration interaction) refers to considering the multi-particle Hamiltonian (4.1) with the chosen particle-number content projected onto the basis of states (4.5) as a matrix and finding its eigenvalues and eigenvectors.

In this chapter we use a single-particle basis constructed from the spinful eigenstates of the two-dimensional harmonic oscillator (4.2). The explicit form of the basis functions used in the numerical procedure and the determination of the corresponding matrix elements are discussed in details in Appendices E and F.

For the numerical procedure we determine the ground state energy with a matrix-free approach: Using a variant of the power method [93], we iteratively rotate an initial state onto the ground state vector without having to construct the matrix explicitly.

4.4 Resolving the Gaussian pseudopotential

4.4.1 Unscaled harmonic oscillator basis

Figure 4.1 shows the ground state energy of three interacting fermions (two spin-up and one spin-down) according to the Hamiltonian (4.1) after full diagonalization with a finite Fock basis. We are using the Fock-Darwin form (E.1) of the (unscaled) harmonic oscillator eigenfunctions of the single-particle Hamiltonian (4.2) up to shell $n = 20$, which yields up to $M = 231$ single-particle basis functions. The maximum dimension of the Hilbert space for the three fermions in the zero total angular momentum slot is approximately 1.6×10^5 , which already requires significant computational resources for deterministic diagonalization.

For panels (a) and (b) in Fig. 4.1, the converged regime can be visibly reached. The expected exponential convergence can be recognized from the insets, where the energies at the infinite basis-set limit are determined by a non-linear fit of the last three data points. In these cases, the width of the pseudopotential $R \approx l$ is close to the length scale of the trapping potential. Since the mean particle separation in the harmonic trap will also be of the same order l , or even smaller, this pseudopotential does not provide a useful approximation for the zero-range contact interactions that are relevant for modeling experiments with ultra-cold neutral atoms.

In the panels (c) and (d), R is about one-third and one-tenth of l respectively, where achieving the converged regime is not possible with the considered basis states. Although the convergence seems exponentially fast, the energies are strongly affected by the errors of finite-basis expansion. As will be seen in Sec. 4.4.3, for $R = 0.3l$ the exact energies can be determined ($E_c \approx -62.38\hbar\omega$), which is significantly different from the energy, which is obtained from the results of panel (c) in Fig. 4.1 ($E_c \approx -44.24\hbar\omega$).

As the lowest energy values reached for each pseudopotential width R change significantly between the different panels of Fig. 4.1, it is also apparent that $R \ll l$ is a necessary condition for a useful, convergent, approximation of the zero-range limit. Even without more sophisticated analysis, it is apparent from the results

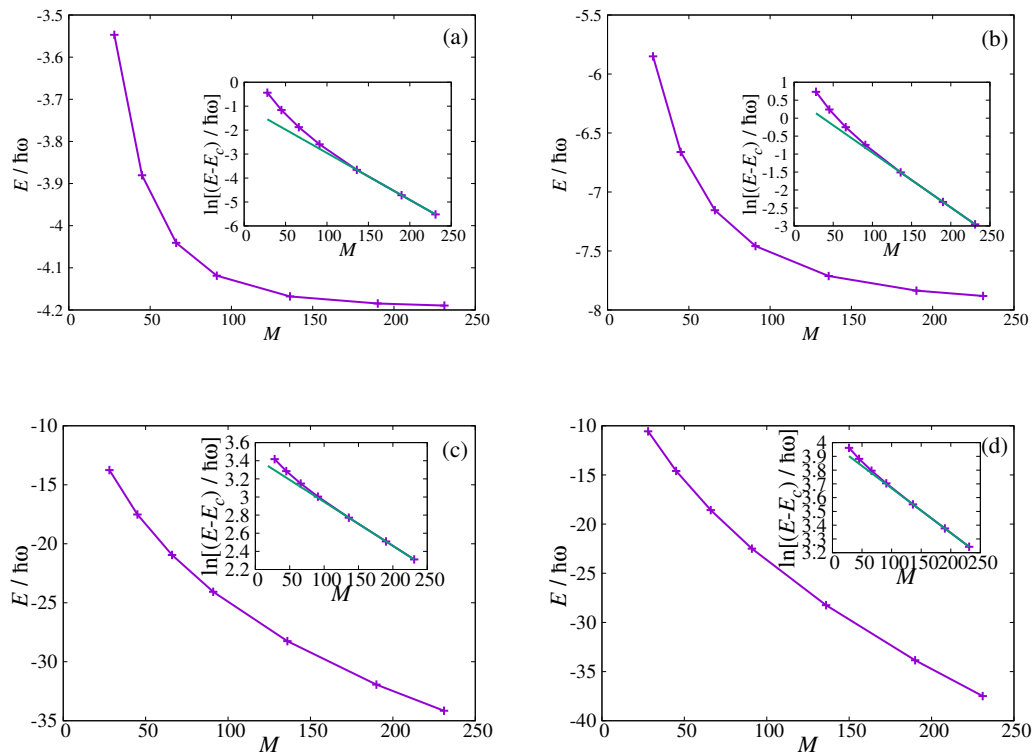


FIGURE 4.1: Convergence of the ground-state energy for three fermions with attractive Gaussian pseudopotential interactions in the unscaled harmonic oscillator basis. The energy from exact diagonalization in the finite multi-particle basis of Eq. (4.5) is plotted vs. the size M of the single-particle basis for Gaussian pseudopotentials of different widths R : (a) $R = l$, (b) $R = 0.8l$, (c) $R = 0.3l$ and (d) $R = 0.1l$, where $l = \sqrt{\hbar/m\omega}$ is the length scale of the harmonic trapping potential. The insets in panels (a) and (b) show logarithmic plots of the same data as the main graph and demonstrate that a regime of exponential convergence is reached. The extrapolated limiting values of the energy E_c are obtained by non-linear fitting of the exponential function $Ae^{-BM} + E_c$ to the last three data points: (a) $E_c = -4.19359\hbar\omega$, (b) $E_c = -7.93323\hbar\omega$, (c) $E_c = -44.2392\hbar\omega$, and (d) $E_c = -63.1069\hbar\omega$. The interaction strength $\ln(l/a_s) = 3.0$ is kept constant for all panels and the corresponding amplitude parameters V_0 are determined numerically following the procedure described in Ref. [139]: (a) $V_0 = 19.8237\hbar\omega$, (b) $V_0 = 19.6329\hbar\omega$, (c) $V_0 = 18.2369\hbar\omega$ and (d) $V_0 = 13.024\hbar\omega$.

of Fig. 4.1 that the necessary extrapolations the infinite basis set ($M \rightarrow \infty$) and zero range ($R \rightarrow 0$) limit will be challenging to achieve.

4.4.2 Length scale resolution

Since we are using a smooth Gaussian pseudopotential, we should expect that, for a sufficiently large basis set, the energy will converge exponentially to a limiting

value with the size of the single-particle basis set. Indeed, it is well known that the Fourier transform of a Gaussian function yields again a Gaussian, which decays, in fact, faster than exponential in the tails. Sampling a Gaussian potential function in momentum space should thus lead to at least exponential convergence, once the basis set is large enough to sample the tails of the Fourier-transformed Gaussian in momentum space. The necessary condition to reach this regime is that the basis set can resolve length scales that are smaller than the length scale R of the Gaussian.

We now use this argument as a motivation to consider the length scale resolution of a two-dimensional harmonic oscillator basis. In order to keep the basis set independent from the Hamiltonian of Eq. (4.2), we consider basis functions that are eigenfunctions of a harmonic oscillator with frequency $\tilde{\omega}$ and corresponding length scale $\tilde{l} = \sqrt{\hbar/m\tilde{\omega}}$. For a one-dimensional harmonic oscillator, the p -th excited state has a spatial extent that can be estimated by the classical turning point x_t :

$$(p + \frac{1}{2})\hbar\tilde{\omega} = \frac{1}{2}m\tilde{\omega}^2 x_t^2, \quad (4.7)$$

or $x_t = \sqrt{2p+1}\tilde{l}$. The set of $M_{1D} = p+1$ harmonic oscillator functions up to the p -th excited states provides an approximately homogeneous sampling of the interval $[-x_t, x_t]$ at a length scale

$$l_{\text{res}} = \frac{2x_t}{M_{1D}} = \frac{2\sqrt{2p+1}\tilde{l}}{p+1}. \quad (4.8)$$

In order to connect this result to the number M of two-dimensional harmonic oscillator basis functions, we construct the latter as a product basis (of Hermite functions) with an energy cutoff. This yields

$$M = \sum_{i,j=0}^{i+j \leq p} 1 = \frac{(p+1)(p+2)}{2}. \quad (4.9)$$

We can thus relate the resolution length scale l_{res} to the size of the basis and obtain

$$l_{\text{res}} = \frac{4\sqrt{\sqrt{8M+1}-2}}{\sqrt{8M+1}-1}\tilde{l}, \quad (4.10)$$

which can be solved for M to yield

$$M \approx 32 \left(\frac{\tilde{l}}{l_{\text{res}}} \right)^4, \quad (4.11)$$

where lower order terms were neglected assuming $\tilde{l} \gg l_{\text{res}}$.

Equation (4.11) provides an estimate for the size of the single-particle basis needed to resolve a length scale l_{res} . For the situation of Sec. 4.4.1 where $\tilde{l} = l$ we can estimate the minimum size of the basis set to be able to resolve the pseudopotential length scale R as

$$M_{\text{min}} \approx 32 \left(\frac{l}{R} \right)^4, \quad (4.12)$$

i.e. the required basis set size increases rapidly when the length scale R (and thus the range) of the pseudopotential is decreased.

Specifically, it means that reaching an exponentially convergent regime should be quite achievable when the pseudopotential width is of the same order of magnitude as the oscillator length l . For $R = l$ and $R = 0.8l$ we would require a minimum of 32 and 78 single-particle basis functions, respectively, which means about 16,000 and 200,000 Fock states for three fermions. This is consistent with the numerical results of Fig. 4.1 obtained with up to $M = 230$ single-particle basis functions.

In order to explore the physics of short-range interactions, however, we may need to use narrower pseudopotentials. With modest choices of $R = 0.3l$ and $R = 0.1l$ the number of required single-particle basis functions already increases to about 4,000 and 300,000, respectively, corresponding to about 3×10^{10} and 10^{16} multi-particle basis function. In this case, even the storage of the wave function is very expensive as it would require 0.2 TByte and 100,000 TByte memory, respectively. Although exploiting symmetries, using approximation schemes, or

stochastic sampling techniques can reduce these requirements [50, 106], the quartic scaling in Eq. (4.11) does not seem pleasant.

4.4.3 Scaled harmonic oscillator basis

The required size of the single-particle basis can be decreased by introducing an appropriate scaling of the basis functions. The main idea is the the following: Increasing the number of basis functions not only improves the resolution length scale l_{res} (by making it smaller) but also increases the largest length scale that can be described by the basis, which is given by $2x_t = 2\sqrt{2p+1} \tilde{l}$, i.e. through the classical turning point. This means that the basis functions can be scaled according to the basis set size while still resolving the largest length scale of the problem (e.g. twice the Thomas-Fermi radius of a cold atomic cloud). Let us denote this largest relevant length scale as γl , where γ is the dimensionless form of this length scale in units of the length scale l of the trapping potential. Note that γ is determined by the physical properties of the system (i.e. particle number, interaction strength, etc.), and is thus independent of the basis set size. For the required basis set length scale we then obtain

$$\tilde{l} = \frac{\gamma}{2\sqrt{2p+1}} l . \quad (4.13)$$

With Eq. (4.8) this yields $l_{\text{res}} = \gamma l / (p + 1)$ and using Eq. (4.9) to solve for M we obtain

$$M = \frac{\gamma^2}{2} \left(\frac{l}{l_{\text{res}}} \right)^2 + \frac{\gamma}{2} \frac{l}{l_{\text{res}}} . \quad (4.14)$$

Applying this result to the problem of resolving a Gaussian pseudopotential with length scale $l_{\text{res}} = R$ and taking the leading term for $l \gg R$, we obtain the revised relation for the minimum size of the single-particle basis

$$M_{\text{min}} \approx \frac{\gamma^2}{2} \left(\frac{l}{R} \right)^2 , \quad (4.15)$$

when the length scale of the single-particle basis is optimally scaled with the size of the basis set. Compared to the result (4.12) for the unscaled basis, the power-law scaling of the required basis set size with the pseudopotential length scale R in Eq. (4.15) is improved by two orders.

4.4.4 Estimating the interaction-dependent prefactor

As γl represents the largest length scale that has to be resolved by the single-particle basis, i.e. the maximal spatial extent of the system, the factor γ depends on the details of the Hamiltonian, which, for our example, are the particle number content and the strength of the contact interaction. Although the exact value of γ is difficult to calculate we can estimate its value and present upper and lower bounds from limiting cases that are simple to analyze.

Specifically for fermions with attractive short-range interactions as per Eq. (4.1), the size of the trapped non-interacting gas cloud will provide an upper bound, while a lower bound can be obtained from the strongly interacting limit where fermion pairs form deeply bound composite bosons, while excess fermions remain with little residual interactions.

Starting with the upper bound, we consider a non-interacting Fermi gas with a possibly unequal population of spin-up and spin-down fermions. The largest length scale is determined by the Fermi pressure of the majority component with the quantum number p^{majority} along a single spatial dimension

$$\gamma_{\text{upper}} = 2\sqrt{2p^{\text{majority}} + 1} . \quad (4.16)$$

The parameter p^{majority} can be expressed in terms of particle number N_{majority} by considering Eq.(4.9) and using the information that only one particle can occupy one spatial orbital from the same spin component to yield

$$\gamma_{\text{upper}} = 2\sqrt{2\left\lceil \frac{\sqrt{8N_{\text{majority}} + 1} - 3}{2} \right\rceil + 1} , \quad (4.17)$$

where $\lceil x \rceil$ is the ceiling function [140].

For strong short-range attractive interactions, pairs of spin-up and spin-down particles form point-like effective bosons [67, 141]. The interactions between the effective bosons are repulsive but vanish in the limit of strong attraction between fermions. In this limit we thus obtain a non-interacting system where all of the bosons occupy the lowest single-particle orbital. In the spin balanced system, the largest length scale will thus be given by the length scale of the harmonic oscillator trapping potential. This length scale provides a lower bound of the largest length scale of the system as the effective repulsive interactions can only increase the average particle-particle distance. We thus obtain a lower bound of

$$\gamma_{\text{lower}}^{\text{sb}} = 2, \quad (4.18)$$

where the index ‘sb’ stands for the spin balanced case.

In the spin-imbalanced case, excess unpaired fermions from the majority component are still present and they maintain Fermi pressure in the whole interaction regime. Indeed, the excess fermions have weak repulsive interactions with the effective bosons that also vanish in the strongly interacting limit (regarding the original interactions between fermions) [67, 141]. Hence, the lower bound for the largest length scale can be tightened by considering a non-interacting Fermi gas of the excess fermions following the same argument as above. We obtain

$$\gamma_{\text{lower}}^{\text{si}} = 2 \sqrt{2 \left\lceil \frac{\sqrt{8 |N_{\uparrow} - N_{\downarrow}| + 1} - 3}{2} \right\rceil + 1}, \quad (4.19)$$

where the index ‘si’ stands for the spin imbalanced case.

We can see from Eqs.(4.17) and (4.19) that the largest relevant length scale γl increases with particle number. To leading order the bounds become

$$\gamma_{\text{upper}} \approx 2 \sqrt[4]{8 N_{\text{majority}}}, \quad (4.20)$$

$$\gamma_{\text{lower}} \approx 2 \sqrt[4]{8 |N_{\uparrow} - N_{\downarrow}|}. \quad (4.21)$$

Comparing with the expression (4.15) for the minimum size of the single-particle basis, we see that M_{min} increases with the square root of the particle number

(that is N_{majority} and $|N_{\uparrow} - N_{\downarrow}|$, respectively), i.e. requiring a larger single-particle basis for a larger particle number. We also see that the largest interaction dependence of M_{min} can be expected in the spin-balanced case, whereas M_{min} will approximately remain independent of interactions for large spin polarization (e.g. polaron physics), where $N_{\text{majority}} \approx |N_{\uparrow} - N_{\downarrow}|$.

For large particle numbers the large length scale γl is well approximated by Thomas-Fermi theory as $\gamma l = 2R_{\text{TF}}$, where R_{TF} is the Thomas-Fermi radius. In Thomas-Fermi theory, the single-particle density $n(r)$ is found from solving

$$\mu_0 = V_{\text{ext}}(r) + \mu[n(r)], \quad (4.22)$$

where $V_{\text{ext}}(r) = \frac{1}{2}m\omega^2 r^2$ is the external potential, $\mu[n(r)]$ represents the chemical potential at local equilibrium [from the equation of state $\mu(n)$ of the homogeneous gas] and the constant μ_0 is the chemical potential of the finite system [17, 56, 62]. The Thomas-Fermi radius R_{TF} is then the value of r where $n(r)$ drops to zero.

For our case of a two-dimensional BCS mean-field theory yields a Thomas-Fermi radius R_{TF} that is independent of particle interactions [142], i.e. the result (4.20). In the strongly interacting limit of the balanced Fermi gas, we may use the known asymptotic form of the equation of state for a two-dimensional gas of bosonic dimers [143, 144]

$$\mu(n) = -\frac{2\pi\hbar^2}{m} \frac{n}{\ln(a_{dd}^2 n)}, \quad (4.23)$$

where the scattering length of bosonic dimers a_{dd} is approximately $a_{dd} \approx 0.55(4)a_s$ [141, 145]. The Thomas-Fermi radius can be determined from Eq.(4.22). After some algebraic manipulations we obtain

$$R_{\text{TF}} \approx \sqrt{a_{dd}^2 N_d + \frac{4\pi l^4}{a_{dd}^2} \ln\left(\frac{8\pi l^4 e^{\gamma_E + 1}}{N_d a_{dd}^4}\right)},$$

where N_d is the number of the bosonic dimers and γ_E is the Euler-Mascheroni constant with approximate value of $\gamma_E \approx 0.577216$. The resulting approximation for the scaling factor γ is $\gamma = 2R_{\text{TF}}/l$.

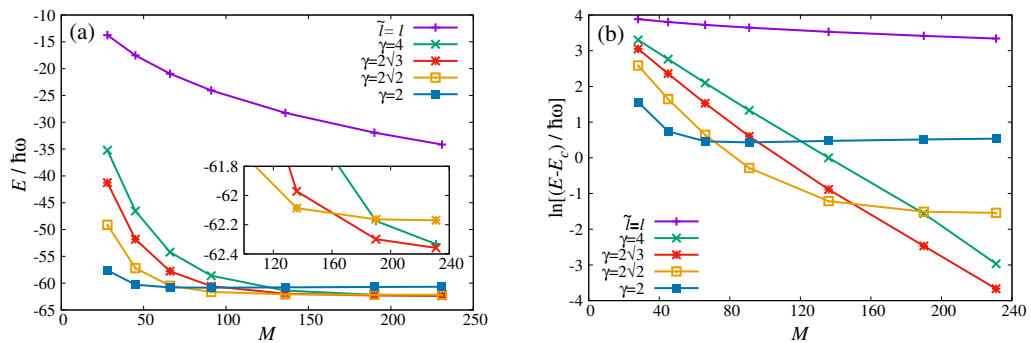


FIGURE 4.2: Energy convergence in a scaled harmonic oscillator basis at $R = 0.3l$ with different values of the factor γ . For reference, we also show results for the unscaled basis (green crosses) identical to Fig. 4.1(c). Panel (b) shows a logarithmic representation of the same data as panel (a). The extrapolated limiting value of the energy E_c is obtained by non-linear fitting of the exponential function $Ae^{-BM} + E_c$ to the last three data points of the $\gamma = 2\sqrt{3}$ data with $E_c = -62.38392715\hbar\omega$. $V_0 = 18.2369\hbar\omega l^2$ corresponding to $\ln(l/a_s) = 3.0$.

In order to test the prediction of Eq. (4.15) for reduced requirements for the size of a scaled single-particle basis we consider again the example of two spin-up particles and one spin-down particle with attractive interactions. The upper and lower bounds for γ can be easily calculated from Eqs.(4.17) and (4.19) to give $\gamma_{\text{upper}} = 2\sqrt{3}$ and $\gamma_{\text{lower}} = 2$. The required minimum number of basis functions M_{min} from Eq. (4.15) then yields 20 and 60, respectively, for $R = 0.3l$ [reduced from $M_{\text{min}} = 4,000$ for the unscaled basis according to Eq. (4.12)]. Similarly for $R = 0.1l$ the number decreases from 300,000 to 200–600 basis functions. In Fig. 4.2 we show the ground state energy for $R = 0.3l$ with different scaling factors γ . The results demonstrate that the regime of exponential convergence can be reached with the scaled basis, even though it was unattainable with the unscaled basis with the available computational resources. The smallest scaling factors of $\gamma = 2$ and $\gamma = 2\sqrt{2}$ are seen to result in an (unphysical) energy bias. This can be understood by the fact the the lower bound $\gamma = 2$ and $\gamma = 2\sqrt{2}$ underestimate the system size and thus the scaled basis set does not cover the whole area occupied by finite particle density. Increasing the value of γ from the lower bound eliminates the bias but also eventually leads to a reduced convergence rate. At the upper bound ($\gamma = 2\sqrt{3}$) the computation is seemingly free of bias but convergence of the energy is greatly improved compared to the unscaled basis set. Hence, we find

that the upper bound can safely be used for the accurate determination of the ground state energy.

4.5 Conclusion and outlook

In this work we considered the question whether smooth pseudopotentials are a good choice for representing short-range interactions in numerical approaches that rely on a Fock-state basis constructed from a finite set of single-particle functions. The combination of smooth pseudopotentials and an asymptotically complete set of (smooth) single-particle basis functions promises exponential convergence. This regime of exponential convergence can only be reached, however, if the basis set is large enough to resolve the relevant length scales of the problem.

In order to isolate the effects of the single-particle basis we have used an exact diagonalization procedure to capture the many-particle quantum physics. For an example system of experimental interest (a two-dimensional harmonic trapping potential with attractively-interacting fermions) we have derived simple expressions for the required minimum size of the single-particle basis in order to resolve a given pseudopotential length scale. The algebraic scaling of $l_{\text{res}}^{1/4}$ can be improved to $l_{\text{res}}^{1/2}$ by scaling the basis set but remains algebraic with the required resolution length scale. An additional algebraic scaling of the required basis set size is found to apply to the particle number. With numerical example calculations for three particles we could demonstrate that the exponential convergence regime could indeed be reached, albeit in a regime where the pseudopotential length scale is not much smaller than the particle separation of length scale of the trapping potential.

In order to faithfully represent the physics of short-range interacting particles, as is relevant for ultracold quantum gases of neutral atoms, it would be necessary to reduce the length scale of the pseudopotential much further and extrapolate to the zero range limit. Although such extrapolation has been demonstrated in few-body systems using different computational approaches [81], it does not seem feasible for the current approach. Looking towards the treatment of larger particle numbers and simultaneous extrapolation to the zero-range limit, one has to consider that the benefits of asymptotically exponential convergence of the single-particle basis

are counter-acted by the algebraically scaling requirements for the minimum size of the single-particle basis, both with particle number and with the ratio of extremal length scales that have to be resolved. A remaining alternative approach is to replace the smooth pseudopotential by a renormalized contact interaction. This has the advantage of removing the artificial length scale of the pseudopotential, while at the same time the property of exponential convergence is lost and replaced by algebraic convergence. Extrapolation to the limit of zero range interactions has been successfully demonstrated for up to 66 fermions in three dimensions with an auxiliary-field quantum Monte Carlo approach [134]. The transcorrelated method, which will be discussed in the next chapter thoroughly, can further improve the power-law scaling. Extending the applicability of this method to trapped systems is a promising avenue for future work.

Chapter 5

Accelerating the convergence of exact diagonalization with the transcorrelated method: Quantum gas in one dimension with contact interactions

5.1 Introduction

In recent years there has been increasing interest in the experimental realization of strongly correlated quantum gases with bosonic or fermionic ultracold atoms [23, 146–149]. Their theoretical description is difficult [62, 150] and efficient numerical methods are required to describe the system reliably and accurately. One straightforward approach is to diagonalize the Hamiltonian in a Fock basis, i.e., a finite basis of appropriately symmetrized products of single-particle wave functions [47, 128, 130, 131, 151–154]. Besides the energy, this approach also provides convenient access to the full wave function from which all system properties can be computed. With the recently developed Full Configuration Interaction Quantum Monte Carlo method [50] it has become possible to solve much larger problems than with conventional, deterministic approaches [51, 155, 156]. Nevertheless, the

exact diagonalization in Fock space is computationally expensive as the size of the many-particle Fock basis grows combinatorially with the number of particles and the size of the single-particle basis. Moreover, the convergence towards exact results with increasing the size of the single-particle basis is painfully slow for short-range interacting ultracold atoms. Specifically, for a one-dimensional model with δ function interactions, which models ultracold atoms in a tightly confining trap [157], the energy converges to the exact result with an error that scales as M^{-1} with a basis set of M plane waves, or $M^{-1/2}$ with a basis set of harmonic-oscillator eigenfunctions [47]. The reason for this slow convergence is the fact that the short-range interaction induces a cusp into the many-body wave functions at particle coalescence, i.e., whenever two particles meet [33, 157]. Mathematically, the wave function belongs to the differentiability class C^0 , i.e., it is continuous but its first derivative is discontinuous. Approximating such a shape of the wave function by linear combinations of products of smooth single-particle functions is highly inefficient.

One possible way to improve energy estimates in a finite basis set is to renormalize the parameters of the Hamiltonian [83, 84, 158]. This approach is closely related to the concept of a running coupling constant in quantum field theory, where the coupling constant depends on a momentum cutoff [159]. In two and three-dimensional systems with contact interaction it is necessary to renormalize the interaction constant with the basis size (momentum cutoff) in order to avoid divergences. While this is not necessary in one dimension, adjusting the interaction strength can still improve convergence properties [84]. The simplest possibility is to adjust the interaction constant such as to yield the exact value of the ground-state energy for two interacting particles from a calculation in the truncated basis. We are not aware whether the improved convergence rate of a many-body calculation has been determined before, but in Sec. 5.3 we report numerical results for three and six fermions that indicate that the convergence rate of the energy error improves by one order from M^{-1} to M^{-2} . Renormalizing the coupling strength based on an exactly solvable limit of the many-body problem was proposed in Ref. [84] and the possibility of adjusting the dispersion relation

of the kinetic energy part of the Hamiltonian in order to improve the convergence rate was discussed in Refs. [134, 158] for two- and three-dimensional Fermi gases. In a similar spirit as the renormalization of the coupling constant, a more elaborate effective Hamiltonian approach has been used to speed up the convergence of few-particle calculations in harmonic trapping potentials [72, 160]. Other approaches to optimize the finite-basis representation of the wave function have suggested modifying the cutoff procedure for the exact diagonalization procedure [132], or scaling the single-particle basis function [161].

A different way to improve the convergence properties of a basis set expansion is to use basis functions that explicitly depend on the interparticle distances instead of a Fock basis [162–165]. However, the cost of the determination of the matrix elements exponentially increases with the number of particles restricting the applicability of the method to the few-particle regime.

The route that we follow in this work is to introduce a Jastrow factor e^τ [166] in order to capture the short-range behavior of the exact N -particle wave function Ψ

$$\Psi(x_1, x_2, \dots, x_N) = e^\tau \Phi(x_1, x_2, \dots, x_N) , \quad (5.1)$$

$$\tau = \sum_{k < l}^N u(x_k - x_l) , \quad (5.2)$$

where the correlation factor τ depends on the pairwise separation distances of particles. The function $u(x)$ is designed to describe important two-particle correlations of Ψ while the function Φ is much smoother. Jastrow factors as in Eq. (5.1) are frequently used in Variational and Diffusion Quantum Monte Carlo approaches for ultracold atoms [145, 167–170], *ab initio* nuclear physics [171], the electronic structure of atoms, molecules [172, 173], and solid-state materials [174, 175].

In this chapter we follow the transcorrelated approach [176], where the Jastrow factor is folded into the Hamiltonian. Starting from the stationary Schrödinger equation

$$\hat{H}\Psi = E\Psi, \quad (5.3)$$

and using Eq. (5.1) we obtain the transcorrelated Schrödinger equation

$$\underbrace{e^{-\tau} \hat{H} e^{\tau}}_{\tilde{H}} \Phi = E \Phi, \quad (5.4)$$

where the transcorrelated Hamiltonian $\tilde{H} = e^{-\tau} \hat{H} e^{\tau}$ is related to the original Hamiltonian \hat{H} by a similarity transformation and thus shares the same eigenvalue spectrum. The transcorrelated method has already been widely used for computations of atomic, molecular [176–179] and solid-state properties [180, 181], where typically the emphasis has been on finding an optimized correlation factor τ , while Φ is taken as a simple reference function with the correct particle exchange symmetry, e.g., a Slater determinant. Here, we follow the idea of Ref. [182] where the function $u(x)$ is designed to exactly reproduce the singular short-range behavior of the exact wave function Ψ , while the transcorrelated function Φ is expanded in a Fock basis. The transcorrelated Schrödinger equation (5.4) is then solved as an exact diagonalization problem. Reference [182] demonstrated that an improved convergence rate and highly accurate energies for the homogeneous Coulomb gas could be achieved with this approach.

In the following, we concentrate on a one-dimensional quantum gas of bosons or fermions with contact interactions. By constructing a correlation factor with an appropriate cusp, we show that the smoothness of the transcorrelated wave function is improved by at least one order, i.e. from C^0 to C^1 where the first derivative is continuous. For spinless bosons where the wave function is symmetric under pairwise particle exchange, the transcorrelated wave function even improves further to C^2 , i.e. the second derivative is continuous as well. The explicit and exact form of the transcorrelated Hamiltonian is derived in real space, and in momentum space in second quantization. Three-particle interactions occur as a consequence of the similarity transformation. While a useful approximation is developed that only requires evaluation of effective two-particle terms, it is also shown that convergence to exact results for the energy can be achieved with a purely one- and two-body effective Hamiltonian if the correlation factor is appropriately adjusted with the basis set size. While the transcorrelated approach developed here is not

restricted to ground states or the absence of trapping potentials, we specifically consider the cases of the homogeneous gas of spin- $\frac{1}{2}$ fermions and spinless bosons and compare with exact solutions based on the Bethe ansatz [33–35]¹.

This allows for easy benchmarking of our numerical results, which are presented for the spin- $\frac{1}{2}$ Fermi gas in a plane-wave basis. We find that the convergence rate of the energy error is improved by the transcorrelated method from M^{-1} to M^{-3} in a basis of M single-particle functions.

This chapter is organized as follows. After introducing the original Hamiltonian with δ interactions and discussing the wave function cusp in Sec. 5.2.1, we construct an appropriate correlation factor in Sec. 5.2.2 before deriving the explicit form of the transcorrelated Hamiltonian in real space in Sec. 5.2.3. In Sec. 5.2.4 we show that the correlation factor improves the smoothness of the wave function by one or two orders before providing an analytical estimate for the convergence rate of the energy in Sec. 5.2.5. Discussing the momentum space form of the transcorrelated Hamiltonian in second quantization and a convenient approximation for the three-body term in Sec. 5.2.6 concludes the theory part 5.2. Numerical results for spin- $\frac{1}{2}$ fermions are presented in Sec. 5.3. After introducing the methods used in Sec. 5.3.1, we present calculations of the energy error for two particles in Sec. 5.3.2, for three particles in Sec. 5.3.3, and for six particles in Sec. 5.3.4 before concluding in Sec. 5.4.

5.2 Theory

5.2.1 One-dimensional quantum gas with contact interaction: cusp of the wave function

We consider a gas of N quantum particles of mass m in one spatial dimension. Either a single or several spin flavors of bosons or fermions may be present. The particles interact with a contact (zero-range) interaction, which can be represented

¹Exact solutions are also available for inhomogeneous systems in the strongly interacting limit, which could be used for further benchmarking in future work [36–39, 69].

by a Dirac delta potential in the Hamiltonian

$$\hat{H} = -\frac{\hbar^2}{2m} \sum_{i=1}^N \left[\frac{\partial^2}{\partial x_i^2} + V(x_i) \right] + g \sum_{i < j} \delta(x_i - x_j), \quad (5.5)$$

where x_i is the spatial coordinate of the i th particle and $V(x)$ a smooth external potential. The external trapping potential $V(x)$ does not change the singular properties of the wave function, which are dominated by the contact interaction term. For this reason, we will omit the potential $V(x)$ for many examples, which allows the comparison to exact solutions obtained by the Bethe ansatz, e.g. for spinless bosons [33] and spin- $\frac{1}{2}$ fermions [34, 35]. Our transcorrelated approach for improving the smoothness of the wave function, however, is not restricted to the homogeneous system and the asymptotic convergence rates that we report in this work are not affected by smooth external potentials.

The Hamiltonian (5.5) can be realized with ultracold atoms in a tightly confining wave-guide-like trapping potential [157]. The potential strength g can be expressed through a one-dimensional scattering length a as

$$g = -\frac{2\hbar^2}{ma}. \quad (5.6)$$

The contact interaction can be also expressed as boundary condition for the wave function at coalescence, i.e. when two particles meet [33]. Note that fermions only feel the presence of the contact interaction term between different spin flavors due to the Pauli exclusion principle. Near the coalescence point the wave function takes the form (in analogy to Refs. [65, 68, 158])

$$\begin{aligned} \Psi(x_1, x_2, \dots) &\stackrel{x_{ij} \rightarrow 0}{\sim} (a - |x_{ij}|) \cdot \\ &\cdot A_{ij}(X_{ij}, x_1, \dots, x_{i-1}, x_{i+1}, \dots, x_{j-1}, x_{j+1}, \dots) + \mathcal{O}(x_{ij}), \end{aligned} \quad (5.7)$$

where $x_{ij} = x_i - x_j$ is the relative and $X_{ij} = (x_i + x_j)/2$ is the center-of-mass coordinate relating to the pair with the i th and j th particles. The $\mathcal{O}(x_{ij})$ term is regular at coalescence. For fermions the function $A_{ij}(X_{ij}, x_1, \dots)$ is equal to zero if both particles i and j belong to the same spin flavor due to the Pauli exclusion

principle, which also means that they do not feel the contact interaction. The term $a - |x_{ij}|$ in Eq.(5.7) describes a cusp in the wave function with a discontinuity in the first derivative and a singularity in the second derivative. The wave function thus belongs to the differentiability class C^0 . The cusp in the wave function further has the consequence that the Fourier transform of the wave function to momentum space has k^{-2} tails for large k and, thus, the single-particle momentum distribution falls off as k^{-4} , as is well known for quantum gases in one dimension with contact interactions [65].

5.2.2 Correlation factor for 1D system with contact interaction

In this work we follow a similar procedure to Ref. [182] and design the correlation factor τ of Eq. (5.2) such that the boundary condition (5.7) is satisfied automatically. To this end it is sufficient to require the function $u(x)$ to have the form

$$u(x) \stackrel{x \rightarrow 0}{\equiv} u(0) - \frac{1}{a}|x| + \mathcal{O}(x^2) . \quad (5.8)$$

This restriction is enough to obtain the correct boundary condition, which can be seen by substituting Eq.(5.8) into the Jastrow factor

$$e^\tau = \left(\prod_{k \neq i, l \neq j} e^{u(x_{kl})} \right) e^{u(0)} \underbrace{e^{-\frac{1}{a}|x_{ij}| + \mathcal{O}(x_{ij}^2)}}_{1 - \frac{1}{a}|x_{ij}| + \mathcal{O}(x_{ij}^2)} . \quad (5.9)$$

It is convenient to define the correlation factor in momentum space to have the correct large- k dependence and a simple cutoff for small k

$$\tilde{u}(k) = \begin{cases} \frac{2}{ak^2} & \text{if } |k| \geq k_c , \\ 0 & \text{if } |k| < k_c , \end{cases} \quad (5.10)$$

where the parameter k_c sets an inverse length scale. The advantages of choosing this specific form of the correlation factor will become fully clear in the following

sections. An important feature is the free parameter k_c , which controls the size of the correlation factor and becomes important for suppressing three-particle contributions in the transcorrelated Hamiltonian. The function $u(x)$ can be obtained by the inverse Fourier transform $u(x) = (2\pi)^{-1} \int \exp(-ikx) \tilde{u}(k) dk$, as

$$u(x) = \frac{2}{a\pi} \left(\frac{\cos(k_c x)}{k_c} + x \operatorname{Si}(k_c x) - \frac{\pi}{2} |x| \right), \quad (5.11)$$

where $\operatorname{Si}(x)$ is the sine integral function [183]. The function $u(x)$ is found to be smooth except at the origin. Considering the case when x is close to zero we obtain the expression

$$u(x) = \frac{2}{ak_c\pi} - \frac{1}{a} |x| + \mathcal{O}(x^2), \quad (5.12)$$

which satisfies the condition (5.8).

The Jastrow factor with $u(x)$ from Eq.(5.11) is shown in Fig. 5.1. Close to the coalescence point it resembles the absolute value function, as is expected from Eqs.(5.7) and (5.9). It can be also read from these equations that the slopes of the two sides of the absolute value function linearly depend on the inverse of the scattering length. When the scattering length tends to infinity the slope goes to zero and the cusp disappears. This is the non-interacting limit.

The parameter k_c adjusts the width of the Jastrow factor. As we choose larger momentum cutoff in the momentum space it makes the function narrower in real space.

The physically relevant information about the scattering length comes exclusively from the cusp of the Jastrow factor near the coalescence point. The long-range behavior is an artifact from the definition (5.10). Since the long-range part of the correlation factor is smooth, however, it is easier to correct it with the Fock-space expansion of the transcorrelated wave function Φ . Moreover, the long-range part can be easily damped by increasing the parameter k_c . In Sec. 5.3 we will numerically examine the accuracy of the transcorrelated method and we will show that it improves the efficiency of the numerical approach.

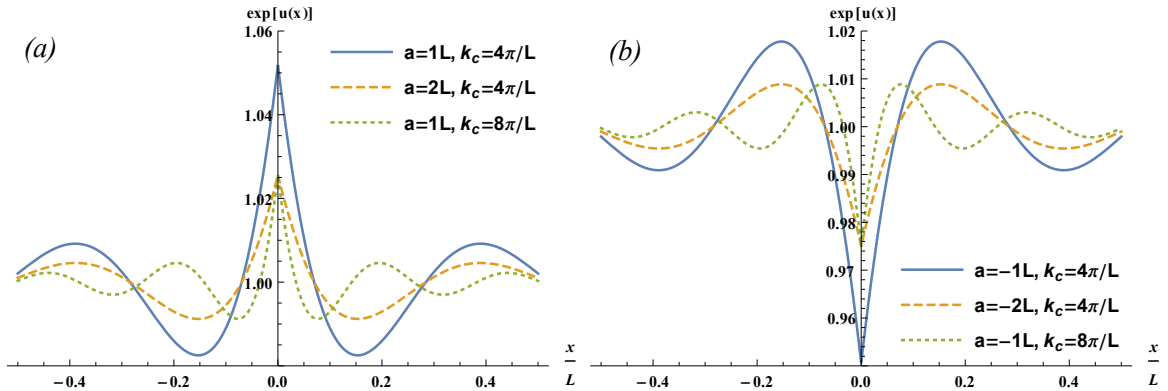


FIGURE 5.1: Jastrow factor $\exp[u(x)]$ with $u(x)$ from Eq.(5.11). (a) Attractive and (b) repulsive interactions with parameter values for a_s and k_c as indicated.

5.2.3 Transcorrelated Hamiltonian in real space

The explicit form of the effective Hamiltonian in Eq.(5.4) can be determined from the expansion

$$\tilde{H} = \hat{H} + [\hat{H}, \tau] + \frac{1}{2} [[\hat{H}, \tau], \tau] + \dots \quad (5.13)$$

The external and the particle-particle interaction potentials commute with the function τ as they can be expressed as a function of the particle positions. The only non-zero commutators come from the kinetic term, where only the first three terms are different from zero. Thus the expansion (5.13) terminates to yield

$$\tilde{H} = \hat{H} - \frac{\hbar^2}{2m} \sum_i \left[\frac{\partial^2}{\partial x_i^2}, \tau \right] - \frac{\hbar^2}{4m} \sum_i \left[\left[\frac{\partial^2}{\partial x_i^2}, \tau \right], \tau \right].$$

The remaining commutators can be calculated analytically [176, 182],

$$\tilde{H} = \hat{H} - \sum_i \left[\frac{1}{2} \frac{\partial^2 \tau}{\partial x_i^2} + \frac{\partial \tau}{\partial x_i} \frac{\partial}{\partial x_i} + \frac{1}{2} \left(\frac{\partial \tau}{\partial x_i} \right)^2 \right] \frac{\hbar^2}{m}. \quad (5.14)$$

As it can be seen from the term $\frac{\partial \tau}{\partial x_i} \frac{\partial}{\partial x_i}$ in the summation on the right-hand side, the resulting effective Hamiltonian is not Hermitian. As a consequence, the left and right eigenvectors are different and connected by the linear transformation

$$|\Phi^L\rangle = e^{2\tau} |\Phi\rangle,$$

where $|\Phi^L\rangle$ is the adjoint of the left eigenvector and $|\Phi\rangle$ is the right eigenvector. Since the transcorrelated transformation of Eq. (5.4) is a similarity transformation, the effective Hamiltonian \tilde{H} nevertheless has the same real-valued eigenvalue spectrum as the original (Hermitian) Hamiltonian \hat{H} .

Properties such as correlation functions or expectation values of general operators can be expressed through the transcorrelated wave function as

$$\frac{\langle\Psi|\hat{A}|\Psi\rangle}{\langle\Psi|\Psi\rangle} = \frac{\langle\Phi|e^\tau\hat{A}e^\tau|\Phi\rangle}{\langle\Phi|e^{2\tau}|\Phi\rangle}. \quad (5.15)$$

Evaluating such expectation values involves high-dimensional integrals, which is usually prohibitive in a Fock basis. If the correlation factor is small, however, one can make use of the cumulant expansion

$$\frac{\langle\Phi|e^\tau\hat{A}e^\tau|\Phi\rangle}{\langle\Phi|e^{2\tau}|\Phi\rangle} = \langle\Phi|\hat{A}|\Phi\rangle_c + \langle\Phi|\{\hat{A}, \tau\}|\Phi\rangle_c + \frac{1}{2}\langle\Phi|\{\{\hat{A}, \tau\}, \tau\}|\Phi\rangle_c + \dots, \quad (5.16)$$

to obtain approximate results. Here $\{\cdot, \cdot\}$ is the anti-commutator and $\langle\Phi|\dots|\Phi\rangle_c$ denotes the cumulant of operator products [184].

5.2.4 Smoothness of the transcorrelated wave function

The transcorrelated transformation improves the smoothness of the wave function, which eventually leads to faster convergence of the basis expansion. Here we consider two interacting particles in a smooth and separable external potential, where we will prove that the transcorrelated eigenfunction is at least C^1 , i.e. it can be differentiated at least once with a continuous derivative. In the case of additional even exchange symmetry of the wave function, the smoothness further improves to C^2 , i.e. the second derivative of the wave function is also continuous. This is an improvement to the eigenfunctions of the original Hamiltonian which are only C^0 .

We consider two particles, e.g. two bosons, or fermions in different spin states, and introduce the center-of-mass and relative coordinates

$$X = \frac{1}{2}(x_1 + x_2) , \quad (5.17)$$

$$x = (x_1 - x_2) , \quad (5.18)$$

respectively. For convenience, we assume that the smooth external trapping potential $V(x)$ is further separable, as it is the case for harmonic trapping potentials frequently employed for ultracold atoms:

$$\sum_{i=1}^2 V(x_i) = v(x) + \mathcal{V}(X). \quad (5.19)$$

It follows that the Hamiltonian of Eq. (5.5) can be written as the sum $H = H_{\text{COM}} + H_{\text{rel}}$, with terms that only depend on either the center-of-mass or relative coordinate, respectively. The Schrödinger equation (5.3) is thus solved with a wave function of the form

$$\Psi(x_1, x_2) = \chi(X)\psi(x), \quad (5.20)$$

and eigenvalue $E = E_{\text{COM}} + E_{\text{rel}}$. The equation for the center-of-mass motion is free of singular operators and thus leads to a smooth wave function $\chi(X)$. The equation for the relative motion, however, contains the particle-particle contact interaction

$$\left[-\frac{\hbar^2}{2m} \frac{\partial^2}{\partial x^2} + v(x) + g\delta(x) \right] \psi = E_{\text{rel}}\psi. \quad (5.21)$$

The wave function of relative motion $\psi(x)$ is not smooth but rather has a cusp as we discussed earlier in Sec. 5.2.1.

Since we are only interested in the smoothness properties at the particle coalescence point $x = 0$, we may take the simplified correlation factor

$$\tau(x) = -\frac{1}{a}|x| , \quad (5.22)$$

which has the same small- x expansion up to first order as the function of Eq. (5.11).

Applying the transcorrelated similarity transformation Eq.(5.4) with $\psi(x) = e^{\tau(x)}\phi(x)$, the δ -function interaction term is eliminated. The transcorrelated equation (5.21) then can be written in the form

$$-\frac{\hbar^2}{2m} \frac{d^2\phi}{dx^2} = \frac{\hbar^2}{ma} S(x) \frac{d\phi}{dx} - v(x)\phi + E'\phi, \quad (5.23)$$

where a constant term from the first derivative of τ has been absorbed as a shift in the energy $E' = E_{\text{rel}} + \hbar^2/2ma^2$, and

$$S(x) = \frac{d|x|}{dx} = \begin{cases} 1, & x > 0, \\ -1, & x < 0. \end{cases} \quad (5.24)$$

In order to examine the smoothness of the function $\phi(x)$, we follow the idea of Kato [185] by designing an elementary solution of $\frac{d^2}{dx^2}$,

$$G(x) = \frac{|x|}{2} \zeta(x), \quad (5.25)$$

where ζ is a sufficiently smooth function that equals 1 for $|x| \leq 1$ and 0 for $|x| > 2$. Then we have

$$\frac{d^2}{dx^2} G(x) = \begin{cases} \delta(x), & |x| < 1, \\ S(x)\zeta'(x) + \frac{|x|}{2}\zeta''(x), & \text{otherwise.} \end{cases}$$

We apply a convolution with respect to G on both sides of Eq.(5.23)

$$G * \left(\frac{d^2}{dx^2} \phi \right) = -2G * \left(\frac{1}{a} S(x) \frac{d\phi}{dx} - \frac{m}{\hbar^2} v(x)\phi + \frac{mE'}{\hbar^2} \phi \right),$$

and we find the leading singular term for ϕ

$$\phi(x) = -\frac{1}{a} \int_{-\infty}^{\infty} |x-y| \zeta(x-y) S(y) \phi'(y) dy + \text{smooth part}.$$

Using partial integration we obtain an integral equation that depends on $\phi(x)$ instead of its derivative

$$\phi(x) = \frac{1}{a} \int_{-\infty}^{\infty} \left\{ \zeta(x-y)[S(y-x)S(y) + 2|x-y|\delta(y)] + |x-y|S(y)\zeta'(x-y) \right\} \phi(y) dy + \text{smooth part.}$$

By noticing that $S(y-x)S(y) = 1$ in the whole integration domain except $(0, x)$ or $(x, 0)$ (depending on whether $x > 0$ or $x < 0$), we obtain

$$\phi(x) = \frac{2}{a} \begin{cases} x\zeta(x)\phi(0) - \int_0^x \phi(y)\zeta(x-y)dy + \text{smooth part}, & x > 0, \\ -x\zeta(x)\phi(0) - \int_x^0 \phi(y)\zeta(x-y)dy + \text{smooth part}, & x < 0. \end{cases}$$

Hence, $\phi(x)$ is continuous. Since the singularity only takes place at $x = 0$, we can simply take $\zeta(x) = 1$ for small variables. Then we get the expressions for the first, second and third derivatives ($\phi' \equiv d\phi/dx$)

$$\phi'(x) = \frac{2}{a} \begin{cases} \phi(0) - \phi(x) + \text{smooth part}, & x > 0, \\ -\phi(0) + \phi(x) + \text{smooth part}, & x < 0, \end{cases} \quad (5.26)$$

$$\phi''(x) = \frac{2}{a} \begin{cases} -\phi'(x) + \text{smooth part}, & x > 0, \\ \phi'(x) + \text{smooth part}, & x < 0, \end{cases} \quad (5.27)$$

$$\phi'''(x) = \frac{2}{a} \begin{cases} -\phi''(x) + \text{smooth part}, & x > 0, \\ \phi''(x) + \text{smooth part}, & x < 0. \end{cases} \quad (5.28)$$

It follows from Eq. (5.26) that the first derivative ϕ' is continuous and thus the relative wave function is C^1 . Since the center-of-mass wave function $\chi(X)$ is smooth, it follows that also the full wave function $\Psi(x_1, x_2)$ of Eq. (5.20) is at least C^1 .

Even stronger results follow when the wave function is known to be symmetric under particle exchange, i.e. $\Psi(x_1, x_2) = \Psi(x_2, x_1)$. This is manifestly the

case when the particles are spinless bosons but also for the ground state of distinguishable particles if the Hamiltonian is symmetric (e.g. as well for fermions with different spin quantum numbers in the absence of spin-dependent terms in the Hamiltonian). From the symmetry of Ψ it then follows that the relative wave function is even, $\phi(x) = \phi(-x)$, and, as a consequence, its first derivative is an odd function. From Eq.(5.26) it can be seen that the first derivative is also continuous, which means that it must have a node at the origin, i.e. $\phi'(0) = 0$. Using this fact it can be seen from Eq.(5.27) that the second derivative is continuous as well, and the third derivative is the first one where a discontinuity may appear. In this case of even particle exchange symmetry, the transcorrelated wave function is thus C^2 , i.e. the smoothness has improved by two orders compared to the original wave function $\Psi(x_1, x_2)$.

These results derived for two particles can be expected to carry over to multi-particle wave functions since the only singular term in the Hamiltonian is two-particle interaction in the form of a Dirac δ . For spinless bosons the multi-particle wave function is symmetric under the exchange of an arbitrary pair of particle coordinates. Hence we expect the transcorrelated multi-particle wave function to be C^2 and thus have improved smoothness by two orders compared to the original wave function. We have checked this property by explicitly constructing the two- and three-particle wave functions of the Lieb-Liniger model of interacting bosons in a one-dimensional box with periodic boundary conditions [33], and found that the transcorrelated wave functions have continuous first and second derivatives while the third derivatives are discontinuous.

For fermions the wave function has to be antisymmetric under the exchange of fermions, which carries over to an antisymmetry of the spatial wave function under exchange of two-particle coordinates with the same spin (like-spin pairs are thus not affected by the δ interaction). Pairs of particles with opposite spin are affected by the δ interaction but, for more than two (spin- $\frac{1}{2}$) fermions, the wave function is in general not symmetric under the exchange of the coordinates. Thus it is expected that the transcorrelated wave function is C^1 with a discontinuous second derivative. We have explicitly constructed the ground-state wave function for three

fermions (one spin- \uparrow and two spin- \downarrow) in the Yang-Gaudin model of interacting fermions in a box with periodic boundary conditions and verified that the second derivative of the transcorrelated wave function has a discontinuous jump at the coalescence of different-spin particles. We will discuss further numerical evidence for the C^1 nature of the transcorrelated three-particle wave function for fermions in Sec. 5.3.3.

5.2.5 Convergence rate for ground-state energy

In the numerical procedure we have to truncate the many-particle Hilbert space and work with a finite basis. Let us consider the case where we truncate the single-particle Hilbert space with a momentum cutoff k_{\max} and otherwise perform an exact diagonalization. We want to estimate the size of the error $\delta E = E - E_a$ that is made by replacing the exact energy E by the eigenvalue E_a obtained in the truncated basis with cutoff k_{\max} .

Let us write

$$\tilde{H}|\Phi\rangle = E|\Phi\rangle, \quad (5.29)$$

for the eigenvalue equation in full Hilbert space and

$$\tilde{H}_{PP}|\Phi_a\rangle = E_a|\Phi_a\rangle \quad (5.30)$$

for the approximate, truncated eigenvalue equation solved by the computer. Here, we have introduced the truncated Hamiltonian $\tilde{H}_{PP} = P\tilde{H}P$, where P is the projector onto the N -particle linear space spanned by the Fock states constructed from plane waves with momentum $-k_{\max} \leq k \leq k_{\max}$. Noting that \tilde{H} is not necessarily Hermitian and has a left eigenvector equation

$$\langle\Phi_a^L|\tilde{H}_{PP} = E_a\langle\Phi_a^L|, \quad (5.31)$$

we may obtain an expression for the energy error δE from projecting Eq. (5.29) onto $\langle \Phi_a^L |$. Simple manipulation yields

$$\delta E \langle \Phi_a^L | \Phi \rangle = \langle \Phi_a^L | \tilde{H}_{PQ} | \Phi \rangle, \quad (5.32)$$

where $\tilde{H}_{PQ} = P\tilde{H}Q$ and $Q = 1 - P$ is the projector onto the complement of the projected space, i.e. where at least one momentum is $|k| > k_{\max}$. We may choose $\langle \Phi_a^L | \Phi \rangle = 1$ as a normalization condition for the approximate eigenstate and are thus left with evaluating the overlap on the right-hand side of Eq. (5.32). Let us, for simplicity, consider the situation of Sec. 5.2.4 of two-particles in the relative motion frame and assume that the exact wave function decays with a power-law

$$\Phi(k) \sim k^{-\alpha} \quad (5.33)$$

with an integer exponent $\alpha \geq 1$. Then we obtain

$$\delta E = \langle \Phi_a^L | \tilde{H}_{PQ} | \Phi \rangle \sim \int_{k_0}^{k_{\max}} dp \int_{k_{\max}}^{\infty} dq \Phi_a^L(p) q^{-\alpha} \tilde{H}_{pq}, \quad (5.34)$$

where we have replaced the summation of momenta by integrals and the projection operators determine the range of integration. We have applied a small momentum cutoff k_0 , which is related to the inverse system size. The expression (5.34) is general enough to apply both to the original exact diagonalisation problem of the Hamiltonian (5.5) and to the transcorrelated Schrödinger equation (5.4).

5.2.5.1 Standard method

The original Hamiltonian (5.5) for two particles in the relative motion frame can be written in momentum space with the matrix elements

$$H_{pq} = \frac{\hbar^2 p^2}{m} \delta_{pq} + g, \quad (5.35)$$

where the off-diagonal term results from the short-range interaction and couples any momenta equally. The diagonal term of the kinetic-energy does not contribute

in Eq. (5.34) and we are left with

$$\int_{k_0}^{k_{\max}} dp \int_{k_{\max}}^{\infty} dq \Phi_a^L(p) q^{-\alpha} \tilde{H}_{pq} = k_{\max}^{-\alpha+1} \frac{g}{\alpha} \int_{k_0}^{k_{\max}} dp \Phi_a^L(p). \quad (5.36)$$

Since the p integral is finite, the scaling of the energy error becomes

$$\delta E \sim k_{\max}^{-\alpha+1} \quad (5.37)$$

$$= k_{\max}^{-1}, \quad (5.38)$$

where in the last equality we have used the result from Sec. 5.2.4 that $\alpha = 2$ as a consequence of the C^0 cusp of the exact wave function with δ function interactions.

5.2.5.2 Transcorrelated method

In the transcorrelated approach, the δ function interaction is removed and replaced by the less singular operator $S(x) d/dx$ as discussed in Sec. 5.2.4. The matrix elements of the transcorrelated Hamiltonian in momentum space become

$$\tilde{H}_{pq} = \frac{\hbar^2 p^2}{m} \delta_{pq} + 2g \frac{q \sin^2[L(p-q)/4]}{p-q}. \quad (5.39)$$

We want to use Eq. (5.34) in order to estimate the energy error,

$$\delta E \sim 2g \int_{k_0}^{k_{\max}} dp \Phi_a^L(p) q^{-\alpha} \frac{q \sin^2[L(p-q)/4]}{q-p}, \quad (5.40)$$

where we omitted a minus sign as we interested only the absolute value of the error. As the integrand is positive everywhere we can consider the following upperbound $\sin^2[x] \leq 1$,

$$\delta E \sim 2g \int_{k_0}^{k_{\max}} dp \Phi_a^L(p) F(\alpha - 1), \quad (5.41)$$

where the q -integral can be separately performed as

$$F(n) = \int_{k_{\max}}^{\infty} dq \frac{q^{-n}}{p-q}. \quad (5.42)$$

For integer-valued $n \geq 1$ it is easy to show that $F(n)$ has the series representation

$$F(n) = \sum_{\nu=0}^{\infty} \frac{p^{\nu}}{(n + \nu)k_{\max}^{n+\nu}} \quad (5.43)$$

In order to evaluate the p -integral in Eq. (5.41) it is relevant to estimate the p -dependence of the left eigenfunction $\Phi_a^L(p)$. Since the left eigenfunction of the transcorrelated Hamiltonian does not benefit from the removal of the cusp by the Jastrow factor it will have the same asymptotics of the original relative wave function, i.e. $\Phi_a^L(p) \sim p^{-2}$. Now the integral (5.41) can be done term by term for the power series. The asymptotic scaling turns out to be dominated by the first term, which gives

$$\delta E \sim k_{\max}^{-\alpha+1}. \quad (5.44)$$

This is the same result as the expression (5.37) for the original short-range interaction, i.e. the scaling of the energy error is completely determined by the large- k asymptotics of the wave function.

Specifically, for the smooth transcorrelated wave function of class C^2 for the case of completely symmetric wave functions (bosons or fermions with different spin quantum numbers only), we have $\alpha = 4$ and thus the expected scaling of the energy error with the momentum cutoff is

$$\delta E \sim k_{\max}^{-3}. \quad (5.45)$$

5.2.6 Transcorrelated Hamiltonian in second quantization and three-body term

In the following we examine the homogeneous system in a discrete plane wave basis. In order to examine the matrix elements of the transcorrelated Hamiltonian,

let us rewrite Eq.(5.14) in second quantized form [182],

$$\begin{aligned} \tilde{H} = & \frac{\hbar^2}{2m} \sum_{k\sigma} k^2 a_{k,\sigma}^\dagger a_{k,\sigma} + \sum_{\substack{pqk \\ \sigma\sigma'}} T_{pqk} \Theta_{\sigma\sigma'} a_{p-k,\sigma}^\dagger a_{q+k,\sigma'}^\dagger a_{q,\sigma'} a_{p,\sigma} + \\ & + \sum_{\substack{pqs \\ kk' \\ \sigma\sigma'}} Q_{kk'} \Theta_{\sigma\sigma'} a_{p-k,\sigma}^\dagger a_{q+k',\sigma}^\dagger a_{s+k-k',\sigma'}^\dagger a_{s,\sigma'} a_{q,\sigma} a_{p,\sigma} , \end{aligned} \quad (5.46)$$

where $a_{k,\sigma}^\dagger$ create a one-particle plane wave state with momentum k and spin σ , L is the length of the unit cell, and $\Theta_{\sigma\sigma'} = \delta_{\sigma\sigma'}$ for bosons and $\Theta_{\sigma\sigma'} = 1 - \delta_{\sigma\sigma'}$ for fermions. The tensors \mathbf{T} and \mathbf{Q} can be expressed explicitly with the correlation factor,

$$\begin{aligned} T_{pqk} &= \frac{g}{L} + \frac{\hbar^2}{mL} \left(k^2 \tilde{u}(k) - (p-q)k \tilde{u}(k) + \frac{W(k)}{L} \right) , \\ W(k) &= \sum_{k'} (k-k')k' \tilde{u}(k-k') \tilde{u}(k') , \\ Q_{kk'} &= -\frac{k'k \tilde{u}(k) \tilde{u}(k') \hbar^2}{2mL^2} . \end{aligned} \quad (5.47)$$

The summation in Eq.(5.47) contains infinitely many terms. It can be evaluated exactly. The results and derivations are detailed in the Appendix.

Treating the three-body term in the explicit calculation is cumbersome. In order to improve the numerical efficiency we approximated this term with an effective two-body term. For the approximation we considered only the diagonal part of the three-body term, where momentum exchanges are equal to each other ($k = k'$). We can recognize the number operator ($\sum_{s\sigma} a_{s\bar{\sigma}}^\dagger a_{s\bar{\sigma}}$). Its effect can be evaluated in advance,

$$\sum_{\substack{pqsk \\ \sigma\sigma'}} Q_{kk'} \Theta_{\sigma\sigma'} a_{p-k,\sigma}^\dagger a_{q+k,\sigma}^\dagger a_{s,\sigma'}^\dagger a_{s,\sigma'} a_{q,\sigma} a_{p,\sigma} |\Phi\rangle = \sum_{\substack{pqk \\ \sigma}} Q_{kk'} \mathcal{N}_\sigma a_{p-k,\sigma}^\dagger a_{q+k,\sigma}^\dagger a_{q,\sigma} a_{p,\sigma} |\Phi\rangle ,$$

where $\mathcal{N}_\sigma = N_\sigma = N - 2$ for bosons and $\mathcal{N}_\sigma = N - N_\sigma$ for fermions. This approximation is very closely related to the Random Phase Approximation (RPA) [186, 187]. The approximated Hamiltonian with only one- and two-body terms

can be given in the form:

$$\begin{aligned} \tilde{H}_{\text{ATB}} = & \frac{\hbar^2}{2m} \sum_{k\sigma} k^2 a_{k,\sigma}^\dagger a_{k,\sigma} + \sum_{\substack{pqk \\ \sigma \neq \bar{\sigma}}} T_{pqk} \Theta_{\sigma\sigma'} a_{p-k,\sigma}^\dagger a_{q+k,\bar{\sigma}}^\dagger a_{q,\bar{\sigma}} a_{p,\sigma} + \\ & + \sum_{\substack{pqk \\ \sigma}} Q_{kk} \mathcal{N}_\sigma a_{p-k,\sigma}^\dagger a_{q+k,\sigma}^\dagger a_{q,\sigma} a_{p,\sigma} , \end{aligned} \quad (5.48)$$

where the "ATB" index in the Hamiltonian stands for "approximate three-body." In the two-particle case and in the limit when the system is noninteracting, this approximation becomes irrelevant, because the three-body term does not have any effects. This approximation introduces an uncontrolled bias in the calculations. In the next section, we introduce a procedure, where this bias can be eliminated in a controlled manner.

5.3 Numerical examinations

5.3.1 Methods and implementation

In this section we study numerically the homogeneous spin- $\frac{1}{2}$ Fermi gas in one dimension with Hamiltonian of Eq. (5.5) with $V(x) = 0$ in a box of length L with periodic boundary conditions (ring configuration) for two to six particles. Exact solutions for this system are available using the Bethe ansatz [34, 35], which we use to calculate exact reference energies. We then diagonalize the original Hamiltonian (5.5) and the transcorrelated Hamiltonian (5.48) with approximated three-body terms. To this end we use a single-particle basis with M plane waves truncated according to

$$|k| \leq k_{\text{max}} \equiv \frac{M-1}{2} \frac{2\pi}{L}, \quad (5.49)$$

and construct the full multi-particle Fock basis with dimension $\binom{M}{N_\uparrow} \binom{M}{N_\downarrow}$, where N_\uparrow and N_\downarrow are the spin-up and spin-down particle numbers. We then express the Hamiltonian as a matrix in this finite Fock basis and numerically obtain the ground-state energy and eigenvector (often referred to as "exact diagonalization").

We also compare our results with the lattice renormalization approach [83, 84]. The truncated plane wave basis expansion discretizes real space by creating an underlying reciprocal lattice. The lattice renormalization approach then adjusts the potential strength g of the discretized δ interaction in order to recover the correct scattering amplitude for two particles [83] or, equivalently, yield the correct two-particle ground-state energy to leading order [84]. In order to apply this approach, one simply replaces the interaction constant g in the Hamiltonian (5.5) by the renormalized coupling constant

$$\tilde{g} = \frac{g}{1 + \frac{g}{g_0}}, \quad (5.50)$$

where

$$g_0 = \frac{M\pi^2\hbar^2}{mL} \approx \frac{k_{\max}\pi\hbar^2}{m}. \quad (5.51)$$

While the exact diagonalization of the Hamiltonian (5.5) in the Fock bases with or without renormalized interaction strength can be calculated with any diagonalization algorithm, the transcorrelated method has an additional complication due to the non-Hermiticity of the transcorrelated Hamiltonian. We apply power iterations to obtain the ground-state energy and eigenvector [91], which can be done for non-Hermitian eigenvalue problems. The power method can be scaled to very large Hilbert spaces with the stochastic implementation provided by the Full Configuration Interaction Quantum Monte Carlo [50, 188]. Very recently, this approach was combined with the transcorrelated method for the homogeneous electron gas [182].

5.3.2 Two particles

The convergence of the energy with respect to the size of the single-particle basis is shown in Figs. 5.2 and 5.3 for two particles (one spin-up and one spin-down fermion or, equivalently, two spinless bosons) with attractive and repulsive interactions, respectively. The two-particle system has the advantage that the three-body interaction term in the transcorrelated Hamiltonian of Eq. (5.46) does

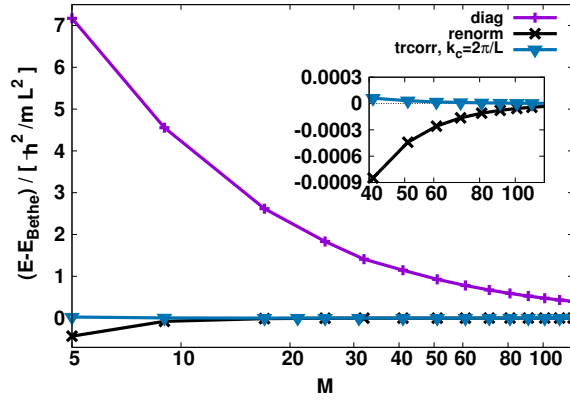


FIGURE 5.2: *Two particles with attractive interaction* ($g = -10\hbar^2/mL$): the error of the approximate ground-state energy vs. the number of one-particle basis functions M , on linear-log scale. “diag”: exact diagonalization of the Hamiltonian (5.5); “renorm”: with renormalized interaction constant of Eq. (5.50); “trcorr”: transcorrelated Hamiltonian of Eq. (5.46); “ k_c ” truncation parameter for fixed correlation factor of Eq. (5.10).

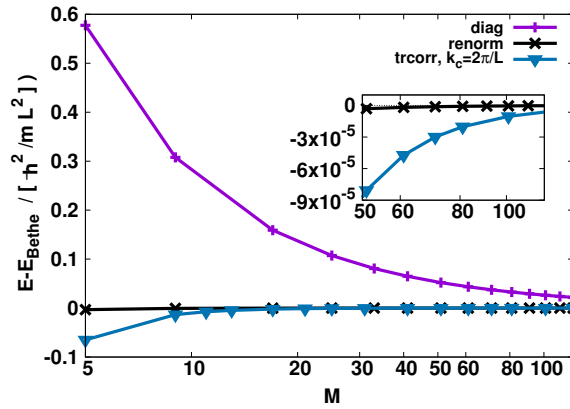


FIGURE 5.3: *Two particles with repulsive interaction* ($g = 10\hbar^2/mL$): the error of the ground-state energy vs. the number of one-particle basis functions M on linear-log scale. Legend labels as in Fig. 5.2.

not contribute and thus the effects of the transcorrelated transformation on the two-particle interactions can be studied in isolation without the need for further approximations. The energy error $\delta E \equiv E - E_{\text{Bethe}}$ is calculated as the difference of the numerically obtained approximate value and the exact ground-state energy value obtained from the Bethe ansatz [34, 35].

As we discussed earlier in Sec. 5.2.5 the energy is expected to converge polynomially, hence, by using the identity of the logarithmic function the relation between δE and M can be written in the following form:

$$\log_{10} \left(\frac{\delta E}{\hbar\omega} \right) = -b \log_{10} (M) ,$$

where b is the convergence rate. Therefore, b can be given as a slope in a double logarithmic scale. In Fig. 5.4 the energy obtained by exact diagonalization of the original Hamiltonian of Eq. (5.5) in the truncated Fock basis (“diag”) is found to converge linearly with the inverse number M^{-1} of single-particle basis functions in Figs. 5.4 and 5.5 for attractive and repulsive interaction respectively. This agrees nicely with the theoretical prediction of Eq. (5.38) in Sec. 5.2.5.

The transcorrelated approach (“trcorr”) is seen to generally improve upon the exact diagonalization results. From Sec. 5.2.5 we also may expect a faster convergence rate of $\delta E \sim M^{-3}$ (since the two-particle ground-state wave function is symmetric under particle exchange). From the numerical results presented in Figs. 5.4 - 5.7 we see that this is the case asymptotically for basis sets that are large enough to resolve the modified singular feature of the transcorrelated wave function. A more detailed description of these figures, especially about the cutoff procedure will be discussed in the next two subsections.

5.3.2.1 Correlation factor with fixed parameter k_c

In Figs. 5.4 and 5.5 the data labeled with k_c values are obtained with fixed correlation factors and variable number of single-particle basis functions M . The smallest value, $k_c = 2\pi/L$, shows significantly improved energy errors following the power law $\delta E \sim M^{-3}$ for all considered basis set sizes $M \geq 5$. Increasing the correlation factor cutoff k_c leads to an overall smaller correlation factor due to

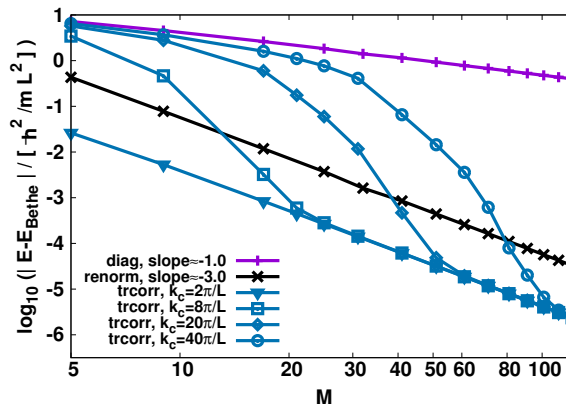


FIGURE 5.4: Power-law convergence with fixed correlation factor - two particles with attractive interaction ($g = -10\hbar^2/mL$): the error of the ground-state energy vs. the number of single-particle basis functions M on a log-log scale for different values of the k_c parameter (“trcorr”). Exact diagonalization (“diag”) and renormalized results (“renorm”) are shown for comparison (cf. Fig. 5.2).

“slope”: approximate exponent of fitted power-law $\delta E \sim M^{\text{slope}}$.

fewer Fourier components contributing, and an associated smaller length scale for its real-space version $u(x)$ of Eq. (5.11). Unsurprisingly, the smaller correlation factors are less effective in reducing the energy error for the small (fixed-size) basis sets. However, when the number of single-particle functions M is increased, all curves collapse onto the same asymptotic power-law with $\delta E \sim M^{-3}$. From our numerical data we find that the correlation factor is fully effective when $k_{\max} \gtrsim 3k_c$ for the attractive case of Fig. 5.4 and $k_{\max} \gtrsim 2k_c$ for repulsive interactions as seen in Fig. 5.5, where $k_{\max} = (M/2 - 1)2\pi/L$ determines the number of single-particle functions M .

5.3.2.2 Correlation factor with sliding parameter k_c

The observation that the correlation factor is fully effective when k_{\max} is larger than a value determined by k_c suggests that it makes sense to adjust k_c with the size of the basis set M (or, equivalently, k_{\max}), in order to find the smallest correlation factor necessary, for given basis set size M , to fully reap the benefits of the accelerated convergence of the transcorrelated approach. We thus introduce a

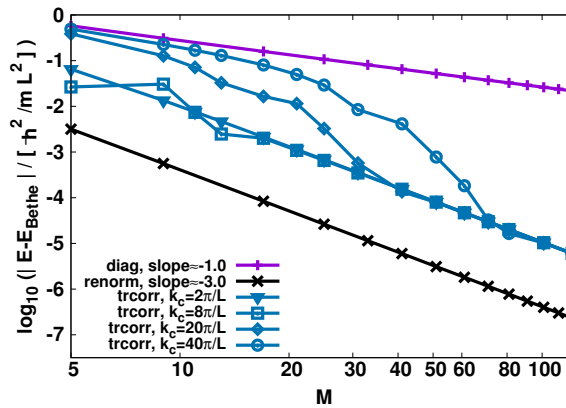


FIGURE 5.5: Power-law convergence with fixed correlation factor - two particles with repulsive interaction ($g = 10\hbar^2/mL$): the error of the ground-state energy vs. the number of one-particle basis functions M in a log-log plot. Legend labels as in Fig. 5.4.

way of scaling the correlation factor cutoff k_c with the basis set size according to

$$k_c = \beta k_{\max} . \quad (5.52)$$

A similar way of scaling the correlation factor with the size of the single-particle basis set was previously suggested in Ref. [182] (with fixed $\beta = 1$) in order to control the size of the three-body term in the transcorrelated Hamiltonian. We will discuss this issue in Secs. 5.3.3 and 5.3.4. In Figs. 5.6 and 5.7 we show, respectively, the energy error obtained with this approach for different values of β . Our data suggest that each value of β leads to a different power-law, until the value of β is small enough to reach the theoretical limit with $\delta E \sim M^{-3}$. Reducing the value of β further, does not change the power-law. We also see that different values of β are needed to reach the theoretical limit depending on the nature of the interaction.

5.3.2.3 Comparison with the renormalization approach

Energies obtained with renormalized interaction strength according to Eq. (5.50) are also shown in Figs. 5.2 - 5.7 for comparison. The renormalization method works

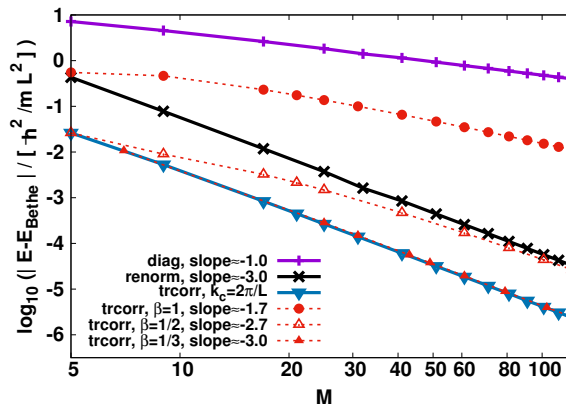


FIGURE 5.6: Correlation factor with sliding parameter k_c - two particles with attractive interaction ($g = -10\hbar^2/mL$) with sliding k_c : the error of the approximate ground-state energy vs. the number of one-particle basis functions M in a log-log plot. Legend labels as in Fig. 5.4. “ β ” parameter for scaled correlation factor of Eq. (5.52).

well for estimating the ground-state energy for two particles, which is not surprising because the renormalized coupling constant is determined by comparison with an exact solution to a two-particle problem. We here find that the energy error scales again as $\delta E \sim M^{-3}$. Even though the scaling is the same as the transcorrelated method, we find that the prefactors are different (leading to different off-sets of the curves in Figs. 5.6 and 5.7). It is interesting to note that the transcorrelated approach works better than the renormalized one for attractive interactions but worse for repulsive interactions. This is probably due to the Jastrow factor resembling the bound-state wave function that dominates the ground state for attractive interactions (see Fig. 5.1). Since the prefactor of the transcorrelated energy error certainly depends on the details of the cutoff procedure used in Eq. (5.10), it could probably be further reduced by optimizing this procedure.

5.3.2.4 Single-particle momentum density

In order to obtain information about the approximate wave function, we calculate the single-particle momentum density

$$\rho_\sigma(k) = \langle a_{k,\sigma}^\dagger a_{k,\sigma} \rangle, \quad (5.53)$$

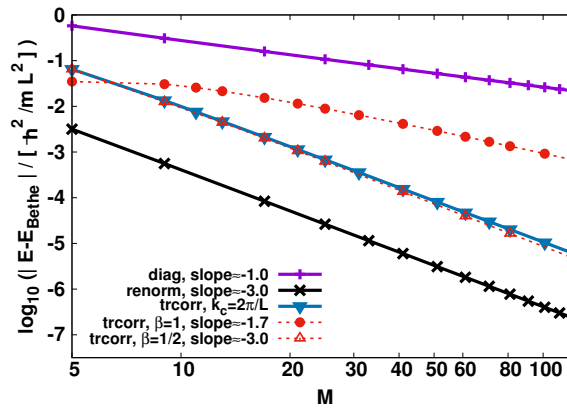


FIGURE 5.7: Correlation factor with sliding parameter k_c - two particles with repulsive interaction ($g = 10\hbar^2/mL$) with sliding k_c : the error of the ground-state energy vs. the number of one-particle basis functions M in a log-log plot. Legend labels as in Figs. 5.4. “ β ” parameter for scaled correlation factor of Eq. (5.52).

where the expectation value is taken with respect to the finite basis set approximation of either the original ground-state $|\Psi\rangle$ or the transcorrelated eigenstate $|\Phi\rangle$, respectively.

The results for two particles, shown in Fig. 5.8, are independent of the spin σ and the sign of k . The momentum distribution of the original ground-state $|\Psi\rangle$ shows a clear power-law decay $\sim k^{-4}$ for almost the entire momentum interval shown in the figure. As discussed in Sec. 5.2.1, this behavior is expected, since the momentum density contains the square of the wave function, which possesses k^{-2} tails as a consequence of the cusp in real space [65]. The renormalization method leads to the same power-law for the momentum density, since the analytic properties of the wave function are not changed.

The momentum distributions of the transcorrelated ground-state $|\Phi\rangle$ are seen to decay much faster for large k and asymptotically converge to a power-law of k^{-8} . This observation is consistent with the analytic results about the smoothness of the transcorrelated wave function of Sec. 5.2.4. Improving the smoothness (differentiability class) of the real-space wave function by one order also decreases the power-law of the large- k tail in momentum space by one order. Thus the C^2 character of the transcorrelated two-particle wave function implies $\sim k^{-4}$ scaling of the

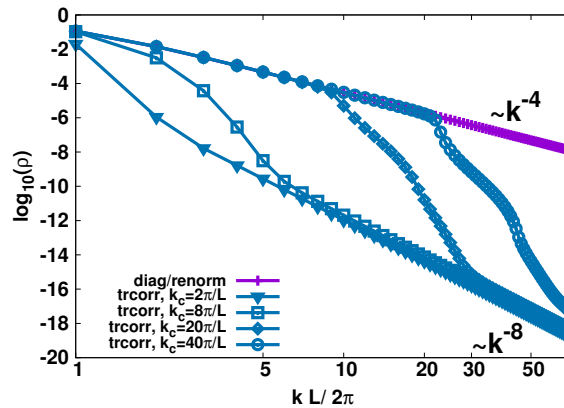


FIGURE 5.8: Single particle momentum density $\rho(k)$ for two particles with attractive interactions $g = -10\hbar^2/mL$, with $M = 139$ on a log–log scale showing the transition from the k^{-4} behavior of the original Hamiltonian to the k^{-8} asymptotics of the effective Hamiltonian as an effect of the correlation factor. Legend labels as in Fig. 5.4. Asymptotic power-laws from approximate fits to the large- k tails as indicated. The data from exact diagonalization with the bare interaction (“diag”) and renormalized interaction (“renorm”) are indistinguishable on the scale of the plot.

wave function and thus $\sim k^{-8}$ scaling of the momentum density. The parameter k_c defines an inverse length scale characterizing the “size” of the correlation factor. For larger length scales the correlation factor does not have any significant effect and hence the momentum density follows the original k^{-4} power-law for $k < k_c$. For smaller length scales (larger k) there is a transition region after which the smoothing effect of the correlation factor on the transcorrelated wave function becomes fully effective. In this regime of the smallest length scales (large k), the short-range correlations are suppressed and the momentum density shows a $1/k^8$ decay.

Smaller correlation factors (corresponding to larger k_c) reach the asymptotic scaling at larger wave numbers, which is expected because the wavelength of the basis functions needs to be small enough to resolve the features of the smaller correlation factor in order to take advantage of the improved smoothness of the wave function.

A remarkable feature of Fig. 5.8 is that the momentum density of the transcorrelated wave function for $k_c = 20\pi/L$ and $k_c = 40\pi/L$ coincides with the momentum

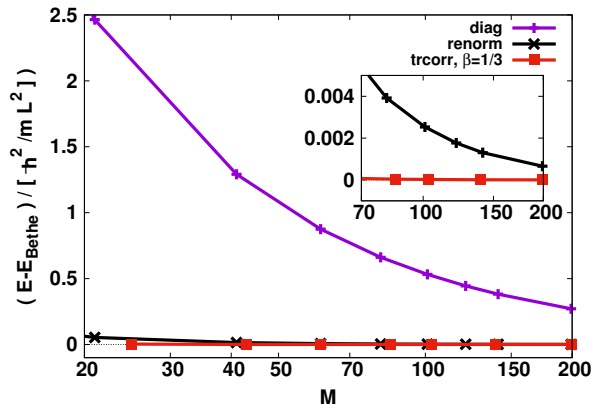


FIGURE 5.9: *Three fermions (two spin-up and one spin-down) with attractive interactions $g = -10\hbar^2/mL$: the error of the ground-state energy vs. the number of one-particle basis functions M on a linear-log scale. The labels “diag”, “renorm” and “tcorr” stand for the exact diagonalization, renormalization, and transcorrelated approaches, respectively. The correlation factor cutoff k_c is linearly scaled with M according to Eq. (5.52).*

density of the original wave function accurately for the smaller values of k up to critical value that is approximately given by k_c . This means that the exact momentum density can be extracted from Eq. (5.15) for the small wave numbers already from the first term of the expansion (5.16), i.e.

$$\langle \Psi | a_k^\dagger a_k | \Psi \rangle \approx \langle \Phi | a_k^\dagger a_k | \Phi \rangle. \quad (5.54)$$

Increasing k_c will further increase the range of wave numbers (equivalently decrease the length scale) over which the momentum density is accurately approximated.

5.3.3 Three fermions

In order to study the role of the three-body term and the effects of approximations we need to consider more than two particles. It is also interesting to study the efficacy of renormalizing the interaction strength in a multi-particle system, as Eq. (5.50) was derived considering only two interacting particles.

We consider three spin- $\frac{1}{2}$ fermions with two spin-up and one spin-down particles with attractive interactions. The energy error compared to the exact Bethe-ansatz

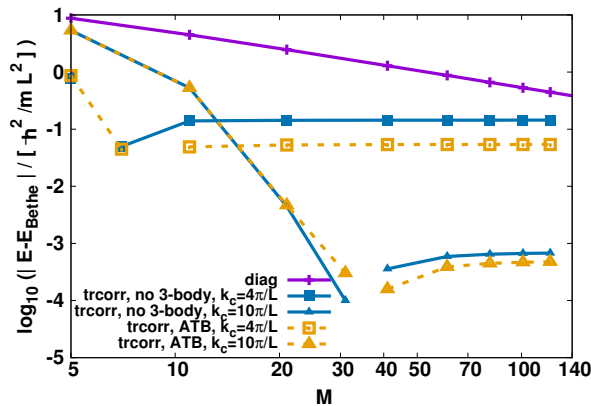


FIGURE 5.10: *Relevance of three-body terms - three fermions (two spin-up and one spin-down) with attractive interactions $g = -10\hbar^2/mL$ with constant k_c : the error of the ground-state energy vs. the number of one-particle basis functions M in a log-log plot. Legend labels as in Fig. 5.9. The label “no 3-body” means that the three-body term was omitted from the transcorrelated Hamiltonian Eq.(5.46), while for “ATB”-labelled data the three-body term is approximated as per Eq.(5.48).*

solution for the various approximations is shown in Fig. 5.9. Here (and also in Figs. 5.2-5.16), the lines connecting data points are a guide to the eye only. Where connecting lines are omitted in the logarithmic plot, a sign change of the error has occurred, i.e. the approximate energy curve crosses the exact one. The energy error from the exact diagonalization of the original Hamiltonian (5.5) is shown for reference in Figs. 5.9 and 5.11a. As expected it follows the power-law scaling $\sim k^{-1}$. The approach of renormalizing the interaction strength for a given basis set size by Eq. (5.50) is shown in Figs. 5.9 and 5.11a, and clearly demonstrates power-law scaling $\sim M^{-2}$. The convergence rate has decreased by one order compared to the two-particle case. This can be understood by the fact that the renormalized interaction strength was determined by solving a two-particle problem.

5.3.3.1 Correlation factor with fixed parameter k_c : Bias from the approximation of the three-body term

Results from the transcorrelated approach with fixed cutoff parameter k_c are shown in Fig. 5.10. Since we are not including the full three-body terms in our

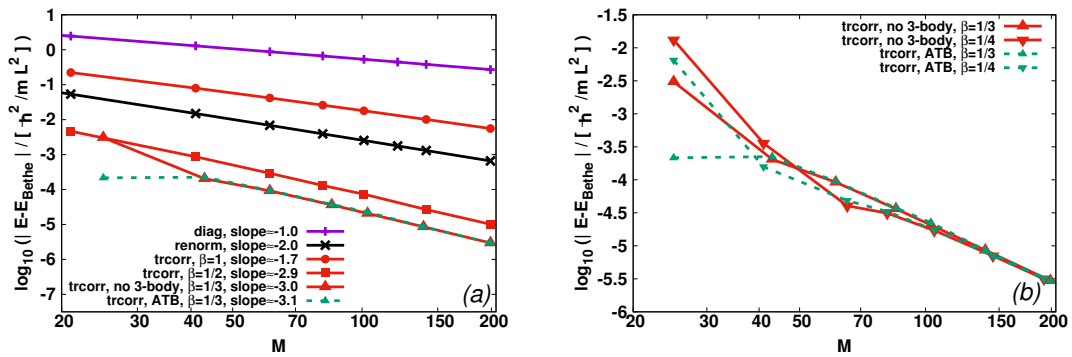


FIGURE 5.11: *Power-law convergence with sliding correlation parameter k_c - three fermions (two spin-up and one spin-down) with attractive interactions $g = -10\hbar^2/mL$* : the error of the ground-state energy vs. the number of one-particle basis functions M in a log-log plot. Legend labels as in Fig. 5.9. The label “no 3-body” means that the three-body term was omitted from the transcorrelated Hamiltonian Eq.(5.46), while for “ATB”-labelled data the three-body term is approximated as per Eq.(5.48). Where these labels are not indicated the results of the two approaches are indistinguishable from each other on the scale of this plot.

diagonalization procedure, the results converge to a finite value, which quantifies the contribution of the neglected three body terms. It can be seen that the approximate inclusion of the three-body term as per Eq. (5.48) (labelled “ATB”) leads to smaller errors than the complete neglect of three-body contributions [“no 3-body”; Eqs. (5.46) and (5.47) with $Q_{kk'} = 0$]. By increasing the value of k_c , the three-body error decreases dramatically providing a more accurate approximation for the energy. This can be understood as follows: increasing k_c reduces the length scale associated to the correlation factor and with it the range of the newly generated terms in the effective Hamiltonian, including the three-body term. In a dilute gas, the significance of the three-body terms thus diminishes.

5.3.3.2 Correlation factor with sliding parameter k_c : Treatment of the three-body term

We may expect that scaling the parameter k_c of the correlation factor with the size of the basis set as per Eq. (5.52) is a way to asymptotically eliminate the error introduced by neglecting or approximating the three-body term and converge to

exact results. Figs. 5.9 and 5.11 show that this is indeed the case (and a similar observation was previously made in Ref. [182]). Data for different values of the scaling factor β in Eq. (5.52) all show algebraic convergence to the exact ground-state energy. The numerically extracted power-law exponents vary, with generally a smaller value of β resulting in faster convergence in the asymptotic (large M) regime. As in the case for two particles in Fig. 5.6, the fastest convergence is reached with $\beta \leq \frac{1}{3}$ yielding the approximate power law $\delta E \sim M^{-3}$. As seen in Fig. 5.11b, decreasing the factor β below this value does not yield a further improvement of the asymptotic power law, but on the other hand, leads to larger errors for smaller basis sets (due to the smaller correlation factor being less effective in capturing pair correlations). It is also seen from the data in Fig. 5.11 that the approximate treatment of the three-body term (“ATB”) of Eq. (5.48) does not change the asymptotic power law, or even the value of the energy error in the asymptotic regime, but it does improve the energy error for smaller basis sets. We conclude that the value of $\beta = \frac{1}{3}$ and the inclusion of approximate three-body terms gives the best performance.

5.3.3.3 Single-particle momentum density

The single-particle momentum density $\rho_{\downarrow}(k)$ is shown in Fig. 5.12 and shows similar features as seen in the two-particle case of Fig. 5.8. The original ground-state wave function for three fermions leads to a $\sim k^{-4}$ algebraic decay of the momentum density as in the case of two particles, or more generally, for the Bose gas [65]. The transcorrelated ground-state $|\Phi\rangle$, however, asymptotically decays as $\sim k^{-6}$, which is slower by two orders than in the two particle case. This observation suggests that the wave function has the differentiability class C^1 , i.e. is less smooth by one order than the two-particle wave function. This result provides further evidence for the conclusion of Sec. 5.2.4 that the transcorrelated fermionic multi-particle wave function is C^1 .

The remarkable result from the numerical investigation of the three-fermion system is that the ground-state energy convergence $\sim M^{-3}$ is faster than expected from the analytical estimates of Sec. 5.2.5.2. The analytical arguments as well

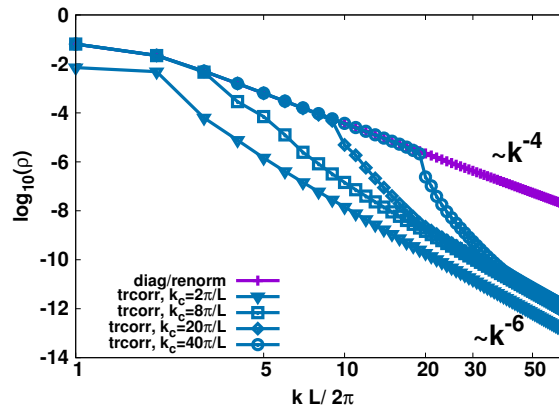


FIGURE 5.12: Single particle momentum density $\rho_{\downarrow}(k)$ for the minority spin component for three fermions (two spin-up, one spin-down) with attractive interactions of $g = -10\hbar^2/mL$ and $M = 139$ on a log-log scale. Labels as in Fig. 5.9. Asymptotic power laws from approximate fits to the large- k tails as indicated. The data from exact diagonalization with the bare interaction (“diag”) and renormalized interaction (“renorm”) are indistinguishable on the scale of the plot.

as the numerical analysis of the momentum density of the transcorrelated wave function indicate that the large momentum asymptotics scale as $\Phi(k) \sim k^{-3}$, which, by Eq. (5.44), should lead to an energy error scaling as $\delta E \sim M^{-2}$. The faster-than-expected convergence of the transcorrelated energy is well supported by the data shown in Fig. 5.11 and comes as a pleasant surprise.

5.3.4 Six fermions

We also examined the spin-balanced six-particle system in order to study the convergence properties for the larger particle number. Figs. 5.13 and 5.14 show the convergence of the energy error for attractive and repulsive interactions, respectively. As it can be seen by using the sliding scaled correlation factor k_c with $\beta = 1/2$, the transcorrelated method performs the best among the three methods. The improvement is even more significant in the attractive case, where in this scale it can barely be differentiated from the exact curve.

In order to examine the convergence rate and the effect of the different cutoff procedures, the double logarithmic scale is applied in Figs. 5.15 and 5.15. The

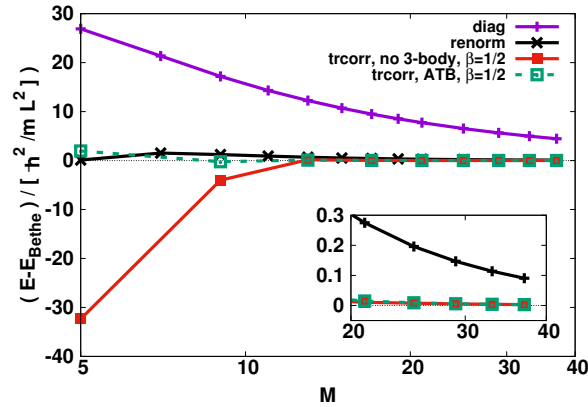


FIGURE 5.13: Six fermions (three spin-up and three spin-down) with attractive interactions $g = -10\hbar^2/mL$: the error of the ground-state energy vs. the number of one-particle basis functions M on a linear-log scale. Labels as in Figs. 5.9 and 5.11.

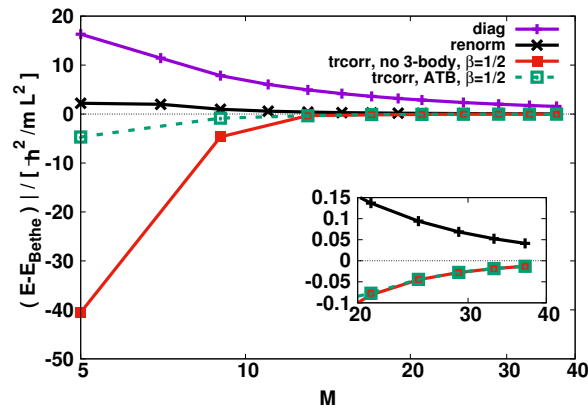


FIGURE 5.14: Six fermions (three spin-up and three spin-down) with repulsive interaction $g = 10\hbar^2/mL$: the error of the ground-state energy vs. the number of one-particle basis functions M on a linear-log scale. Labels as in Figs. 5.9 and 5.11.

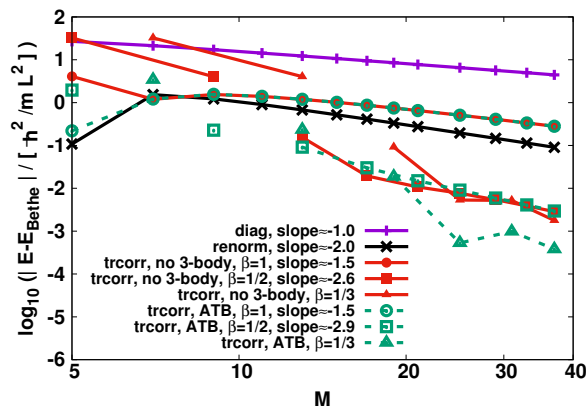


FIGURE 5.15: Power-law convergence with sliding correlation parameter k_c - six fermions (three spin-up and three spin-down) with attractive interactions $g = -10\hbar^2/mL$: the error of the ground-state energy vs. the number of one-particle basis functions M on a log-log scale. Labels as in Figs. 5.9 and 5.11.

results are largely consistent with the case of the three fermions. Exact diagonalization of the original Hamiltonian yields an M^{-1} convergence, as expected, and also the convergence rate of M^{-2} for the renormalization approach has not changed compared to three particles. This confirms that the faster convergence of the renormalization method in the two-particle system is a special case.

The transcorrelated approach with scaled correlation factor cutoff k_c seems a bit complicated for the smaller basis sets especially at attractive interactions 5.15, due to the several crossings of the exact energy value. However, at a larger number of basis states, it can be seen that it converges algebraically towards the exact ground-state energy, even though the three-body terms have been either approximated or fully omitted. The two curves merge together at the scaling factor of $\beta = \frac{1}{2}$ showing the elimination of the bias from the calculations. This indicates that the required β -factor for optimal convergence has no strong dependence on the particle number. The six-particle results also confirm the faster-than-expected M^{-3} scaling of the transcorrelated approach that we already saw for the three-particle and two-particle cases.

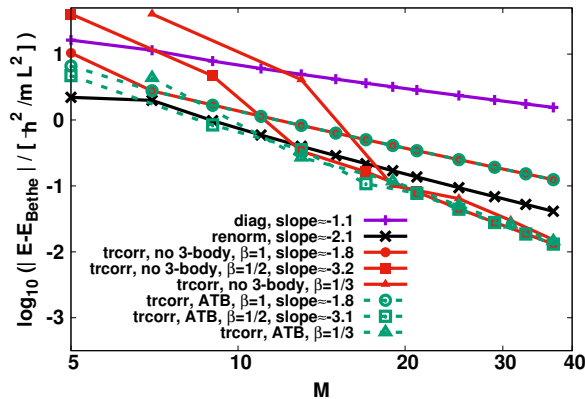


FIGURE 5.16: Power-law convergence with sliding correlation parameter k_c - six fermions (three spin-up and three spin-down) with repulsive interaction $g = 10\hbar^2/mL$: the error of the ground-state energy vs. the number of one-particle basis functions M on a log-log scale. Labels as in Figs. 5.9 and 5.11.

5.4 Conclusion and outlook

We have constructed an effective Hamiltonian based on a transcorrelated transformation that replaces the singular contact interaction by less singular, but non-Hermitian terms, which also include artificial three-body interactions. We have shown that an explicit treatment of the three-body terms can be avoided, while nevertheless achieving fast convergence to the exact results by scaling the correlation factor with the size of the single-particle basis. This scaling is controlled with the parameter β through Eq.(5.52) and effectively reduces the error due to neglected three-body terms when the basis set is increased by reducing the size of the correlation factor. While small values of β will lead to the optimal asymptotic scaling of the error for large basis sets, larger values will lead to improved benefits of the correlation factor for smaller basis set but compromise the asymptotic scaling beyond an optimal value. The optimal value of β was seen to depend weakly on the sign of the interaction strength and may also depend on the value.

Including the full three-body terms would allow one to achieve unbiased results for a Fock-space diagonalization even for fixed-size correlation factors. This could potentially be useful for reducing the amount of correlation in the effective Hamiltonian, which may be beneficial for the convergence of stochastic or approximate

approaches. Our numerical results indicate that the transcorrelated method improves the convergence of the energy from M^{-1} of the exact diagonalization of the original Hamiltonian to M^{-3} , where M is the number of single-particle basis functions. For two particles we could show that the faster convergence rate originates in the improved smoothness of the transcorrelated wave function from C^0 of the original cusp-like wave function to C^2 . For more than two spin- $\frac{1}{2}$ fermions, where the smoothness of the wave function improves only to C^1 , the convergence rate is not yet fully understood.

We have also examined an alternative approach based on a simple renormalization of the interaction constant. While not affecting the smoothness of the wave function, this approach improves the convergence rate of ground-state energies by one order to M^{-2} .

Based on such promising results for the ground state of the one-dimensional homogeneous gas, it will be interesting to examine the efficiency of the transcorrelated approach in a trapped system or for excited states, where the presence of a cusp at the two-particle coalescence causes slow convergence [47]. Due to the non-Hermitian nature of the transcorrelated Hamiltonian, care must be taken when choosing an appropriate excited state method, but projective operation based approaches [189, 190], for example, are well suited.

In future work we also would like to extend the treatment of the three-body terms to include all six-index interaction terms, of which the explicit form is given in Sec. 5.2.6. Using the exact expressions it is not necessary to adjust the correlation factor cutoff with the size of the basis. Potentially better results can be expected by simply selecting the largest correlation factor in the calculations. Moreover, we plan to investigate two- and three-dimensional systems, where the singular behavior at the coalescence point is even more severe. Considering this singularity in the correlation factor potentially can greatly improve the convergence behavior even more significant than the improvements found in the present study.

Chapter 6

Summary

In this thesis, we discussed methodological developments, which improved the efficiency of the Fock-space based approaches for ultracold atoms. The inefficiency of most numerical methods stem from the combinatorial scaling of the Hilbert space, thus we investigated the possibility to decrease the required number of single-particle basis functions and thus enable calculations for larger particle numbers and strong interaction regimes. For this, first, we considered the smooth Gauss pseudopotential, which is known to converge exponentially fast in the asymptotic limit with the number of single-particle basis functions. Then we considered the transcorrelated method, where a similarity transformation was applied to reduce the convergence rate.

For the Gauss pseudopotential, a numerical approach is necessary to determine the s -wave scattering length. These techniques are generally inaccurate around the zero-energy bound states, where the s -wave scattering length is singular. We derived analytic expressions around these singularities, which accurately describe the singular behavior but they are inaccurate for deeply bound and the unbound states. Therefore, a general ansatz was considered, where applying a non-linear fit for the numerical results far from the singularity provides an accurate description for the whole attractive interaction regime.

Next, we had a closer look at the convergence properties of the Gauss pseudopotential. Despite the exponentially fast convergence, using only a small number of basis functions cannot resolve the finite length scale of the Gauss potential. In this

case, the finite basis expansion of the Gauss potential is equivalent to the pathological bare Dirac-delta contact interaction. We investigated the minimal number of single-particle basis functions, which can resolve the finite-range of the potential. We showed, through the example of few particles in a two-dimensional harmonic trap, that the minimal number of single-particle harmonic oscillator basis functions scales with $(l/R)^4$, where l is the characteristic length scale of the trapping potential and R is the length scale of the Gaussian potential. This can be reduced to a $(l/R)^2$ convergence rate by optimizing the length scale of the single-particle basis functions. However, this scaling property makes the computation inaccessible for physically realistic short-range potentials, where the length-scale of the system is several magnitudes larger than the length scale of the particle-particle interaction.

In order to improve the slow convergence properties of the exact diagonalization, we have applied the so-called transcorrelated approach. Instead of modifying the potential itself, the wave function ansatz is improved by considering the correct boundary conditions at the point of particle-particle coalescence with a Jastrow-factor². In order to solve the Schrödinger equation, the Jastrow-factor is transformed into the Hamiltonian with a similarity transformation. The obtained transcorrelated Hamiltonian is not Hermitian and apart from one- and two-body interactions contains a three-body interaction term as well. In order to improve the efficiency of the numerical implementation, we have suggested to approximate the three-body term with an effective two-body term. The energy can still easily be determined with imaginary time evolution. Although, the approximation of the three-body term introduces an error in the calculations, it can be eliminated by simultaneously decreasing the Jastrow-factor with increasing the size of the single-particle basis set. We examined the homogeneous gas in one dimension. In this case, the convergence of the energy is M^{-1} , where M is the number of single-particle plane-wave basis functions. Applying the well-known renormalization approach the convergence can be increased to M^{-2} , which can be further improved to M^{-3} by the transcorrelated approach.

Comparing the obtained cubic convergence of the transcorrelated approach with

an exponential convergence of the Gaussian potential we find that the later one still performs better in the asymptotic limit. However, in practice to access the exponentially fast converging regime the required number of single-particle basis functions has to be extremely large, which is not accessible with the current computational resources. The cubic convergence of the transcorrelated approach can be accessible at least in the few-particle regime. Although we have only tested this approach on a homogeneous gas, the convergence is expected to be the same for an inhomogeneous gas in a trap, because the convergence is primarily determined by the particle-particle interaction itself.

Chapter 7

Outlook

Based on the significant improvement of the convergence behavior in the transcorrelated approach, we plan to continue the investigation in that direction. First, we would like to analyze the effect of the three-body terms, which are approximated by effective two-body terms in Sec. 5.2.6. There the correlation factor has to be decreased simultaneously by the increasing number of single-particle basis functions in order to eliminate the artificial bias from the calculations. Considering the exact form of the three-body terms it is possible to consider an optimal fixed correlation factor, which can improve the convergence properties.

Alternative improvement in our methodology can be the optimization of the correlation factor itself. The correlation factor has to reproduce the cusp at the coalescence point. As the long-range property of the wave function is unknown, we would like to describe that part completely with the exact diagonalization approach. Therefore, the correlation factor is required to quickly decay to a constant function to avoid any numerical difficulties. In Sec. 5.3 we considered the homogeneous system, where due to the plane-wave basis the correlation factor is considered in momentum space. In this case, the correlation factor has a $1/k^2$ momentum tail, while for small momentums it has to decay to a constant function. The two limits are matched together with a simple cutoff in Sec. 5.2.2 providing a simple way to evaluate the matrix elements. However, it introduces slowly decaying oscillations in the real space, which can lead to possible numerical artifacts in the calculations. We plan to examine the effect of this oscillations and consider

different correlation factors, where the oscillation can be damped and the decay can be accelerated.

A natural extension of this approach is to apply it to trapped inhomogeneous systems. As the convergence rate at strong interactions principally determined by the interaction between the particles, the convergence properties should be the same for trapped and for homogeneous systems. Moreover, the implementation of these systems should be straightforward. Applying the plane-wave basis functions it is only necessary to derive matrix elements of the trapping potential. The matrix elements of the particle-particle interaction described in Sec. 5.2.6 can be directly applied to inhomogeneous systems as well.

Another possible generalization can be the extension to two and three dimensions. While in one dimension at the coalescence point only the second derivative of the wave functions diverges, in higher dimensions the wave function itself is singular. Considering this singularity in the Jastrow factor, the convergence properties will potentially improve even more than in the one-dimensional case.

These methodological developments pave the way to describe reliably the strongly correlated Fermi gases. They can give a deeper understanding of the present experiments of ultracold fermions and can also suggest a parameter regime, where the indications of the elusive strongly correlated systems (e.g.: fractional quantum Hall effect, high-temperature superconductors) can be looked for. An alternative more direct advantage comes from the universality of these systems at the unitary regime. Improving these numerical approaches we can get a more accurate values for the universal parameters (e.g.: Bertsch, contact parameters), which are necessary to describe the physics of peculiar solid-state systems or neutron stars [191].

Appendix A

Boundary conditions for the scattering problem

For the case of simplicity we suppose a smooth non-singular interaction potential, which implies at least a second order smoothness of the wave function due to the second derivative in the Schrödinger equation (3.6). However, the obtained boundary conditions are correct for the more general class of potentials defined by Eqs. (3.2) and (3.3), as well [192, 193].

In order to obtain the boundary conditions, let us multiply Eq.(3.6) by r^2 and consider the limit of $r \rightarrow 0$ as

$$\lim_{r \rightarrow 0} \left[-\frac{\hbar^2}{2\mu} \left(r^2 \frac{d^2}{dr^2} + r(n-1) \frac{d}{dr} \right) \Phi_{nD}(r) + r^2 (V(r) - E) \Phi_{nD}(r) \right] = 0 . \quad (\text{A.1})$$

Assuming to the potential and wave function are non-singular, the second term in Eq.(A.1) goes to zero in the limit of $r \rightarrow 0$. Therefore, it is enough to consider only the following differential equation:

$$\lim_{r \rightarrow 0} \left[-\frac{\hbar^2}{2\mu} \left(r^2 \frac{d^2}{dr^2} + r(n-1) \frac{d}{dr} \right) \Phi_{nD}^a(r) \right] = 0 , \quad (\text{A.2})$$

where $\Phi_{nD}^a(r)$ is asymptotic solution of $\Phi_{nD}(r)$ in the origin. Let us consider first the two- and three dimensional cases, where we have the following solutions:

$$\Phi_{2D}^a(r) = d_{2D} \ln(r) + c_{2D} , \quad (\text{A.3})$$

$$\Phi_{3D}^a(r) = \frac{d_{3D}}{r} + c_{3D} . \quad (\text{A.4})$$

The parameters d_{2D} , c_{2D} , d_{3D} and c_{3D} are arbitrary constants. The functions $\ln(r)$ and $1/r$ are singular at $r = 0$, which would provide a non-smooth wave function. Moreover, in the kinetic part the second derivative would be a Dirac-delta function, which cannot be compensated by the potential part in the Schrödinger equation [192]. Hence, these irregular parts should be eliminated by setting the scalar factors d_{2D} and d_{3D} to 0. Choosing the coefficients $c_{nD,1}$ and $c_{nD,2}$ to 1, we obtain the following boundary conditions:

$$\Phi_{2D}^a(r) = 1 , \quad \Phi_{3D}^a(r) = 1 . \quad (\text{A.5})$$

In one dimension the parity is a good quantum number, which can be shown by interchanging of r to $-r$ in Eq.(A.2),

$$\lim_{r \rightarrow 0} \left[-\frac{\hbar^2}{2\mu} r^2 \frac{d^2}{dr^2} \Phi_{1D}^a(-r) \right] = 0 . \quad (\text{A.6})$$

Matching Eq.(A.2) with Eq.(A.6), we find that $\Phi_{nD}(r)$ can either be an even or an odd function. The s -wave symmetry demands an even solution, and hence we can choose a solution with

$$\Phi_{1D}^a(r) = 1 , \quad (\text{A.7})$$

fixing the normalisation constant. Collecting the asymptotic solutions (A.5) and (A.7) into one expression and calculating the derivative, we obtain suitable boundary conditions for an arbitrary number of dimensions (1–3):

$$\Phi_{nD}(0) = 1 \quad \text{and} \quad \Phi'_{nD}(0) = 0 .$$

Here, the first condition sets the norm of the wave function, while the second one selects the correct symmetry in one dimension, and excludes the singular solutions in two and three dimensions.

Appendix B

Accuracy of the s -wave scattering length in three dimensions at the singularity

In three dimensions the accuracy of the s -wave scattering length is limited mainly by the accuracy of the position W_1 of the first singularity. We determine this position using the numerical differential equation solver by finding the value of V_0 where the scattering length changes sign. The accuracy of this position can be checked by increasing the accuracy of the calculation itself. We found that W_1 can be determined with very good accuracy of 12 digits when $p = 11$.

The value of W_1 can in principle also be obtained by diagonalizing the Hamiltonian in a plane-wave basis and determining the value of V_0 where the ground state energy crosses zero, extrapolating to the limits of infinite box size and basis set. We found a value that is consistent with the result from the differential equation solver to three digits of accuracy but were not able to reach higher accuracy with the diagonalization procedure due to limitations of the extrapolation procedures. Thus we have used values extracted from the differential equation solver for the numerical results presented in this paper.

The s -wave scattering length is plotted with different accuracy of W_1 in Fig. B.1. The parameters α_i and the W_j ($j > 1$) are set according to Table 3.3 and are kept unchanged. The poles with the minimums on the error curves correspond to

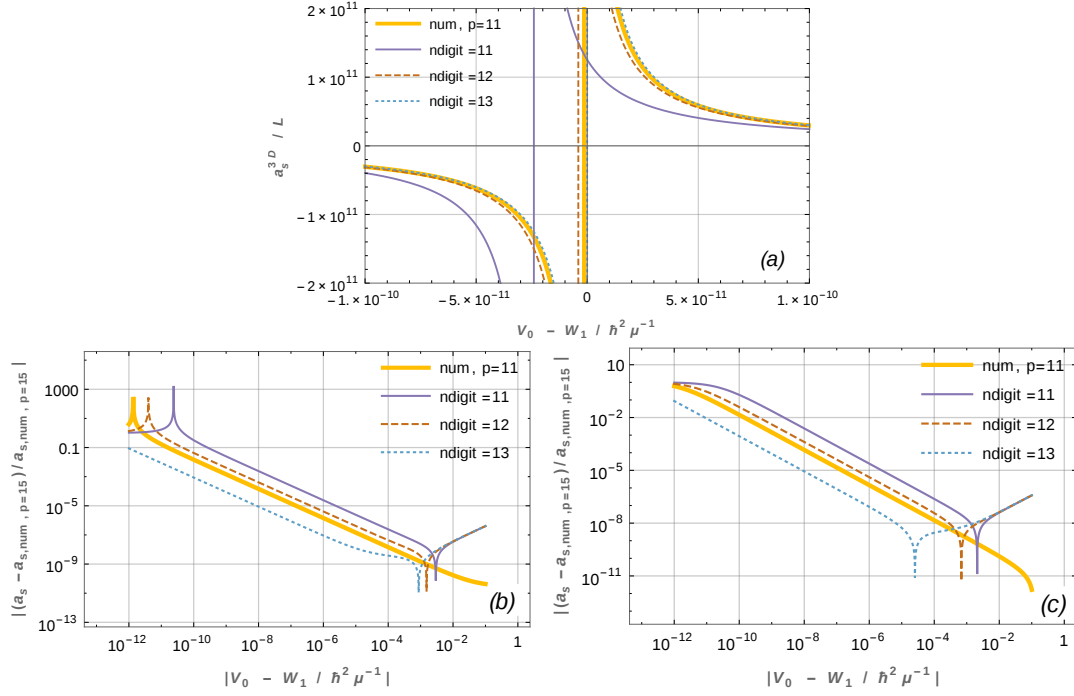


FIGURE B.1: Importance of the location of the first pole on the accuracy of the scattering length in three dimensions. Panel (a): s -wave scattering length from the numerical and the approximate expressions. In the approximate expressions, the scattering length is calculated with varying precision (ndigit decimal digits) of the position of the first singularity W_1 . Panels (b) and (c): The errors of the approximate and numerical values of the scattering length. $V_0 < W_1$ for panel (b) and $V_0 > W_1$ for panel (c). Reference values for determining the zero points of the x and y axes, respectively, are calculated by numerical calculations with high level of accuracy ($p = 15$ for a_s ; reference value $W_1 = 2.684004650924\hbar^2/\mu$).

the crossing of the reference curve. The poles with the maximums come from the inaccurate position of the singularity. Increasing the accuracy of W_1 significantly improves a_s^{3D} as well. In the main part of the paper ndigit = 12 decimal digits of accuracy are used for W_1 , where the relative error is below 10^{-5} , if the potential strength is within $W_1 - 10^{-6}\hbar^2/\mu < V_0 < W_1 + 10^{-6}\hbar^2/\mu$.

Appendix C

Alternative derivation of the approximate expressions for the s -wave scattering length

C.1 Three-dimensional case

Let us introduce new dimensionless variables

$$y = r/L, \tag{C.1}$$

$$\eta = V_0\mu/\hbar^2, \tag{C.2}$$

with which the Schrödinger equation (3.6) can be written in the following form

$$\left(\frac{d^2}{dy^2} + 2y \frac{d}{dy} + \eta \exp(-y^2) \right) \tilde{\Phi}_{3D}(y) = E \tilde{\Phi}_{3D}(y). \tag{C.3}$$

One can see from the definitions of the scattering length (3.10) and Eqs. (C.1), (C.3) that the ratio a_s/L depends only on the single dimensionless parameter η . In the following let us consider the $E = 0$ case in order to determine the s -wave scattering length.

The Schrödinger equation (C.3) can be transformed [with $\tilde{u}_{3D}(y) = y\tilde{\Phi}_{3D}(y)$] to the Lippmann-Schwinger equation [194],

$$\tilde{u}_{3D}(y) = y - \eta \int_0^y dx (y-x) \exp(-x^2) \tilde{u}_{3D}(x) . \quad (\text{C.4})$$

The *s*-wave scattering length can be expressed with a simple form if we substitute Eqs.(C.1) and (C.4) into Eq.(3.10),

$$a_s^{3D}/L = c_2/(c_1 + 1) , \quad (\text{C.5})$$

where

$$c_1 = -\eta \int_0^\infty dx \exp(-x^2) \tilde{u}_{3D}(x) , \quad (\text{C.6})$$

$$c_2 = -\eta \int_0^\infty dx x \exp(-x^2) \tilde{u}_{3D}(x) . \quad (\text{C.7})$$

Let us solve Eq. (C.4) with iterations. In the first step, we consider $\eta = 0$ on the right hand side,

$$\tilde{u}_{3D}^{(0)}(y) = y .$$

Substituting it into Eqs.(C.5)-(C.7) the zero-order approximation for the scattering length can be obtained,

$$\frac{\bar{a}_s^{3D}}{L} = -\frac{\sqrt{\pi}}{4} \frac{\eta}{1 - \frac{\eta}{2}} , \quad (\text{C.8})$$

which is equivalent to the analytical expression (3.27) in the main text.

C.2 One-dimensional case

In one dimension the Lippmann-Schwinger equation and the approximate expression of scattering length are derived analogously to the three dimensional case,

$$\tilde{u}_{1D}(y) = 1 - \eta \int_0^y dx (y-x) \exp(-x^2) \tilde{u}_{1D}(x) , \quad (\text{C.9})$$

$$a_s^{1D}/L = (c_2 - 1)/c_1 , \quad (\text{C.10})$$

with the same relations (C.6) and (C.7) for the constants c_1 and c_2 as in the three dimensional case. The difference from the three-dimensional solution arises from the different boundary conditions (3.17) and (3.18).

We solve Eq.(C.9) iteratively. In the first step we consider $\tilde{u}_{1D}^{(0)}(y) = 1$, from which the first order wave function and zero-order scattering length can be obtained,

$$\bar{u}_{1D}(y) = 1 - \frac{\eta}{2} \left[e^{-y^2} + \sqrt{\pi} y \operatorname{erf}(y) - 1 \right] , \quad (\text{C.11})$$

$$\frac{\bar{a}_s^{1D}}{L} = \frac{2}{\sqrt{\pi}} \frac{1}{\eta} + \frac{1}{\sqrt{\pi}} . \quad (\text{C.12})$$

The first-order scattering length, obtained with Eq. (C.11), is given by

$$\frac{\bar{a}_s^{1D}}{L} = \frac{2}{\sqrt{\pi}} \frac{1}{\eta} + \sqrt{\frac{2}{\pi}} + O(\eta) . \quad (\text{C.13})$$

Interestingly, the zeroth- and first-order term recover Eqs. (3.31) and (3.32) from the main text.

C.3 Two-dimensional case

In two dimensions, the Lippmann-Schwinger equation for the function $\tilde{\Phi}_{2D}(y)$, obeying the Schrödinger equation (C.3), takes the form [195]

$$\tilde{\Phi}_{2D}(y) = 1 - \eta \int_0^y dx x \ln(y/x) \exp(-x^2) \tilde{\Phi}_{2D}(x) . \quad (\text{C.14})$$

Comparing its long-range asymptotics with the definition (3.10) and using Eq. (C.1), we derive

$$a_s^{2D}/L = e^{\frac{c_1-1}{c_2}-\gamma+\log 2}, \quad (\text{C.15})$$

where

$$c_1 = -\eta \int_0^{+\infty} dx \log(x) \exp(-x^2) \tilde{\Phi}_{2D}(x), \quad (\text{C.16})$$

$$c_2 = -\eta \int_0^{+\infty} dx x \exp(-x^2) \tilde{\Phi}_{2D}(x). \quad (\text{C.17})$$

Similar to the previous sections, the zero-order approximation for the scattering length is obtained with the zero-order function $\tilde{\Phi}_{2D}^{(0)}(x) = 1$,

$$\bar{a}_s^{2D}/L = 2e^{\frac{-3\gamma}{2}+\frac{2}{\eta}}. \quad (\text{C.18})$$

The first-order wave function, obtained with the first iteration, is given by

$$\bar{\tilde{\Phi}}_{2D}(y) = 1 - \frac{\eta}{4} [\gamma + 2 \log(y) - \text{Ei}(-y^2)], \quad (\text{C.19})$$

where $\text{Ei}(z) = -\int_{-z}^{\infty} \frac{e^{-t}}{t} dt$ is the exponential integral function. Substituting it into Eqs. (C.16), (C.17) and using (C.15) gives us

$$\bar{\bar{a}}_s^{2D}/L = \sqrt{8} e^{\frac{-3\gamma}{2}+\frac{2}{\eta}+O(\eta)}. \quad (\text{C.20})$$

As it can be seen the obtained Eqs.(C.18) and (C.20) are equivalent to Eqs.(3.37) and (3.38) from the main text.

Appendix D

Derivation of approximate formula (3.32) for the one-dimensional s -wave scattering length

As we previously discussed in Appendix (A), the one-dimensional wave function $u_{1D}(r)$ is even, hence, its power series expansion can be written in the following form:

$$u_{1D}(r) = \sum_{k=1}^{\infty} b_k r^{2k} . \quad (\text{D.1})$$

Substituting back Eq.(D.1) into Eq.(3.15), we got the following differential equation:

$$u_{1D}''(r) = -V_0 e^{-r^2} \sum_{k=1}^{\infty} b_k r^{2k} , \quad (\text{D.2})$$

where b_0 is chosen to one due to the boundary condition (3.17). Using the usual Taylor-expansion identity as

$$b_k = \frac{1}{(2k)!} \left. \frac{d^{2k} u_{1D}(r)}{dr^{2k}} \right|_{r=0} ,$$

the parameters can be determined from Eq.(D.2) or its corresponding derivative form as

$$b_k = -\frac{V_0}{(2k)!} \sum_{l=0}^{k-1} \left[\binom{2k-2}{2l} (2k-2-2l)! b_{k-l-1} \frac{d^{2k}}{dr^{2k}} e^{-r^2} \Big|_{r=0} \right].$$

Using the following identities of the Hermite-polynomials:

$$\frac{d^{2k}}{dr^{2k}} e^{-r^2} \Big|_{r=0} = \mathcal{H}_{2k}(0) = (-1)^k \frac{(2k)!}{k!},$$

parameter b_k can be expressed as a linear combination of b_m ($m < k$) as

$$b_k = \frac{V_0}{2k(2k-1)} \sum_{l=0}^{k-1} (-1)^{l+1} \frac{b_{k-1-l}}{l!}. \quad (\text{D.3})$$

With Eq.(D.3) all the b_k -s can be determined, hence function $u_{1D}(r)$ can be given explicitly in the power series form.

In order to determine the s -wave scattering length, function $u_{1D}(r)$ should be examined in the asymptotic limit $r \rightarrow \infty$, which is difficult to handle in Eq.(D.1). However, a different form of $u_{1D}(r)$ can be considered as

$$u_{1D}(r) = 1 + V_0 c_0 - V_0 \left(e^{-r^2} \sum_{k=0}^{\infty} c_k r^{2k} + d\sqrt{\pi} r \operatorname{erf}(r) \right), \quad (\text{D.4})$$

where c_k and d are real coefficients. Equation (D.4) satisfies the Schrödinger equation (3.15), if the coefficients c_k and d are chosen properly. We can make a relation between Eqs.(D.2) and (D.4) by expanding in Taylor series of Eq.(D.4), where we obtain the following relations:

$$\begin{aligned} b_0 &= -2c_0 + 2c_1 + 4d, \\ b_1 &= 4c_0 - 10c_1 + 12c_2 - 4d, \\ b_{i+1} &= 4c_i - 2(4i+5)c_{i+1} + 2(i+2)(2i+3)c_{i+2}, \end{aligned} \quad (\text{D.5})$$

where $i \geq 1$. Considering the asymptotic limit of $r \rightarrow \infty$ in Eq.(D.4), the scattering length can be determined as

$$u_{1D}(r) \approx -d\sqrt{\pi}V_0 \left(r - \underbrace{\frac{1 + V_0c_0}{d\sqrt{\pi}V_0}}_{a_s^{1D}} \right). \quad (\text{D.6})$$

As it can be seen in Eq.(D.6), a_s^{1D} depends only two parameters: c_0 and d . However, these parameters are determined through an infinitely large system of linear equations (D.5). The s -wave scattering length can be further separated to two terms as

$$a_s^{1D} = \frac{2}{\sqrt{\pi}V_0} + \underbrace{\frac{1 + V_0c_0 - 2d}{d\sqrt{\pi}V_0}}_{a_{sc}^{1D}}. \quad (\text{D.7})$$

Considering only the first few terms of the summation in Eq.(D.2), the explicit values of the parameters c_k and d can be obtained assuming the following expressions:

$$c_0 = \frac{1}{2} + \sum_{k=1}^{\infty} \frac{k!}{2} b_k, \quad (\text{D.8})$$

$$d = \frac{1}{2} + \sum_{k=1}^{\infty} \frac{(2k-1)!!}{2^{k+1}} b_k. \quad (\text{D.9})$$

These statements can be proofed by induction. First, we suppose that Eqs.(D.8) and (D.9) are true up to the first n -th terms as

$$c_0^{(n)} = \frac{1}{2} + \sum_{k=1}^n \frac{k!}{2} b_k, \quad (\text{D.10})$$

$$d^{(n)} = \frac{1}{2} + \sum_{k=1}^n \frac{(2k-1)!!}{2^{k+1}} b_k, \quad (\text{D.11})$$

where parameters $c_0^{(n)}$ and $d^{(n)}$ gives back the original parameters c_0 and d as n goes to infinity. Considering a finite number of b_k , Eq.(D.5) terminates with the

following last two equations:

$$b_{n-1} = 4c_{n-2}^{(n)} - 2(4n-3)c_{n-1}^{(n)}, \quad (\text{D.12})$$

$$b_n = 4c_{n-1}^{(n)}. \quad (\text{D.13})$$

Increasing n to $n+1$, equations Eqs.(D.12) and (D.13) are supplemented with additional terms as

$$b_{n-1} = 4c_{n-2}^{(n+1)} - 2(4n-3)c_{n-1}^{(n+1)} + 2(2n-1)nc_n^{(n+1)}, \quad (\text{D.14})$$

$$b_n = 4c_{n-1}^{(n+1)} - 2(4n+1)c_n^{(n+1)}, \quad (\text{D.15})$$

$$b_{n+1} = 4c_n^{(n+1)}. \quad (\text{D.16})$$

Let us express $c_n^{(n+1)}$ in Eq.(D.16) and substitute back to Eqs.(D.14) and (D.15). If we introduce the following notations:

$$b'_{n-1} = b_{n-1} - \frac{(2n-1)n}{2}b_{n+1}, \quad (\text{D.17})$$

$$b'_n = b_n + \frac{4n+1}{2}b_{n+1}, \quad (\text{D.18})$$

then Eqs.(D.14) and (D.15) can be expressed in the following form:

$$b'_{n-1} = 4c_{n-2}^{(n+1)} - 2(4n-3)c_{n-1}^{(n+1)}, \quad (\text{D.19})$$

$$b'_n = 4c_{n-1}^{(n+1)}. \quad (\text{D.20})$$

Therefore by recognizing the similarity between the expressions (D.19)-(D.20) and (D.12)-(D.13) the equations (D.8) and (D.9) for $c_0^{(n+1)}$ and $d^{(n+1)}$ can be extended for the $n+1$ case as

$$c_0^{(n+1)} = \frac{1}{2} + \sum_{k=1}^{n-2} \frac{k!}{2} b_k + \frac{(n-1)!}{2} b'_{n-1} + \frac{n!}{2} b'_n, \quad (\text{D.21})$$

$$d^{(n+1)} = \frac{1}{2} + \sum_{k=1}^{n-2} \frac{(2k-1)!!}{2^{k+1}} b_k + \frac{(2n-3)!!}{2^n} b'_{n-1} + \frac{(2n-1)!!}{2^{n+1}} b'_n. \quad (\text{D.22})$$

Substituting back Eqs.(D.17) and (D.18) into Eqs.(D.21) and (D.22), we obtain

back Eqs.(D.10) and (D.11), but the sum goes until $n + 1$ justifying Eqs.(D.8) and (D.9).

Therefore, using Eqs.(D.8) and (D.9), the correction for the scattering length (D.7) can be given explicitly in the following form:

$$a_{sc}^{1D} = \frac{1 + \sum_{k=1}^{\infty} \left(k! b_k - \frac{(2k-1)!!}{2^{k-1}} \frac{b_k}{V_0} \right)}{\sqrt{\pi} \left(1 + \sum_{l=1}^{\infty} \frac{(2l-1)!!}{2^l} b_l \right)} .$$

Considering the limit $V_0 \rightarrow 0$ the following identities can be derived from Eq.(D.3):

$$\begin{aligned} \lim_{V_0 \rightarrow 0} b_k &= 0 , \\ \lim_{V_0 \rightarrow 0} \frac{b_k}{V_0} &= \frac{(-1)^k}{2(2k-1)k!} . \end{aligned}$$

Using the expression above the a_{sc}^{1D} can be expressed in the following simple form:

$$\lim_{V_0 \rightarrow 0} a_{sc}^{1D} = \frac{1}{\sqrt{\pi}} \left(1 + \sum_{k=1}^{\infty} (-1)^{k+1} \frac{(2k-3)!!}{(2k)!!} \right) = \sqrt{\frac{2}{\pi}} ,$$

where in the last equation we recognize the Taylor series of $\sqrt{1+x}$ at $x = 1$.

Appendix E

Fock-Darwin orbitals

In the main text of the paper, we discussed the convergence properties from an analytic point of view, where a product basis of one-dimensional basis functions provides an intuitive picture for the analysis. For numerical calculations it is more advantageous to apply a set of orbitals that satisfy the symmetries of the system. This helps to restrict the problem to a single irreducible representation of the symmetry operator, which reduces the required number of the many-body basis functions and thus the requirements for computer memory and CPU time.

We here use simultaneous eigenfunctions of the harmonic oscillator and the angular momentum operator known as Fock-Darwin orbitals

$$L \varphi_{n\ell} = \hbar \ell \varphi_{n\ell} ,$$

where L is the angular momentum operator, $\varphi_{n\ell}$ is the single-particle eigenfunction function, n and ℓ are quantum numbers with non-negative integer and integer values. The eigenfunction $\varphi_{n\ell}$ can be easily given in polar coordinates,

$$\varphi_{n,\ell}(r,\vartheta) = \sqrt{\frac{n!}{\tilde{l}^2 \pi (n + |\ell|)!}} \left(\frac{r}{\tilde{l}}\right)^{|\ell|} e^{-\frac{(r/\tilde{l})^2}{2}} e^{i\ell\vartheta} \mathcal{L}_n^{|\ell|} \left(\frac{r^2}{\tilde{l}^2}\right) , \quad (\text{E.1})$$

where $\mathcal{L}_n^{|\ell|}(x)$ is the associated Laguerre polynomial.

In the numerical calculation the finite single-particle basis set is chosen according to the total quantum number $\bar{n} = 2n + \ell$, representing a “shell”. All

single-particle orbitals are selected where \bar{n} is smaller or equal to a maximal value \bar{n}_{\max} .

The number M of spatial single-particle orbitals can be expressed with \bar{n}_{\max} ,

$$M = \frac{(\bar{n}_{\max} + 2)(\bar{n}_{\max} + 1)}{2} . \quad (\text{E.2})$$

In this paper the largest \bar{n}_{\max} is 20, which corresponds to 231 spatial orbital. The total number of the many-body basis functions for the three particles equal to around 6×10^6 . Considering only those many-body states with projected angular momentum of $0\hbar$, the computational space can be reduced about an order to 1.6×10^5 basis functions.

Appendix F

Evaluation of the matrix elements

The matrix elements of the Hamiltonian can be evaluated according to the Slater-Condon rules [98–100], which expresses them as a linear combination of one-particle integrals

$$\langle \varphi_{n_1 \ell_1} | H_{\text{osc}} | \varphi_{n_2 \ell_2} \rangle = \int d\mathbf{r} \varphi_{n_1 \ell_1}^*(\mathbf{r}) H_{\text{osc}} \varphi_{n_2 \ell_2}(\mathbf{r}),$$

and two-particle integrals

$$\langle \varphi_{n_1 \ell_1} \varphi_{n_2 \ell_2} | V | \varphi_{n_3 \ell_3} \varphi_{n_4 \ell_4} \rangle = \int d\mathbf{r}_1 d\mathbf{r}_2 \varphi_{n_1 \ell_1}^*(\mathbf{r}_1) \varphi_{n_2 \ell_2}^*(\mathbf{r}_2) V(\mathbf{r}_1 - \mathbf{r}_2) \varphi_{n_3 \ell_3}(\mathbf{r}_1) \varphi_{n_4 \ell_4}(\mathbf{r}_2).$$

The integrals are calculated with the single-particle basis described in Appendix E. The explicit expressions are given in the following sections.

F.1 Evaluation of one-particle integrals

The one-particle integral can be evaluated analytically providing an easily implementable formula

$$\begin{aligned} \langle \varphi_{n_1 \ell_1} | \hat{H}_{\text{osc}} | \varphi_{n_2 \ell_2} \rangle &= \frac{\delta_{\ell_1 \ell_2} \hbar \omega}{2} \left(\frac{1 + (\tilde{l}/l)^4}{(\tilde{l}/l)^2} (2n_1 + |\ell_1| + 1) \delta_{n_1 n_2} + \right. \\ &\quad \left. + \frac{1 - (\tilde{l}/l)^4}{(\tilde{l}/l)^2} \sqrt{n_1(n_1 + |m_1|)} \delta_{n_1, n_2+1} + \frac{1 - (\tilde{l}/l)^4}{(\tilde{l}/l)^2} \sqrt{(n_1 + 1)(n_1 + |m_1| + 1)} \delta_{n_1, n_2-1} \right). \end{aligned}$$

F.2 Evaluation of two-particle integrals

First, let us transform out the unit length of the harmonic oscillator

$$\begin{aligned} \langle \varphi_{n_1 \ell_1} \varphi_{n_2 \ell_2} | -\frac{V_0/\hbar\omega}{(R/l)^2} e^{-\frac{|\mathbf{r}_2/l - \mathbf{r}_1/l|^2}{(R/l)^2}} | \varphi_{n_3 \ell_3} \varphi_{n_4 \ell_4} \rangle = \\ = \frac{l^2}{\tilde{l}^2} \langle \varphi_{n_1 \ell_1} \varphi_{n_2 \ell_2} | -\frac{V_0/\hbar\omega}{(R/\tilde{l})^2} e^{-\frac{|\mathbf{r}_2/\tilde{l} - \mathbf{r}_1/\tilde{l}|^2}{(R/\tilde{l})^2}} | \varphi_{n_3 \ell_3} \varphi_{n_4 \ell_4} \rangle , \end{aligned}$$

which transfers the dependence of the unit length to a scale factor. In the following we consider only the remaining matrix element on the right hand side, where both the basis function and the operator have the same unit length.

The direct evaluation of the matrix elements with the single-particle orbitals $\varphi_{n\ell}$ defined in Appendix E is numerically unstable. Therefore, the integrals are calculated in Cartesian orbitals

$$\phi_{n_x n_y}(x, y) = \chi_{n_x}(x) \chi_{n_y}(y) , \quad (\text{F.1})$$

$$\chi_n(x) = \frac{1}{\sqrt{\sqrt{\pi} 2^n n! \tilde{l}}} e^{-\frac{x^2}{2\tilde{l}^2}} \mathcal{H}_n(x/\tilde{l}) , \quad (\text{F.2})$$

where $\phi_{n_x n_y}(x, y)$ is the two-dimensional and $\chi_{n_x}(x)$ is the one-dimensional Cartesian function, and $\mathcal{H}_n(x)$ is the n -th order Hermite polynomial. The function $\phi_{n_x n_y}(x, y)$ can be used as a basis for expanding the single-particle basis $\varphi_{n\ell}$ [196],

$$|\varphi_{n\ell}\rangle = \sum_{n_x n_y}^{n_x + n_y = 2n + |\ell|} d_{n_x n_y}^{n\ell} |\phi_{n_x n_y}\rangle , \quad (\text{F.3})$$

where $d_{n_x, n_y}^{n, \ell}$ is the Wigner's small d -matrix [60]. Then the two-particle integral in the basis of $\varphi_{n\ell}$ can be calculated with multiple unitary transformations

$$\begin{aligned} \langle \varphi_{n\ell} \varphi_{m\ell'} | V | \varphi_{p\ell''} \varphi_{q\ell'''} \rangle = \\ = \sum_{\substack{n_x n_y m_x m_y \\ p_x p_y q_x q_y}} d_{n_x n_y}^{n\ell*} d_{m_x m_y}^{m\ell'*} d_{p_x p_y}^{p\ell''} d_{q_x q_y}^{q\ell'''} \langle \phi_{n_x n_y} \phi_{m_x m_y} | V | \phi_{p_x p_y} \phi_{q_x q_y} \rangle , \end{aligned} \quad (\text{F.4})$$

where the summation indices are restricted similarly to Eq.(F.3). Using Eq.(F.1) the Cartesian integral can be separated according to the spatial variables

$$\langle \phi_{n_x n_y} \phi_{m_x m_y} | \hat{V} | \phi_{p_x p_y} \phi_{q_x q_y} \rangle = -\frac{V_0 \tilde{l}^4}{\pi R^2} I_{p_x q_x}^{n_x m_x} I_{p_y q_y}^{n_y m_y}, \quad (\text{F.5})$$

where the tensor I_{pq}^{nm} can be given as

$$I_{pq}^{nm} = \frac{1}{\sqrt{2^{n+m+p+q} (n!) (m!) (p!) (q!)}} \cdot \int_{-\infty}^{\infty} dx_1 \int_{-\infty}^{\infty} dx_2 \mathcal{H}_n(x_1) \mathcal{H}_m(x_2) \mathcal{H}_p(x_1) \mathcal{H}_q(x_2) e^{-(x_1^2+x_2^2)} e^{-\frac{(x_1-x_2)^2}{R'^2}},$$

where $R' = R/l$. Using the expansion of the Hermite polynomials

$$\frac{\mathcal{H}_n(x)}{2^n n!} = \sum_i^n h_i^n x^i,$$

the tensor I_{pq}^{nm} can be expressed with the following summations:

$$I_{pq}^{nm} = \delta_{\text{mod}(n+m+p+q,2),0} \sum_i^n \sum_k^p \sum_j^m \sum_l^q h_i^n h_k^p h_j^m h_l^q g_{i+k,j+l}, \quad (\text{F.6})$$

$$g_{a,b} = \int_{-\infty}^{\infty} dx_1 \int_{-\infty}^{\infty} dx_2 x_1^a x_2^b e^{-(x_1^2+x_2^2)} e^{-\frac{(x_1-x_2)^2}{R'^2}}. \quad (\text{F.7})$$

Although integral (F.7) can be evaluated analytically, the summation in Eq.(F.6) contains the difference of large numbers, which decreases the numerical accuracy. In order to improve the numerical determination, we expand $g_{a,b}$ as a sum of $g_{r,0}$,

$$g_{a,b} = \sum_{r=a}^{a+b} e_r^{ab} g_{r,0} \delta_{\text{mod}(r,2),0}, \quad (\text{F.8})$$

where $\text{mod}(x, y)$ is the modulo function [197] and the coefficients e_r^{ab} can be obtained with a recursive algorithm:

$$e_r^{a,b} = \frac{(b-1)R'^2 e_r^{a,b-2} + e_r^{a+1,b-1}}{2R'^2 + 1}, \quad (\text{F.9})$$

$$e_a^{a,0} = 1, \quad (\text{F.10})$$

$$e_a^{a-1,1} = \frac{1}{2R'^2 + 1}. \quad (\text{F.11})$$

The equations (F.9) – (F.11) can be derived with integration by parts from the integral (F.7).

Let us substitute Eq.(F.8) into Eq.(F.6)

$$I_{pq}^{nm} = \delta_{\text{mod}(n+m+p+q,2),0} \sum_i^n \sum_k^p \sum_j^m \sum_l^q h_i^n h_k^p h_j^m h_l^q \sum_{r=i+k}^{i+k+j+l} e_r^{i+k,j+l} g_{r,0} \delta_{\text{mod}(r,2),0}, \quad (\text{F.12})$$

where the obtained expression is still numerically unstable due to alternating signs of the coefficients h_i^n and the increasing value of $g_{r,0}$ with r . In order to alleviate these numerical inaccuracies we extend the definition of the coefficient $e_r^{i+k,j+l}$ to smaller indices of r ,

$$e_r^{i+k,j+l} = 0, \quad \text{if} \quad 0 \leq r < i+k. \quad (\text{F.13})$$

Hence, the summation in Eq.(F.12) can be reordered and all of the coefficients can be wrapped into the coefficient D_r ,

$$I_{pq}^{nm} = \delta_{\text{mod}(n+m+p+q,2),0} \sum_{r=0}^{n+m+p+q} D_r g_{r,0}, \quad (\text{F.14})$$

$$D_r = \sum_i^n \sum_k^p \sum_j^m \sum_l^q h_i^n h_k^p h_j^m h_l^q e_r^{i+k,j+l}. \quad (\text{F.15})$$

The relation between the neighboring $g_{a,0}$ can be determined with integration by parts of the integral (F.7),

$$g_{a,0} = \frac{(a-1)(2R'^2 + 1)}{4R'^2 + 4} g_{a-2,0}. \quad (\text{F.16})$$

n_1	ℓ_1	n_2	ℓ_2	n_3	ℓ_3	n_4	ℓ_4	$\langle \varphi_{n_1 \ell_1} \varphi_{n_2 \ell_2} V \varphi_{n_3 \ell_3} \varphi_{n_4 \ell_4} \rangle$
0	0	0	0	0	0	0	0	-0.248756219
4	2	15	-5	8	4	13	11	-0.005826144139
15	5	15	-7	15	-3	15	1	0.003990385223
20	0	20	0	20	0	20	0	-0.02335706042

 TABLE F.1: Examples for the integrals at $R/\tilde{l} = 0.05$ and at $V_0 = 1\hbar\omega$.

The numerical accuracy of the summation in Eq.(F.14) can be increased if we apply the relation (F.16) and evaluate coefficient D_r starting from the largest index:

$$\tilde{D}_{r-2} = \frac{(r-1)(2R'^2+1)}{4R'^2+4} \tilde{D}_r + D_{r-2}, \quad (\text{F.17})$$

$$\tilde{D}_{n+m+p+q} = D_{n+m+p+q}. \quad (\text{F.18})$$

The coefficient \tilde{D}_0 provides a simple expression for Eq.(F.12)

$$I_{pq}^{nm} = \delta_{\text{mod}(n+m+p+q,2),0} \tilde{D}_0 g_{0,0}, \quad (\text{F.19})$$

where $g_{0,0}$ can be determined by explicitly integrating the integral (F.7)

$$g_{0,0} = \frac{R'}{\sqrt{R'^2+1}}. \quad (\text{F.20})$$

For determining the two-particle integrals on the computer, we use the following algorithm: First, we determine the coefficients $e_r^{i+j+k+l}$ with Eqs.(F.9)–(F.11) and Eq.(F.13). After that, we calculate the coefficients D_r and \tilde{D}_r with Eqs.(F.15), (F.17), and (F.18). Then the tensor I_{pq}^{nm} can be determined from Eqs.(F.19) and (F.20), with which the two-particle integrals can be easily evaluated from Eqs.(F.5) and (F.4). With the described algorithm the two-particle integrals are accurate at least for the first eight decimal digits, where the maximal total quantum number $(2n + \ell)$ is set to 20 for the single-particle basis function $\varphi_{n\ell}$. Examples for the numerical values of the integral can be found in Table F.1.

Appendix G

Evaluation of the infinite sum in Eq.(5.47)

The infinite summation is easier to evaluate if we make the substitutions $k = 2\pi n/L$, $k' = 2\pi n'/L$ and $k_c = 2\pi n_c/L$ into the sum as

$$W\left(\frac{2\pi n}{L}\right) = \frac{L^2}{a^2\pi^2} \sum_{n'}^{|n'|, |n-n'| \geq n_c} \frac{1}{n'} \frac{1}{n-n'}, \quad (\text{G.1})$$

where the summation index is integer.

Let us first consider the case $n = 0$, where the sum is symmetric to the swap of the sign of n' . Therefore, we can write Eq.(G.1) in the following way:

$$W(0) = -\frac{2L^2}{a^2\pi^2} \sum_{n'=n_c}^{\infty} \frac{1}{n'^2}. \quad (\text{G.2})$$

Using the identity of $\sum_{n'=1}^{\infty} = \pi^2/6$, we can expand Eq.(G.2) with finite summations, as

$$W(0) = -\frac{2L^2}{a^2\pi^2} \left(\frac{\pi^2}{6} - \sum_{n'=1}^{n_c-1} \frac{1}{n'^2} \right).$$

Now let us consider the case $n > 0$. If $n < 2n_c$ we get the following expression:

$$W\left(\frac{4\pi n_c}{L} > \frac{2\pi n}{L} > 0\right) = \frac{L^2}{a^2\pi^2} \left(\sum_{n'=-\infty}^{-n_c} \frac{1}{n'} \frac{1}{n-n'} + \sum_{n'=n+n_c}^{\infty} \frac{1}{n'} \frac{1}{n-n'} \right), \quad (\text{G.3})$$

which is supplemented by an additional term, if $n \geq n_c$, as

$$W\left(\frac{2\pi n}{L} \geq \frac{4\pi n_c}{L}\right) = \frac{L^2}{a^2\pi^2} \left(\sum_{n'=-\infty}^{-n_c} \frac{1}{n'} \frac{1}{n-n'} + \sum_{n'=n+n_c}^{\infty} \frac{1}{n'} \frac{1}{n-n'} + \sum_{n'=n_c}^{n-n_c} \frac{1}{n'} \frac{1}{n-n'} \right). \quad (\text{G.4})$$

Let us consider first Eq.(G.3), and swap the sign of n' in the first sum and merge all the terms, where n' is larger than $n + n_c$,

$$W\left(\frac{4\pi n_c}{L} > \frac{2\pi n}{L} > 0\right) = \frac{L^2}{a^2\pi^2} \left(- \sum_{n'=n_c}^{n+n_c-1} \frac{1}{n'} \frac{1}{n+n'} + \sum_{n'=n+n_c}^{\infty} \frac{1}{n'} \underbrace{\left(\frac{1}{n-n'} - \frac{1}{n+n'} \right)}_{\frac{2}{n^2-n'^2}} \right). \quad (\text{G.5})$$

The digamma function $\psi(x)$, can be used to simplify the sum above by using the following identities:

$$\sum_{n'=a}^{\infty} \frac{1}{n^2 - n'^2} = \frac{\psi(a-n) - \psi(a+n)}{2n}, \quad (\text{G.6})$$

$$\sum_{n'=a}^b \frac{1}{n'} \frac{1}{n+n'} = \frac{\psi(1+b) + \psi(a+n) - \psi(1+b+n) - \psi(a)}{n}, \quad (\text{G.7})$$

which can be derived from the series expansion of the digamma function as

$$\psi(x) = -\gamma + \sum_{l=0}^{\infty} \frac{x-1}{(l+1)(l+x)}.$$

Using Eqs.(G.6) and (G.7), Eq.(G.5) can be written in the following form:

$$W\left(\frac{4\pi n_c}{L} > \frac{2\pi n}{L} > 0\right) = \frac{2L^2}{a^2\pi^2 n} [\psi(n_c) - \psi(n+n_c)]. \quad (\text{G.8})$$

By using the following property of the digamma function:

$$\psi(x+1) = \psi(x) + \frac{1}{x},$$

equation (G.8) can be written in the following numerically treatable form:

$$W\left(\frac{4\pi n_c}{L} > \frac{2\pi n}{L} > 0\right) = -\frac{2L^2}{a^2\pi^2 n} \sum_{n'=n_c}^{n+n_c-1} \frac{1}{n'}.$$

In the case of $n \geq 2n_c$ and $n < 0$, with a similar derivation, we got the following expressions:

$$\begin{aligned} W\left(\frac{2\pi n}{L} \geq \frac{4\pi n_c}{L}\right) &= -\frac{2L^2}{a^2\pi^2} \left(\frac{1}{n} \sum_{n'=n_c}^{n+n_c-1} \frac{1}{n'} - \frac{1}{2} \sum_{n'=n_c}^{n-n_c} \frac{1}{n'} \frac{1}{n-n'} \right), \\ W\left(-\frac{4\pi n_c}{L} < \frac{2\pi n}{L} < 0\right) &= \frac{2L^2}{a^2\pi^2 n} \sum_{n'=n_c}^{n_c-n-1} \frac{1}{n'}, \\ W\left(\frac{2\pi n}{L} \leq -\frac{4\pi n_c}{L}\right) &= \frac{2L^2}{a^2\pi^2} \left(\frac{1}{n} \sum_{n'=n_c}^{n_c-n-1} \frac{1}{n'} + \frac{1}{2} \sum_{n'=n_c-n}^{-n_c} \frac{1}{n'} \frac{1}{n-n'} \right). \end{aligned}$$

The asymptotic expression of $W\left(\frac{2\pi n}{L}\right)$ for large n can be also given,

$$W\left(\frac{2\pi n}{L}\right) = \frac{2L^2}{a^2\pi^2 |n|} \ln(|n|) + \mathcal{O}\left(\frac{1}{n^2}\right), \quad (\text{G.9})$$

where we use the following asymptotic expression of the digamma function,

$$\psi(x) = \ln(x) + \mathcal{O}\left(\frac{1}{x}\right).$$

Bibliography

- [1] L. H. Greene, J. Thompson, and J. Schmalian, *Rep. Prog. Phys.* **80**, 030401 (2017).
- [2] P. W. Anderson, *Science* **235**, 1196 (1987).
- [3] P. A. Lee, N. Nagaosa, and X.-G. Wen, *Rev. Mod. Phys.* **78**, 17 (2006).
- [4] A. Garg, M. Randeria, and N. Trivedi, *Nature Physics* **4**, 762 (2008).
- [5] H. Li, X. Zhou, S. Parham, T. J. Reber, H. Berger, G. B. Arnold, and D. S. Dessau, *Nature Communications* **9**, 26 (2018).
- [6] R. B. Laughlin, *Phys. Rev. Lett.* **50**, 1395 (1983).
- [7] F. D. M. Haldane, *Phys. Rev. Lett.* **51**, 605 (1983).
- [8] J. Maciejko and G. A. Fiete, *Nature Physics* **11**, 385 (2015).
- [9] A. Gezerlis and J. Carlson, *Phys. Rev. C* **77**, 032801 (2008).
- [10] D. J. Dean and M. Hjorth-Jensen, *Rev. Mod. Phys.* **75**, 607 (2003).
- [11] S. Gandolfi, A. Gezerlis, and J. Carlson, *Annual Review of Nuclear and Particle Science* **65**, 303 (2015).
- [12] A. Fabrocini, S. Fantoni, A. Y. Illarionov, and K. E. Schmidt, *Phys. Rev. Lett.* **95**, 192501 (2005).
- [13] E. Gull, O. Parcollet, and A. J. Millis, *Phys. Rev. Lett.* **110**, 216405 (2013).

-
- [14] J. LeBlanc, A. E. Antipov, F. Becca, I. W. Bulik, G. K.-L. Chan, C.-M. Chung, Y. Deng, M. Ferrero, T. M. Henderson, C. A. Jiménez-Hoyos, E. Kozik, X.-W. Liu, A. J. Millis, N. Prokof'ev, M. Qin, G. E. Scuseria, H. Shi, B. Svistunov, L. F. Tocchio, I. Tupitsyn, S. R. White, S. Zhang, B.-X. Zheng, Z. Zhu, and E. Gull, [Phys. Rev. X](#) **5**, 041041 (2015).
- [15] R. P. Feynman, [Int J Theor Phys](#) **21**, 467 (1982).
- [16] C. Gross and I. Bloch, [Science](#) **357**, 995 (2017).
- [17] C. Pethick and H. Smith, *Bose-Einstein Condensation in Dilute Gases*, 1st ed. (Cambridge University Press, 2002).
- [18] A. Görlitz, J. M. Vogels, A. E. Leanhardt, C. Raman, T. L. Gustavson, J. R. Abo-Shaeer, A. P. Chikkatur, S. Gupta, S. Inouye, T. Rosenband, and W. Ketterle, [Phys. Rev. Lett.](#) **87**, 130402 (2001).
- [19] M. C. Revelle, J. A. Fry, B. A. Olsen, and R. G. Hulet, [Phys. Rev. Lett.](#) **117**, 235301 (2016).
- [20] C. Chin, R. Grimm, P. Julienne, and E. Tiesinga, [Rev. Mod. Phys.](#) **82**, 1225 (2010).
- [21] C. A. Regal, C. Ticknor, J. L. Bohn, and D. S. Jin, [Nature](#) **424**, 47 (2003).
- [22] I. Boettcher, L. Bayha, D. Kedar, P. Murthy, M. Neidig, M. Ries, A. Wenz, G. Zürn, S. Jochim, and T. Enss, [Physical Review Letters](#) **116**, 045303 (2016).
- [23] K. Hueck, N. Luick, L. Sobirey, J. Siegl, T. Lompe, and H. Moritz, [Physical Review Letters](#) **120**, 060402 (2018).
- [24] A. Mazurenko, C. S. Chiu, G. Ji, M. F. Parsons, M. Kanász-Nagy, R. Schmidt, F. Grusdt, E. Demler, D. Greif, and M. Greiner, [Nature](#) **545**, 462 (2017).
- [25] F. Serwane, G. Zurn, T. Lompe, T. B. Ottenstein, A. N. Wenz, and S. Jochim, [Science](#) **332**, 336 (2011).

-
- [26] A. N. Wenz, G. Zurn, S. Murmann, I. Brouzos, T. Lompe, and S. Jochim, *Science* **342**, 457 (2013).
- [27] S. Murmann, F. Deuretzbacher, G. Zürn, J. Bjerlin, S. Reimann, L. Santos, T. Lompe, and S. Jochim, *Physical Review Letters* **115**, 215301 (2015).
- [28] G. Zürn, A. N. Wenz, S. Murmann, A. Bergschneider, T. Lompe, and S. Jochim, *Physical Review Letters* **111**, 175302 (2013).
- [29] A. M. Kaufman, B. J. Lester, C. M. Reynolds, M. L. Wall, M. Foss-Feig, K. R. A. Hazzard, A. M. Rey, and C. A. Regal, *Science* **345**, 306 (2014).
- [30] M. Popp, B. Paredes, and J. I. Cirac, *Phys. Rev. A* **70**, 053612 (2004).
- [31] N. Regnault and T. Jolicoeur, *Physical Review B* **70**, 241307 (2004).
- [32] H. Bethe, *Z. Physik* **71**, 205 (1931).
- [33] E. H. Lieb and W. Liniger, *Physical Review* **130**, 1605 (1963).
- [34] C. N. Yang, *Physical Review Letters* **19**, 1312 (1967).
- [35] M. Gaudin, *Physics Letters A* **24**, 55 (1967).
- [36] M. Girardeau, *Journal of Mathematical Physics* **1**, 516 (1960).
- [37] F. Deuretzbacher, D. Becker, J. Bjerlin, S. M. Reimann, and L. Santos, *Physical Review A* **90**, 013611 (2014).
- [38] A. G. Volosniev, D. V. Fedorov, A. S. Jensen, M. Valiente, and N. T. Zinner, *Nature Communications* **5**, 5300 (2014).
- [39] J. Levinsen, P. Massignan, G. M. Bruun, and M. M. Parish, *Science Advances* **1**, e1500197 (2015).
- [40] L. Pollet, *Reports on Progress in Physics* **75**, 094501 (2012).
- [41] M. Troyer and U.-J. Wiese, *Physical Review Letters* **94** (2005), [10.1103/PhysRevLett.94.170201](https://doi.org/10.1103/PhysRevLett.94.170201).

- [42] M. Iazzi, A. A. Soluyanov, and M. Troyer, *Physical Review B* **93**, 115102 (2016).
- [43] C. Wu and S.-C. Zhang, *Physical Review B* **71**, 155115 (2005).
- [44] Lei Wang, Ye-Hua Liu, Mauro Iazzi, Matthias Troyer, and Gergely Harcos, *Physical Review Letters* **115**, 250601 (2015).
- [45] A. Szabo and N. S. Ostlund, *Modern quantum chemistry: introduction to advanced electronic structure theory* (Dover Publications, Mineola, N.Y, 1996).
- [46] J. M. Zhang and R. X. Dong, *Eur. J. Phys.* **31**, 591 (2010).
- [47] T. Grining, M. Tomza, M. Lesiuk, M. Przybytek, M. Musiał, P. Massignan, M. Lewenstein, and R. Moszynski, *New Journal of Physics* **17**, 115001 (2015).
- [48] J. Carlson, S. Gandolfi, K. E. Schmidt, and S. Zhang, *Phys. Rev. A* **84**, 061602 (2011).
- [49] H. Shi, S. Chiesa, and S. Zhang, *Physical Review A* **92**, 033603 (2015).
- [50] G. H. Booth, A. J. W. Thom, and A. Alavi, *The Journal of Chemical Physics* **131**, 054106 (2009).
- [51] G. H. Booth, A. Grüneis, G. Kresse, and A. Alavi, *Nature* **493**, 365 (2012).
- [52] M. Lewenstein, A. Sanpera, and V. Ahufinger, *Ultracold atoms in optical lattices: simulating quantum many-body systems* (Oxford University Press, 2017) oCLC: 984744682.
- [53] G. Carleo and M. Troyer, *Science* **355**, 602 (2017).
- [54] J. Weiner, V. S. Bagnato, S. Zilio, and P. S. Julienne, *Reviews of Modern Physics* **71**, 1 (1999).
- [55] A. J. Leggett, *Reviews of Modern Physics* **73**, 307 (2001).
- [56] W. Ketterle and M. W. Zwierlein, *La Rivista del Nuovo Cimento* , 247 (2008).

- [57] E. Tiesinga, C. Williams, P. Julienne, K. Jones, P. Lett, and W. Phillips, [Journal of Research of the National Institute of Standards and Technology](#) **101**, 505 (1996).
- [58] Eric W. Weisstein, “[Legendre Polynomial](#),” (2018), from MathWorld—A Wolfram Web Resource.
- [59] H. Friedrich, *Theoretical Atomic Physics*, 3rd ed. (Springer-Verlag, Berlin Heidelberg, 2006).
- [60] L. D. Landau and E. M. Lifshitz, *Course of Theoretical Physics - Quantum Mechanics, Non-relativistic theory*, 3rd ed., Vol. 3 (Pergamon Press, 1977).
- [61] J. J. Sakurai and S. F. Tuan, *Modern quantum mechanics*, rev. ed ed. (Addison-Wesley Pub. Co, Reading, Mass, 1994).
- [62] S. Giorgini, L. P. Pitaevskii, and S. Stringari, [Reviews of Modern Physics](#) **80**, 1215 (2008).
- [63] E. Tiesinga, C. J. Williams, F. H. Mies, and P. S. Julienne, [Physical Review A](#) **61**, 063416 (2000).
- [64] P. R. Johnson, D. Blume, X. Y. Yin, W. F. Flynn, and E. Tiesinga, [New Journal of Physics](#) **14**, 053037 (2012).
- [65] M. Olshanii and V. Dunjko, [Physical Review Letters](#) **91**, 090401 (2003).
- [66] B. J. Verhaar, L. P. H. de Goey, J. P. H. W. van den Eijnde, and E. J. D. Vredenbregt, [Physical Review A](#) **32**, 1424 (1985).
- [67] J. Levinsen and M. M. Parish, in *Annual Review of Cold Atoms and Molecules*, Vol. 3 (World Scientific, 2015) pp. 1–75, doi: 10.1142/9789814667746_0001.
- [68] H. Bethe and R. Peierls, [Proceedings of the Royal Society A: Mathematical, Physical and Engineering Sciences](#) **148**, 146 (1935).
- [69] F. Deuretzbacher, K. Fredenhagen, D. Becker, K. Bongs, K. Sengstock, and D. Pfannkuche, [Physical Review Letters](#) **100**, 160405 (2008).

-
- [70] T. Busch, B.-G. Englert, K. Rzażewski, and M. Wilkens, *Foundations of Physics* **28**, 549 (1998).
- [71] M. A. García-March, B. Juliá-Díaz, G. E. Astrakharchik, J. Boronat, and A. Polls, *Physical Review A* **90**, 063605 (2014).
- [72] A. Dehkharghani, A. Volosniev, J. Lindgren, J. Rotureau, C. Forssén, D. Fedorov, A. Jensen, and N. Zinner, *Scientific Reports* **5**, 10675 (2015).
- [73] F. Werner and Y. Castin, *Phys. Rev. A* **86**, 013626 (2012).
- [74] X.-J. Liu, H. Hu, and P. D. Drummond, *Physical Review A* **82**, 023619 (2010).
- [75] X.-J. Liu, H. Hu, and P. D. Drummond, *Physical Review B* **82**, 054524 (2010).
- [76] B. D. Esry and C. H. Greene, *Physical Review A* **60**, 1451 (1999).
- [77] M. Rontani, G. Eriksson, S. Åberg, and S. M. Reimann, *Journal of Physics B: Atomic, Molecular and Optical Physics* **50**, 065301 (2017).
- [78] K. Huang and C. N. Yang, *Physical Review* **105**, 767 (1957).
- [79] K. Wódkiewicz, *Phys. Rev. A* **43**, 68 (1991).
- [80] M. Olshanii and L. Pricoupenko, *Physical Review Letters* **88**, 010402 (2001).
- [81] D. Blume, *Reports on Progress in Physics* **75**, 046401 (2012).
- [82] Z. Luo, C. E. Berger, and J. E. Drut, *Physical Review A* **93**, 033604 (2016).
- [83] Y. Castin, *Journal de Physique IV (Proceedings)* **116**, 89 (2004).
- [84] T. Ernst, D. W. Hallwood, J. Gulliksen, H.-D. Meyer, and J. Brand, *Physical Review A* **84**, 023623 (2011).
- [85] P. O. Bugnion, P. López Ríos, R. J. Needs, and G. J. Conduit, *Physical Review A* **90**, 033626 (2014).

-
- [86] A. Galea, H. Dawkins, S. Gandolfi, and A. Gezerlis, [Physical Review A **93**, 023602 \(2016\)](#).
- [87] J. von Stecher, C. H. Greene, and D. Blume, [Physical Review A **77**, 043619 \(2008\)](#).
- [88] K. S. Ranade, [Fortschritte der Physik **63**, 644 \(2015\)](#).
- [89] B. Mercier, *An Introduction to the Numerical Analysis of Spectral Methods* (Springer Berlin, Berlin, 2014) oCLC: 888455148.
- [90] S. Kvaal, [Phys. Rev. B **80**, 045321 \(2009\)](#).
- [91] W. H. Press, ed., *Numerical recipes: the art of scientific computing*, 3rd ed. (Cambridge University Press, Cambridge, UK ; New York, 2007) oCLC: ocn123285342.
- [92] Eric W. Weisstein, [“Exponential,”](#) (2018), from MathWorld—A Wolfram Web Resource.
- [93] R. V. Mises and H. Pollaczek-Geiringer, [ZAMM - Journal of Applied Mathematics and Mechanics / Zeitschrift für Angewandte Mathematik und Mechanik **9**, 58 \(1929\)](#).
- [94] C. Lanczos, [Journal of Research of the National Bureau of Standards **45**, 255 \(1950\)](#).
- [95] W. E. Arnoldi, [Quart. Appl. Math. **9**, 17 \(1951\)](#).
- [96] J. W. Demmel, *Applied numerical linear algebra* (Society for Industrial and Applied Mathematics, Philadelphia, 1997).
- [97] A. L. Fetter and J. D. Walecka, *Quantum theory of many-particle systems* (Dover Publications, Mineola, N.Y, 2003).
- [98] J. C. Slater, [Physical Review **34**, 1293 \(1929\)](#).
- [99] E. U. Condon, [Physical Review **36**, 1121 \(1930\)](#).

-
- [100] J. C. Slater, [Physical Review](#) **38**, 1109 (1931).
- [101] L. Pitaevskii and S. Stringari, *Bose-Einstein Condensation and Superfluidity* (Clarendon, Oxford, 2016).
- [102] Roger G. Newton, *Scattering Theory of Waves and Particles*, 2nd ed. (Springer Science+Business Media, LLC, 1982).
- [103] R. A. Doganov, S. Klaiman, O. E. Alon, A. I. Streltsov, and L. S. Cederbaum, [Physical Review A](#) **87**, 033631 (2013).
- [104] T. M. Whitehead, L. M. Schonenberg, N. Kongsuwan, R. J. Needs, and G. J. Conduit, [Physical Review A](#) **93**, 042702 (2016).
- [105] M. M. Forbes, S. Gandolfi, and A. Gezerlis, [Physical Review Letters](#) **106**, 235303 (2011).
- [106] J. Christensson, C. Forssén, S. Åberg, and S. M. Reimann, [Physical Review A](#) **79**, 012707 (2009).
- [107] S. Klaiman, A. U. J. Lode, A. I. Streltsov, L. S. Cederbaum, and O. E. Alon, [Physical Review A](#) **90**, 043620 (2014).
- [108] R. Beinke, S. Klaiman, L. S. Cederbaum, A. I. Streltsov, and O. E. Alon, [Physical Review A](#) **92**, 043627 (2015).
- [109] M. Imran and M. A. H. Ahsan, [Advanced Science Letters](#) **21**, 2764 (2015).
- [110] V. J. Bolsinger, S. Krönke, and P. Schmelcher, [Journal of Physics B: Atomic, Molecular and Optical Physics](#) **50**, 034003 (2017).
- [111] V. J. Bolsinger, S. Krönke, and P. Schmelcher, [Physical Review A](#) **96**, 013618 (2017).
- [112] A. Farrell and B. P. van Zyl, [Canadian Journal of Physics](#) **88**, 817 (2010).
- [113] A. Galea, T. Zielinski, S. Gandolfi, and A. Gezerlis, [Journal of Low Temperature Physics](#) **189**, 451 (2017).

-
- [114] M. M. Parish, B. Mihaila, E. M. Timmermans, K. B. Blagoev, and P. B. Littlewood, [Physical Review B](#) **71**, 064513 (2005).
- [115] A. Farrell and B. P. van Zyl, [Journal of Physics A: Mathematical and Theoretical](#) **43**, 015302 (2010).
- [116] K. M. Case, [Phys. Rev.](#) **80**, 797 (1950).
- [117] W. M. Frank, D. J. Land, and R. M. Spector, [Rev. Mod. Phys.](#) **43**, 36 (1971).
- [118] M. Andrews, [Am. J. Phys.](#) **44**, 1064 (1976).
- [119] B. J. Verhaar, J. P. H. W. v. d. Eijnde, M. A. J. Voermans, and M. M. J. Schaffrath, [Journal of Physics A: Mathematical and General](#) **17**, 595 (1984).
- [120] K. Fenech, P. Dyke, T. Pepler, M. Lingham, S. Hoinka, H. Hu, and C. Vale, [Physical Review Letters](#) **116**, 045302 (2016).
- [121] Wolfram Research, Inc., “Mathematica,” (2014).
- [122] S. Flügge, *Practical Quantum Mechanics* (Springer, Berlin, 1999).
- [123] L. W. Cheuk, M. A. Nichols, K. R. Lawrence, M. Okan, H. Zhang, E. Khatami, N. Trivedi, T. Paiva, M. Rigol, and M. W. Zwierlein, [Science](#) **353**, 1260 (2016).
- [124] M. Feld, B. Fröhlich, E. Vogt, M. Koschorreck, and M. Köhl, [Nature](#) **480**, 75 (2011).
- [125] G. Zürn, F. Serwane, T. Lompe, A. N. Wenz, M. G. Ries, J. E. Bohn, and S. Jochim, [Physical Review Letters](#) **108**, 075303 (2012).
- [126] S. Viefers, [Journal of Physics: Condensed Matter](#) **20**, 123202 (2008).
- [127] G. Möller, T. Jolicoeur, and N. Regnault, [Phys. Rev. A](#) **79**, 033609 (2009).
- [128] F. Deuretzbacher, K. Bongs, K. Sengstock, and D. Pfannkuche, [Phys. Rev. A](#) **75**, 013614 (2007).

-
- [129] M. Rontani, J. R. Armstrong, Y. Yu, S. Åberg, and S. M. Reimann, [Physical Review Letters](#) **102**, (2009).
- [130] M. A. García-March, B. Juliá-Díaz, G. E. Astrakharchik, T. Busch, J. Boronat, and A. Polls, [Physical Review A](#) **88**, 063604 (2013).
- [131] M. A. García-March, B. Juliá-Díaz, G. E. Astrakharchik, T. Busch, J. Boronat, and A. Polls, [New Journal of Physics](#) **16**, 103004 (2014).
- [132] Marcin Płodzień, Dariusz Wiater, Andrzej Chrostowski, and Tomasz Sowiński, arXiv:1803.08387 (2018).
- [133] H.-D. Meyer, F. Gatti, and G. Worth, eds., *Multidimensional quantum dynamics: MCTDH theory and applications* (Wiley-VCH, Weinheim : Chichester, 2009) oCLC: ocn295001065.
- [134] J. Carlson, S. Gandolfi, K. E. Schmidt, and S. Zhang, [Phys. Rev. A](#) **84**, 061602 (2011), arXiv:1107.5848 .
- [135] P. Jeszenszki, H. Luo, A. Alavi, and J. Brand, [Phys. Rev. A](#) **98**, 053627 (2018).
- [136] J. von Stecher, C. H. Greene, and D. Blume, [Physical Review A](#) **76**, 053613 (2007).
- [137] Y. Yan and D. Blume, [Physical Review Letters](#) **112**, 235301 (2014).
- [138] P. Mujal, A. Polls, and B. Juliá-Díaz, [Condensed Matter](#) **3**, 9 (2018).
- [139] P. Jeszenszki, A. Y. Cherny, and J. Brand, [Physical Review A](#) **97**, 042708 (2018).
- [140] Eric W. Weisstein, “[Ceiling](#),” (2018), from MathWorld—A Wolfram Web Resource.
- [141] D. S. Petrov, M. A. Baranov, and G. V. Shlyapnikov, [Physical Review A](#) **67**, 031601 (2003).
- [142] M. Randeria, J.-M. Duan, and L.-Y. Shieh, [Phys. Rev. Lett.](#) **62**, 981 (1989).

-
- [143] M. Schick, *Phys. Rev. A* **3**, 1067 (1971).
- [144] A. Y. Cherny and J. Brand, *Phys. Rev. A* **70**, 043622 (2004).
- [145] G. Bertaina and S. Giorgini, *Physical Review Letters* **106**, 110403 (2011).
- [146] T. Kinoshita, T. Wenger, and D. S. Weiss, *Nature* **440**, 900 (2006).
- [147] E. Haller, M. Gustavsson, M. J. Mark, J. G. Danzl, R. Hart, G. Pupillo, and H.-C. Nagerl, *Science* **325**, 1224 (2009), [arXiv:1006.0739](https://arxiv.org/abs/1006.0739) .
- [148] Y.-a. Liao, A. S. C. Rittner, T. Paprotta, W. Li, G. B. Partridge, R. G. Hulet, S. K. Baur, and E. J. Mueller, *Nature* **467**, 567 (2010).
- [149] P. van Wyk, H. Tajima, D. Inotani, A. Ohnishi, and Y. Ohashi, *Physical Review A* **97**, 013601 (2018).
- [150] M. A. Cazalilla, R. Citro, T. Giamarchi, E. Orignac, and M. Rigol, *Rev. Mod. Phys.* **83**, 1405 (2011).
- [151] P. D'Amico and M. Rontani, *Physical Review A* **91**, 043610 (2015).
- [152] D. Pęcał, M. Gajda, and Tomasz Sowiński, *Few-Body Systems* **58**, 159 (2017).
- [153] T. Sowiński, M. Gajda, and K. Rzażewski, *EPL (Europhysics Letters)* **109**, 26005 (2015).
- [154] L. Rammelmüller, W. J. Porter, J. Braun, and J. E. Drut, *Physical Review A* **96**, 033635 (2017).
- [155] R. E. Thomas, G. H. Booth, and A. Alavi, *Physical Review Letters* **114** (2015), [10.1103/PhysRevLett.114.033001](https://arxiv.org/abs/10.1103/PhysRevLett.114.033001).
- [156] G. Li Manni, S. D. Smart, and A. Alavi, *Journal of Chemical Theory and Computation* **12**, 1245 (2016).
- [157] M. Olshanii, *Physical Review Letters* **81**, 938 (1998).
- [158] F. Werner and Y. Castin, *Phys. Rev. A* **86**, 013626 (2012).

-
- [159] X.-G. Wen, *Quantum Field Theory of Many-Body Systems* (Oxford University Press, Oxford, 2004).
- [160] E. J. Lindgren, J. Rotureau, C. Forssén, A. G. Volosniev, and N. T. Zinner, *New Journal of Physics* **16**, 063003 (2014).
- [161] P. Kościak, *Physics Letters A* **382**, 2561 (2018).
- [162] J. von Stecher and C. H. Greene, *Physical Review A* **80**, 022504 (2009).
- [163] J. Mitroy, S. Bubin, W. Horiuchi, Y. Suzuki, L. Adamowicz, W. Cencek, K. Szalewicz, J. Komasa, D. Blume, and K. Varga, *Reviews of Modern Physics* **85**, 693 (2013).
- [164] I. Brouzos and P. Schmelcher, *Physical Review A* **87**, 023605 (2013).
- [165] P. Kościak, M. Płodzień, and T. Sowiński, *EPL (Europhysics Letters)* **123**, 36001 (2018).
- [166] R. Jastrow, *Physical Review* **98**, 1479 (1955).
- [167] M. Casula, D. M. Ceperley, and E. J. Mueller, *Physical Review A* **78**, 033607 (2008).
- [168] L. M. Schonenberg and G. J. Conduit, *Physical Review A* **95**, 013633 (2017).
- [169] R. Pessoa, S. A. Vitiello, and K. E. Schmidt, *Journal of Low Temperature Physics* **180**, 168 (2015).
- [170] L. Parisi and S. Giorgini, *Physical Review A* **95**, 023619 (2017).
- [171] J. Carlson, S. Gandolfi, F. Pederiva, S. C. Pieper, R. Schiavilla, K. Schmidt, and R. Wiringa, *Reviews of Modern Physics* **87**, 1067 (2015).
- [172] J. B. Anderson, in *Reviews in Computational Chemistry*, edited by K. B. Lipkowitz and D. B. Boyd (John Wiley & Sons, Inc., Hoboken, NJ, USA, 2007) pp. 133–182.
- [173] W. A. Lester, L. Mitas, and B. Hammond, *Chemical Physics Letters* **478**, 1 (2009).

-
- [174] W. M. C. Foulkes, L. Mitas, R. J. Needs, and G. Rajagopal, *Reviews of Modern Physics* **73**, 33 (2001).
- [175] J. Kolorenč and L. Mitas, *Reports on Progress in Physics* **74**, 026502 (2011).
- [176] S. F. Boys and N. C. Handy, *Proceedings of the Royal Society A: Mathematical, Physical and Engineering Sciences* **310**, 43 (1969).
- [177] C. Filippi and C. J. Umrigar, *The Journal of Chemical Physics* **105**, 213 (1996).
- [178] O. Hino, Y. Tanimura, and S. Ten-no, *Chemical Physics Letters* **353**, 317 (2002).
- [179] H. Luo, *The Journal of Chemical Physics* **133**, 154109 (2010).
- [180] M. Ochi, K. Sodeyama, and S. Tsuneyuki, *The Journal of Chemical Physics* **140**, 074112 (2014).
- [181] M. Ochi, Y. Yamamoto, R. Arita, and S. Tsuneyuki, *The Journal of Chemical Physics* **144**, 104109 (2016).
- [182] H. Luo and A. Alavi, *Journal of Chemical Theory and Computation* **14**, 1403 (2018).
- [183] Eric W. Weisstein, “Sine,” (2018), from MathWorld—A Wolfram Web Resource.
- [184] P. Fulde, *Correlated Electrons in Quantum Matter* (WORLD SCIENTIFIC, 2012).
- [185] T. Kato, *Communications on Pure and Applied Mathematics* **10**, 151 (1957).
- [186] T. Gaskell, *Proceedings of the Physical Society* **77**, 1182 (1961).
- [187] E. A. G. Armour, *Journal of Physics C: Solid State Physics* **13**, 343 (1980).
- [188] G. H. Booth, S. D. Smart, and A. Alavi, *Molecular Physics* **112**, 1855 (2014).

-
- [189] N. S. Blunt, S. D. Smart, G. H. Booth, and A. Alavi, *J. Chem. Phys.* **143**, 134117 (2015).
- [190] I. A. Ivanov, M. W. J. Bromley, and J. Mitroy, *Computer Physics Communications* **152**, 9 (2003).
- [191] W. Zwerger, ed., *The BCS-BEC crossover and the unitary fermi gas*, Lecture notes in physics No. 836 (Springer, Heidelberg, 2012) oCLC: 844865150.
- [192] A. M. Perelomov and Y. B. Zel'dovich, *Quantum Mechanics – Selected Topics* (World Scientific, Singapore, 1998).
- [193] A. Y. Cherny and A. A. Shanenko, *Physical Review E* **64**, 027105 (2001).
- [194] B. A. Lippmann and J. Schwinger, *Phys. Rev.* **79**, 469 (1950).
- [195] N. N. Khuri, A. Martin, J.-M. Richard, and T. T. Wu, *J. Math. Phys.* **50**, 072105 (2009).
- [196] N. M. Atakishiyev, G. S. Pogosyan, L. E. Vicent, and K. B. Wolf, *Journal of Physics A: Mathematical and General* **34**, 9381 (2001).
- [197] Eric W. Weisstein, “Mod,” (2018), from MathWorld—A Wolfram Web Resource.



MASSEY UNIVERSITY
GRADUATE RESEARCH SCHOOL

**STATEMENT OF CONTRIBUTION
TO DOCTORAL THESIS CONTAINING PUBLICATIONS**

(To appear at the end of each thesis chapter/section/appendix submitted as an article/paper or collected as an appendix at the end of the thesis)

We, the candidate and the candidate's Principal Supervisor, certify that all co-authors have consented to their work being included in the thesis and they have accepted the candidate's contribution as indicated below in the *Statement of Originality*.

Name of Candidate: Peter Jeszenszki

Name/Title of Principal Supervisor: Joachim Brand

Name of Published Research Output and full reference:

Peter Jeszenszki, Alexander Yu. Cherny, and Joachim Brand, s-wave scattering length of a Gaussian potential, *Physical Review A* 97, 042708 (2018)

In which Chapter is the Published Work: Chapter 3

Please indicate either:

- The percentage of the Published Work that was contributed by the candidate:
and / or
- Describe the contribution that the candidate has made to the Published Work:

The candidate implemented the code based on the preliminary code provided by A. Yu. Cherny and performed the numerical calculations. The candidate also derived the analytic expression in the main text and in Appendix D. The supervisor initiated the project. The main ideas were developed in discussions with major contributions from all co-authors. A. Yu. Cherny suggested and worked out the foundation of the numerical procedure and worked out the derivations in Appendix A and C. The candidate wrote the first draft of the paper, which was modified by the supervisor and A. Yu. Cherny.

Candidate's Signature

27/11/2018

Date

Principal Supervisor's signature

27/11/2018

Date



MASSEY UNIVERSITY
GRADUATE RESEARCH SCHOOL

STATEMENT OF CONTRIBUTION
TO DOCTORAL THESIS CONTAINING PUBLICATIONS

(To appear at the end of each thesis chapter/section/appendix submitted as an article/paper or collected as an appendix at the end of the thesis)

We, the candidate and the candidate's Principal Supervisor, certify that all co-authors have consented to their work being included in the thesis and they have accepted the candidate's contribution as indicated below in the *Statement of Originality*.

Name of Candidate: **Peter Jeszenszki**

Name/Title of Principal Supervisor: **Joachim Brand**

Name of Published Research Output and full reference:

Peter Jeszenszki, Tal Levy, Ali Alavi and Joachim Brand, Are smooth pseudopotentials a good choice for representing short-range interactions?, arXiv:1812.06521, (2018)

In which Chapter is the Published Work: **Chapter 4**

Please indicate either:

- The percentage of the Published Work that was contributed by the candidate:
and / or
- Describe the contribution that the candidate has made to the Published Work:

The candidate performed all the numerical calculations. He also derived and implemented the evaluation of matrix-elements in Appendix B. The supervisor and Ali Alavi initiated the project. The supervisor worked out the relations in Sec. II. B. and the candidate derived the relation in Sec. II. C. The relations in Sec. II. D. are a joint work of the candidate and the supervisor. The candidate wrote the first draft of the paper, which was modified by the supervisor and Ali Alavi.

Candidate's Signature

Date

Principal Supervisor's signature

13 January 2019

Date



MASSEY UNIVERSITY
GRADUATE RESEARCH SCHOOL

**STATEMENT OF CONTRIBUTION
TO DOCTORAL THESIS CONTAINING PUBLICATIONS**

(To appear at the end of each thesis chapter/section/appendix submitted as an article/paper or collected as an appendix at the end of the thesis)

We, the candidate and the candidate's Principal Supervisor, certify that all co-authors have consented to their work being included in the thesis and they have accepted the candidate's contribution as indicated below in the *Statement of Originality*.

Name of Candidate: Peter Jeszenszki

Name/Title of Principal Supervisor: Joachim Brand

Name of Published Research Output and full reference:

Peter Jeszenszki, Hongjun Luo, Ali Alavi and Joachim Brand, Accelerating the convergence of exact diagonalization with the transcorrelated method: Quantum gas in one dimension with contact interactions, *Physical Review A* 98, 053627 (2018)

In which Chapter is the Published Work: Chapter 5

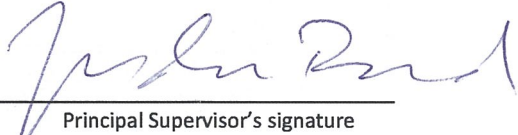
Please indicate either:

- The percentage of the Published Work that was contributed by the candidate:
and / or
- Describe the contribution that the candidate has made to the Published Work:

The candidate derived the expressions in Sec. II. F. and in the Appendix. He implemented the algorithm added the resulting code to the NECI scientific program package. He also performed all the numerical calculations and produced the relevant plots for the paper. The supervisor and Ali Alavi initiated the project. The main ideas were developed with contributions from all co-authors. Hongjun Luo derived the relations in Sec. II. D. and the supervisor derived the relations in Sec II. E. The candidate wrote the first draft of the manuscript, which was modified by the supervisor and there were minor corrections from Hongjun Luo and Ali Alavi.


Candidate's Signature

27/11/2018
Date


Principal Supervisor's signature

27/11/2018
Date